2018

DEVELOPMENT OF CARBONATE ELECTROLYTES FOR LITHIUM METAL ELECTRODES

Zachary Lee Brown
University of Rhode Island, zbrown@uri.edu

DEVELOPMENT OF CARBONATE ELECTROLYTES FOR LITHIUM METAL ELECTRODES

BY

ZACHARY LEE BROWN

A DISSERTATION SUBMITTED IN PARTIAL FULFILLMENT OF THE REQUIREMENTS FOR THE DEGREE OF

DOCTOR OF PHILOSOPHY

IN

CHEMISTRY

UNIVERSITY OF RHODE ISLAND

2018

DOCTOR OF PHILOSOPHY DISSERTATION

OF

ZACHARY L. BROWN

APPROVED:

Dissertation Committee:

Major Professor: Brett Lucht

Jason Dwyer

David Heskett

Nasser H. Zawia

DEAN OF THE GRADUATE SCHOOL

UNIVERSITY OF RHODE ISLAND

2018

ABSTRACT

The development of energy storage technology is an important topic for facilitating the employment of renewable energy in society. Therefore, current energy storage research is heavily focused on enabling rechargeable high-energy density lithium-based batteries. In particular, permitting reversible electrochemical plating and stripping of the lithium metal negative electrode (or lithium metal anode) in carbonate electrolytes can achieve this goal. Unfortunately, the performance of the lithium metal anode in carbonate electrolytes is plagued by unsafe dendrite formation and poor Coulombic efficiency upon cycling. This dissertation attempts to reveal the role of the composition and structure of the Solid Electrolyte Interphase (SEI) in relation to the performance of the lithium metal anode. Galvanostatic voltammetry was used to characterize the electrochemistry of the lithium metal anode, with Infrared Spectroscopy, X-ray Photoelectron Spectroscopy, and Transmission Electron Microscopy to investigate the surface of the lithium metal anode. In chapter 2, a method to electrochemically synthesize lithium metal such that a reliable SEI is generated is introduced, using Cu||$LiFePO_4$ cells. Using this method, in conjunction with the analytical techniques described above, chapters 3 and 4 investigates electrolyte components that significantly improve the performance of the lithium metal anode, fluoroethylene carbonate (FEC) and lithium difluoro(oxalate) borate (LiDFOB), with an explanation proposed. Finally, chapter 5 shows how FEC and LiDFOB can work together to optimize the SEI composition and structure, hence optimizing the performance of the lithium metal anode in carbonate electrolytes.

ACKNOWLEDGMENTS

First, I would like to thank my supervisor, Prof. Brett Lucht. I could not have asked for a better experience during my PhD. I have learned so much about how to properly formulate an idea and then explore it. I also have been fortunate to have many opportunities to travel to different countries, meeting and learning from other people. I am truly thankful for Brett's mentorship.

I am grateful for BASF, DOE, and URI for funding my research throughout my PhD. Without this funding, I could not have pursued this research. I have also learned a great deal from folks within the BASF network. Thank you.

Members of my PhD committee, Prof. Jason Dwyer and Prof. David Heskett have provided guidance for me during my time at URI. In particular, Jason has given me a significant amount of career advice along with academic mentorship. David has given me hands-on experience with impressive scientific instruments, such as a synchrotron. My Chair, Prof. Arijit Bose, has also helped me access experimental techniques, used in this work, along with providing career opportunities to pursue. Thank you all for your help.

There are many Lucht lab members I have had numerous fruitful discussions with, in particular, Cao, Sunhyung, Nina, Satu, Kaveendi, Mickdy, Alex, Taeho, Julien, Bharathy, Jennifer, Maheeka, Navid, and Nuwanthi. Thank you all for putting up with me.

The knowledge I have obtained during my MSc at Dalhousie University has helped me a great deal during my PhD. Thank you to my MSc supervisor, Prof. Mark Obrovac, for his continued mentorship. I am also thankful for lessons that I have

learned from my MSc committee members, Prof Jeff Dahn and Prof. Mary Anne White.

Of course, none of my accomplishments would be possible without my parents, Les and Alex, as I would not exist if it weren't for them. Thank you for all of the time and effort you put into raising me, ensuring that I have a fulfilling childhood. My Brother, Adam, and his family, Frances and Emerson, have taught me more than they realize. Thank you all for continuing to be my life mentors.

My crazy friends from Bridgewater, Max, Darcy, Logan, James, Jory, Andrew, Ben, Matt and Barret, still keep me sane throughout my studies. Thanks boys.

Finally, to Christiana, thank you for listening to my many ideas aloud, no matter how ridiculous they might be. We have already been through so much together, and I can't wait to see what adventures await us in the future.

PREFACE

This dissertation is written in manuscript format. There are five chapters in this dissertation. Chapter 1 is an introduction of the lithium-ion battery and analytical techniques described throughout the dissertation. Chapter 2 was published in the Journal of the Electrochemical Society. Chapter 3 was published in ACS Applied Energy Materials. Chapter 4 was published in RSC Energy & Environmental Science. Chapter 5 is written as a manuscript and is currently submitted to the Journal of the Electrochemical Society.

TABLE OF CONTENTS

LIST OF FIGURES

CHAPTER 1

Dissertation Introduction

MOTIVATION

As the global temperature rises, so does the concern about consuming fossil fuels.[1,2,3] In the United States, 6511 million metric tons of carbon dioxide equivalents of greenhouse gases was emitted in 2016.[2] In particular, US economic sectors of electricity and transportation account for more than 50% of the GHG emissions, plotted in Figure 1-1, with each sector contributing about 28% of emissions.[2] In attempt to reduce this fossil fuel consumption, there has been a surge in the development of energy storage technology to facilitate large-scale grid energy storage and electro mobility.[4] So far, the lithium-ion battery is the leader in energy storage technology, ubiquitous in small-scale mobile devices, now being adopted in electric vehicles, and larger energy storage projects.[5, 6] However, more breakthroughs in battery technology are required to make energy storage affordable to all consumers.

LITHIUM-ION BATTERIES

The lithium-ion battery consists of four important components, a negative electrode (anode), a positive electrode (cathode), the electrolyte, and separator material. An image of a dry, disassembled CR2032 coin cell with common lithium-ion battery components is shown in Figure 1-2 as an example. Graphite is a common anode material in commercial lithium-ion batteries, because of its ability to reversibly intercalate/de-intercalate lithium ions at a low potential, close to $Li^0/Li+$ (-3.04 V vs. standard hydrogen electrode).[7] There are several lithium transition metal oxide materials that can also reversibly intercalate/de-intercalate lithium ions at a high potential relative to Li^0/Li^+, such as $LiCoO_2$, $LiNi_{1/3}Co_{1/3}Mn_{1/3}O_2$, or $LiFePO_4$, that are

used as cathode materials.[7] Commercial electrolytes consist of lithium salts (e. g. lithium hexafluorophosphate ($LiPF_6$)) dissolved in a blend of carbonate ester solvents (e. g. ethylene carbonate (EC), ethyl methyl carbonate (EMC)), which have electrochemical stability over a wide voltage range.[7,8] These carbonate electrolytes enable the pairing of the graphite anode and lithium transition metal oxide cathode, completing the high-voltage, rechargeable electrochemical cell as shown in equations 1-3.[7]

Negative: $$C + x\ Li^+ + x\ e^- \rightleftharpoons Li_xC \quad (1)$$

Positive: $$LiCoO_2 \rightleftharpoons y\ Li^+ + y\ e^- + Li_{1-y}CoO_2 \quad (2)$$

Full Cell: $$LiCoO_2 + \frac{y}{x}\ C \rightleftharpoons \frac{y}{x}\ Li_xC + Li_{1-y}CoO_2 \quad (3)$$

Furthermore, a polyethylene/polypropylene separator does not participate in the electrochemistry, but is wetted with electrolyte and placed in between the anode and cathode materials in order to prevent internal short circuits within the cell. Further, the Coulombic efficiency (CE) is an important parameter used to describe the amount of reversible lithium cations accessed upon each charge/discharge cycle of lithium-ion batteries. The CE for a full cell shown in equation 4,

$$CE = \frac{Q_d}{Q_c} \quad (4)$$

where Q_d is the total charge extracted upon the discharge process and Q_c is the total charge input during the charge process.

SOLID ELECTROLYTE INTERPHASE

The electrolyte can react on the surface of electrode materials to generate a Solid Electrolyte Interphase (SEI), which is important for allowing lithium-ion batteries to be charge/discharged for thousands of cycles with high efficiency.[9] Without the SEI, today's rechargeable lithium-ion batteries could not operate with such impressive efficiency and safety. Specifically, the SEI is an electronically insulating surface film that passivates the electrode, permitting lithium cation mobility and preventing further decomposition of the electrolyte.[9] It is composed of inorganic and organic decomposition products of electrolyte components.[9] Top-performing electrolytes have additives, which are chemicals used in low concentrations to generate an ideal SEI upon initial cycling of the battery. For example, vinylene carbonate is a common commercial additive which polymerizes on the surface of graphite upon reduction, improving the stability of the SEI.[8,10-12]

LITHIUM METAL ELECTRODE

Lithium metal is considered to be the anode to enable next-generation batteries. This is because lithium metal has high theoretical gravimetric capacity of 3861 mAh/g, along with its low electrochemical potential.[13,14] However, especially in carbonate electrolytes, a stable SEI for lithium metal electrodes eludes researchers. Without a stable SEI, the plating and stripping of lithium metal is plagued by dendrite formation, leading to several safety issues, and poor Coulombic efficiency.[8,13,14] Currently, it is difficult to obtain stable Coulombic efficiencies with lithium metal electrodes, where an efficiency of at least 99.9% is required for considering

commercial application.[15] Therefore, researchers are motivated to develop lithium metal electrochemistry to enable next-generation battery technology.

ANALYLTICAL METHODS

The methods used to characterize the lithium metal in this work are summarized below with extreme brevity. Galvanostatic voltammetry is typically employed to investigate the electrochemistry of lithium-ion battery materials, suitable for practical operation of lithium-ion batteries.[7] In this mode, the current between working and counter electrodes is fixed, and the cell voltage is measured. By observing the measured voltage, changes in the chemistry at each electrode can be revealed, as the cell voltage is related to the potential difference (ΔG) between two electrode materials,

$$\Delta G = -nFE \tag{5}$$

where n is the number of electrons transferred in the cell reaction, F is the Faraday constant, and E is voltage of the cell. Cut-off voltages are used in experimental procedures to define the proper operating voltage window for a given cell format. The boundary conditions set by this operating window allow for measurement of the capacity obtainable by the investigated cell format, i. e. the number of lithium ions transferred between electrodes each charge/discharge. From the charge/discharge capacities, Coulombic efficiencies can be calculated from equation 4. The nature of the SEI has a profound effect on these galvanostatic operating conditions. For example, a thick, resistive SEI layer on the anode can cause low capacity and low Coulombic efficiency, whereas a thin, high lithium-ion conductivity SEI on the anode can cause high capacity and high Coulombic efficiency. These changes in

performance are primarily due to the resistance of the SEI heavily influencing the time to reach a cut-off voltage for the chosen current. An ideal SEI formed on the surface of electrodes allows for lithium-ion batteries that can operate at high voltage, high current, and with high efficiency, which is desirable for consumer applications.

In order to characterize the nature of the SEI, employing several techniques that probe the surface of a material is ideal. The first example used throughout this work is Infrared (IR) absorption spectroscopy. Beer's law is applicable to IR spectroscopy,

$$A = \varepsilon bc \tag{6}$$

where A is the absorbance, ε is the molar absorptivity of the analyte, b is the path length of measurement, and c is the concentration of the analyte.[16] When investigating SEI components, IR is particular useful for probing decomposition products of carbonate solvents. The decomposition of products of these carbonate solvents contain carbonyl (C=O) moieties which are particularly sensitive analytes due to the large difference in electronegativity of C and O. Several carbonyl-containing molecules can be resolved by wavenumber, for example, major peaks for Li_2CO_3 are observed at 1550 – 1400 cm^{-1} whereas a major peak for $Li_2C_2O_4$ species can be observed at 1640 cm^{-1}.[17] In this work, both Attenuated Total Reflectance (ATR-IR) and Diffuse Reflectance (DRIFTS) accessories are used.

X-ray Photoelectron Spectroscopy (XPS) is another common technique to probe the surface of electrode materials. XPS is governed by the photoelectric effect,

$$KE = h\nu - BE \tag{7}$$

where KE is the kinetic energy of photoelectrons, BE is binding energy of the electron in the atomic orbital from which it originates, h is Planck's constant, and ν is the X-

ray frequency.[18] Both inorganic and organic SEI components can be identified, as each atomic core is unique, and the penetration depth of XPS is on the order of tens of Ångstroms.[19] In particular, F1s, O1s, and C1s are most useful for this work as they are present in high concentrations in the electrolyte. In this work, Al Kα radiation of hυ = 1486.6 eV is used to probe common SEI components such as LiF, Li_2CO_3, and Li_2O, along with other species and in some cases, other atomic cores of interest.

Transmission Electron Microscopy (TEM) is a versatile imaging technique capable of investigating the morphology at the nanometer scale, ideal for investigating the structure of the SEI. Imaging at this scale for electron microscopes is possible because the wavelength of an electron in a TEM instrument is on the order of 100000x smaller than that of a photon.[20] This significantly smaller wavelength allows for a considerable increase in image resolution according to the Rayleigh criterion,

$$\theta = 1.22\frac{\lambda}{D} \tag{8}$$

where Θ is the minimum resolvable angular separation of two Airy disks, λ is the wavelength of light used, and D is the aperture diameter.[21] Further, TEM instruments can be equipped with energy-dispersive X-ray spectroscopy, allowing for compositional analysis of the imaged object of interest. In this work, lithium metal is plated on Cu TEM grids and its SEI morphology is investigated.

SUMMARY

Overall, this dissertation attempts to reveal the role of the composition and structure of the SEI in relation to the performance of the lithium metal anode. In chapter 2, a method to electrochemically synthesize lithium metal such that a reliable SEI is generated, is introduced. Using this method, in conjunction with the analytical techniques described above, chapters 3 and 4 investigates electrolyte components that significantly improve the performance of the lithium metal anode with an explanation proposed. Finally, chapter 5 shows how these electrolyte components can work together to optimize the SEI composition and structure, hence the optimizing the performance of the lithium metal anode in carbonate electrolytes.

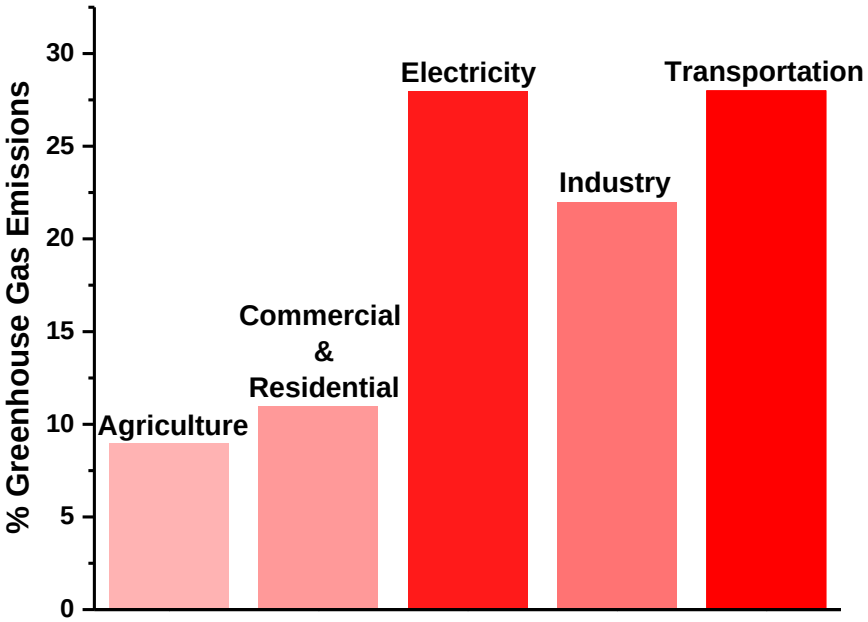

Figure 1-1. Total U. S. Greenhouse Gas Emissions by Economic Sector in 2016. Redrawn from literature[2].

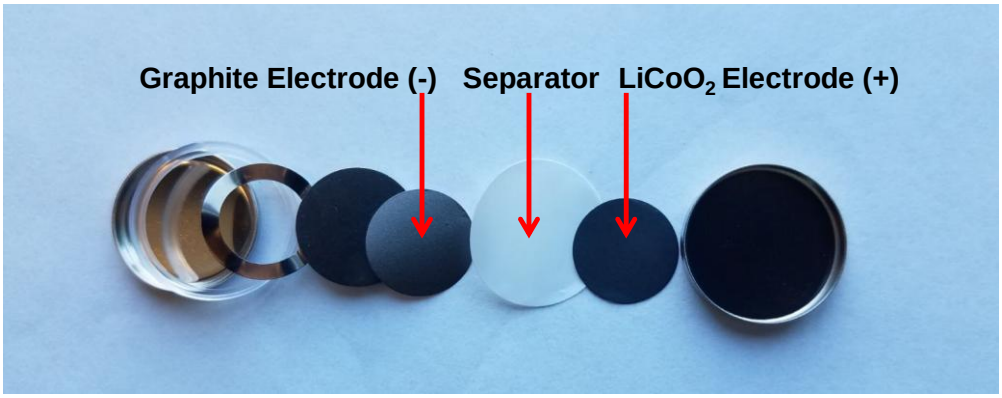

Figure 1-2. A dry, disassembled CR-2032 coin cell containing common lithium-ion battery materials.

REFERENCES

1. Earth Science Communications Team at NASA's Jet Propulsion Laboratory, "Global Climate Change: Vital Signs of the Planet". https://climate.nasa.gov/vital-signs/global-temperature/ (Accessed 10/09/18).
2. United States Environmental Protection Agency, "Overview of Greenhouse Gases", https://www.epa.gov/ghgemissions/overview-greenhouse-gases (Accessed 10/09/18).
3. United Nations Climate Change, "The Paris Agreement". https://unfccc.int/process-and-meetings/the-paris-agreement/the-paris-agreement (Accessed 10/20/18).
4. Bloomberg New Energy Finance (BNEF), "Global Storage Market to Double Six Times by 2030", https://about.bnef.com/blog/global-storage-market-double-six-times-2030/, November 20, 2017.
5. Kokam, http://kokam.com/ess-3/ (Accessed 10/09/18).
6. Tesla, https://www.tesla.com/energy (Accessed 10/09/18).
7. D. Linden and T. B. Reddy, Eds., Lindens Handbook of Batteries, 4th ed., McGrawHill, (2010).
8. K. Xu, *Chem. Rev.*, 2004, **104**, 4303-4418.
9. E. Peled, *J. Electrochem. Soc.*, **126**, 2047–2051 (1979).
10. Simon, B.; Boeuve, J.-P. U.S. Patent 5,626,981, 1997.
11. Barker, J.; Gao, F. U.S. Patent 5,712,059, 1998.
12. Naruse, Y.; Fujita, S.; Omaru, A. U.S. Patent 5,714,281, 1998.

13. X. Cheng, R. Zhang, C.-Z. Zhao, and Q. Zhang, *Chem. Rev.*, **117**, 10403–10473 (2017).

14. B. Liu, J. G. Zhang, and W. Xu, *Joule*, **2**, 833–845 (2018).

15. P. Albertus, S. Babinec, S. Litzelman, and A. Newman, *Nat. Energy*, **3**, 16–21 (2018).

16. D. A. Skoog, J. F. Holler, and S. R. Crouch, *Principles of Instrumental Analysis*, 6th ed.,p. 430 – 480, Thomson Brooks/Cole, (2007).

17. P. Verma, P. Maire, and P. Novák, *Electrochim. Acta*, **55**, 6332–6341 (2010).

18. D. A. Skoog, J. F. Holler, and S. R. Crouch, *Principles of Instrumental Analysis*, 6th ed.,p. 589 – 598, Thomson Brooks/Cole, (2007).

19. J. F. Moulder, W. F. Stickle, P. E. Sobol, and K. D. Bomben, *Handbook of X-ray Photoelectron Spectroscopy* J. Chastan, Editor, p. 11, Perkin-Elmer Corporation, (1992).

20. JEOL Ltd., "Transmission Electron Microscope", https://www.jeol.co.jp/en/science/em.html (Accessed 10/14/18).

21. Lord Rayleigh, *Phil. Mag. S.*, **8**, 261-274 (1879).

CHAPTER 2

Investigation of the Lithium Solid Electrolyte Interphase in Vinylene Carbonate Electrolytes Using Cu||$LiFePO_4$ cells

Zachary L. Brown[1], Sunhyung Jurng[1], and Brett L. Lucht[1]

[1]*Department of Chemistry, University of Rhode Island, Kingston, Rhode Island 02881, USA*

**Corresponding author: blucht@chm.uri.edu*

The following was published in the Journal of The Electrochemical Society, and is presented here in manuscript format

ABSTRACT

The influence of vinylene carbonate (VC) on the plating/stripping of lithium was investigated using Cu||$LiFePO_4$ cells. These cells allow for easy fabrication and in-situ generation of lithium, with no excess lithium to influence performance. Addition of VC to the electrolyte improves both capacity retention and efficiency. IR and XPS spectroscopy of the surface of the plated lithium suggests the presence of a significant amount of poly(VC) when the electrolyte (1.2 M $LiPF_6$ in ethylene carbonate (EC): ethyl methyl carbonate (EMC) (3:7, vol)) contains 5% of added VC. This suggests employing additives that generate polymeric species on the surface of lithium improves plating/stripping performance in carbonate electrolytes.

INTRODUCTION

The plating and stripping of the lithium metal negative electrode in non-aqueous electrolytes has been investigated for decades.[1–3] In particular, carbonate solvents have relatively high voltage stability, making them desirable electrolytes for high-energy density lithium batteries.[3–6] However, the efficiency of plating/stripping lithium in carbonate electrolytes does not meet requirements for commercial application (> 99.9%).[7,8]

It is common to measure the plating/stripping efficiency of lithium by assembling Li||Cu cells.[9–13] In this cell design, a small amount of Li is cycled, with an excess reservoir of lithium present. One limitation of this cell design is the difficulty of controlling the design and construction of the solid electrolyte interphase[14] (SEI) on lithium, as the low reduction potential of the lithium metal electrode present during cell construction will cause immediate reaction with electrolyte upon exposure. Thus, a reaction between the electrolyte and the lithium metal electrode will occur before cycling begins. Further, the excess lithium within the cell can significantly increase the cycle life of the cell making it difficult to compare to commercial cells, with a limited supply of lithium. Contrary to Li||Cu cells, Cu||$LiFePO_4$ cells have air-stable components, facilitating their processing and assembly.[15,16] Further, the in-situ formation of lithium metal and low reactivity of $LiFePO_4$ ensures additives under investigation do not react with the electrode surface upon construction and are only reduced upon initial cycling. This affords the possibility for controlled design and construction of the SEI on lithium metal since the reduction of the electrolyte can be

controlled by current density, cell potential, and the quantity of lithium plated. Finally, given that there is no excess lithium in Cu||$LiFePO_4$ cells, any observed improvements in capacity retention, Coulombic efficiency, or impedance should be applicable to other lithium metal based battery systems.

Vinylene carbonate (VC) is a well known electrolyte additive for lithium-ion batteries, demonstrating exceptional performance for graphite and several cathode materials.[17–24] Further, the reaction products of VC with lithium have been investigated in detail, using Li||Ni cells[25–27] and Li||Cu cells,[10,28] and found to have beneficial performance, typically attributed to poly(VC) within the SEI. However, the effect of added VC has not been investigated with lithium metal anodes in cells without a large excess of lithium. Herein, Cu||$LiFePO_4$ cells are utilized to investigate the influence of VC for plating and stripping lithium.

EXPERIMENTAL

Electrochemical characterization was performed using 2032 coin cells containing Cu||$LiFePO_4$. A minimum of two cells were assembled for each electrolyte, consisting of a copper foil negative electrode (15 mm diameter, MTI Corporation), Celgard 2325 separator (19 mm diameter) for electrolytes with ethylene carbonate: ethyl methyl carbonate (3:7, volume:volume) (EC:EMC) solvents (all electrolyte components were supplied from BASF as battery grade and used as received) or Celgard 3501 separator (19 mm diameter) when VC was employed as a solvent, and a $LiFePO_4$ positive electrode (91% active material, 13.7 mm diameter, MTI corporation), the other 9% of the composite electrode is composed of conductive

carbon and PVDF coated on aluminum. These components were soaked with 75 μL of electrolyte (supplied from BASF). Electrolytes investigated were 1.2 M $LiPF_6$ in EC:EMC (EC:EMC electrolyte), EC:EMC electrolyte with 1% VC (mass%) (1% VC electrolyte), EC:EMC electrolyte with 5% VC (mass%) (5% VC electrolyte), and 1.2 M $LiPF_6$ in VC solvent (VC-S electrolyte). The copper foil was sonicated with 1 M HCl (2×2 minutes) followed by sonication with isopropanol (1×2 minutes), punched to the specified diameter, and dried at 110°C, overnight under vacuum (approx. 3×10^{-3} atm) prior to cell assembly. The $LiFePO_4$ electrodes were punched to the specified diameter, and dried at 110°C overnight under vacuum (approx. 3×10^{-3} atm) prior to cell assembly. Cell assembly and disassembly was conducted in an argon glove box (M-Braun) with water and oxygen contents < 1 ppm. The cycling procedure consisted of plating lithium at 0.1 mA/cm^2 (approx. C/20 rate, where C represents the theoretical capacity of $LiFePO_4$) with subsequent stripping and plating at 0.5 mA/cm^2 (approx. C/4 rate), within a voltage window of 2.0–4.0 V, using an Arbin BT2000 battery cycler at 25°C. There was a rest period of one hour between cell construction and the beginning of the electrochemical protocol.

IR measurements were conducted on a Bruker Tensor 27 spectrometer equipped with an attenuated total reflection (ATR) accessory (Pike Technologies) containing a diamond/ZnSe reflection crystal plate and LaDTG detector. Lithium was plated onto copper foil according to the first charge procedure outlined in the Electrochemistry section (charge to 4.0 V at C/20 rate) and held at rest for approx. 48 hours to ensure cell equilibration before disassembly. Electrodes were washed with 4×500 μL battery grade EMC and dried overnight under vacuum (approx. 3×10^{-3}

atm). The electrodes were transferred from the argon glove box to the nitrogen-filled glove box in a sealed glass vial and immediately analyzed. The spectra were acquired in the nitrogen glove box with a resolution of 4 cm^{-1} and 256 scans. An atmospheric compensation, baseline correction, and extended ATR correction were applied to all spectra using OPUS software, version 7.0. There is no evidence for reaction of the lithium metal anodes with the N_2 during the timeframe of the analysis.

XPS measurements were acquired with a K-alpha, Thermo system using Al Kα radiation (hν = 1486.6 eV) under ultra-high vacuum ($<1\times10^{-12}$ atm) and a measured spot size of 400 μm in diameter. Lithium was plated onto copper foil from a $LiFePO_4$ cathode charged to 4.0 V at a rate of C/20 and held for 48 hours to ensure cell equilibration before disassembly. Electrodes were washed with 4×500 μL battery grade EMC and dried overnight under vacuum ($<2\times10^{-10}$ atm). The samples were transferred from the argon glove box in an air-free transfer case. The binding energy was corrected based in the F1s spectrum, assigning LiF to a position of 685 eV. Relative atomic concentrations were calculated by integrating respective peaks with a Shirley background, using Thermo Avantage v5.932 software. Atomic concentrations were determined from integrations of the XPS peaks taking respective atomic sensitivity factors into account.

RESULTS AND DISCUSSION

The cycling performance of the carbonate electrolytes investigated is provided in Figure 2-1 with stripping capacity (Figure 2-1A), normalized using the active mass of $LiFePO_4$, and Coulombic efficiency (Figure 2-1B) versus cycle number. Since there

is no excess lithium in the Cu||$LiFePO_4$ cells, the reversible capacity of all cells decreases significantly over a short number of cycles as expected.[15] Since VC has been shown to have virtually no reactivity on $LiFePO_4$, the improvement in cell performance is likely due to modification of the SEI on the negative electrode.[22,29] In general, the addition of VC improves the capacity retention and the Coulombic efficiency, as observed with the EC:EMC, 1% VC, 5% VC, and VC-S electrolytes. Electrolytes containing 1% and 5% VC have the highest first cycle Coulombic efficiency ~87%. The 5% VC electrolyte has a longer cycle life and better efficiency (~92%), suggesting that increased concentrations of VC in the electrolyte results in the generation of a more stable SEI for lithium metal anodes. However, when employing VC as the solvent the first cycle Coulombic efficiency is reduced significantly to ~58%. After the first cycle, the efficiency improves to ~95%, comparable to reports in the literature.[10,25] After a significant quantity of lithium is consumed irreversibly on the first cycle, the VC-S electrolyte plates and strips lithium more efficiently than the EC:EMC, 1% VC, or 5% VC electrolytes, leading to improved reversible cycling.

The total quantity of lithium stripped each cycle (or the lithium reversibly cycled), summed over all cycles, for each electrolyte is plotted in Figure 2-2. This plot demonstrates that the amount of lithium reversibly cycled is increased with increasing concentration of VC in the electrolyte. However, the increase of reversibly cycled lithium is not as dramatic when employing VC as a solvent. While increasing the concentration of VC in the electrolyte is beneficial for cycling performance, the beneficial effects diminish at high concentrations of VC.

The first cycle voltage vs. specific capacity plots for all electrolytes investigated are shown in Figure 2-3. The initial plating curves are very similar for all electrolytes, but the stripping voltage curves illustrate the high initial Coulombic efficiency for the 1 and 5% VC electrolytes. Increasing the concentration of VC in the electrolyte increases the hysteresis, consistent with the generation of a resistive SEI. This suggests that the diminishing benefit of VC, discussed above, may result from high resistance of the SEI film.

ATR-IR spectra of lithium plated on copper foil were acquired after the first charge to 4.0 V at 0.1 mA/cm^2 for the EC:EMC and 5% VC electrolytes and are provided in Figure 2-4. The background for the diamond/ZnSe ATR crystal spectrum is also provided to depict spectral artifacts from the ATR crystal. Li_2CO_3 is present on lithium plated from both the EC:EMC and 5% VC electrolytes as evidenced by characteristic peaks[30,31] between 1550–1400 cm^{-1} and at ~875 cm^{-1}. In addition, a peak characteristic of lithium alkyl carbonates[30,32] is observed between 1700–1650 cm^{-1} for the lithium plated with the EC:EMC electrolyte. However, IR absorptions characteristic of lithium alkyl carbonates are not observed for lithium plated with the 5% VC electrolyte. Instead, strong absorptions are observed between 1850–1750 cm^{-1} and 1200–1050 cm^{-1}, consistent with the presence of poly(VC) as previously reported.[26,33]

XPS spectra of lithium plated on copper foil were acquired after the first charge to 4.0 V at 0.1 mA/cm^2. The C1s XPS spectra for electrodes plated from the EC:EMC and 5% VC electrolytes are plotted in Figure 2-5. The C1s spectra for the electrode plated from EC:EMC contains peaks characteristic of Li_2CO_3 or lithium

alkyl carbonates at 290 eV[31,32] along with a C-O peak at 286.7 eV, consistent with the IR spectra. The XPS spectrum of the electrode plated from 5% VC electrolyte is very different and contains intense peaks at 291 and 288 eV characteristic of poly(VC) in the SEI,[26] which is also consistent with IR spectra. The O1s XPS spectra of Li plated with the EC:EMC and 5% VC electrolytes are provided in Figure 2-5. The O1s spectrum for EC:EMC electrolyte, contains a peak characteristic of lithium carbonates (~531.5 eV), consistent with the C1s spectra. A peak characteristic of Li_2O at 528 eV is also present on the surface of the lithium metal plated from the EC:EMC electrolyte.[34] The O1s spectrum for the 5% VC electrolyte contains intense peaks at 534.5 and 533 eV characteristic of poly(VC) in the SEI,[26] consistent with the C1s spectra. The F1s XPS spectra of Li plated with the EC:EMC and 5% VC electrolytes are plotted in Figure 2-5. The F1s spectra for both the EC:EMC and 5% VC electrolytes contain a broad peak characteristic of LixPFy/LixPFyOz[19] at ~687 eV and the related peaks are observed in the P2p spectra at ~137/135 eV (not shown). The XPS spectrum of the lithium plated from the EC:EMC electrolyte also contains a large peak at 685 eV characteristic of LiF. The peak associated with LiF is much smaller for the electrolyte containing VC suggesting that VC inhibits $LiPF_6$ reduction. The surface of the SEI generated from the 5% VC electrolyte is primarily composed of poly(VC).

A chart of the corresponding relative atomic concentrations is provided in Figure 2-6. The surface of the lithium plated from the 5% VC electrolyte is primarily composed of organic species as evidenced by high concentrations of C and O. The IR and XPS data suggest that the surface is dominated by poly(VC). Alternatively, the surface plated from the EC:EMC electrolyte has much higher concentrations of

inorganic species, Li and F, consistent with the presence of high concentrations of LEDC and LiF. Given the improvement of the electrochemistry, the results suggest that incorporating polymeric species into the SEI are beneficial for plating/stripping lithium.

CONCLUSION

The influence of vinylene carbonate (VC) on plating/stripping lithium was investigated using Cu||$LiFePO_4$ cells. This allows for in-situ generation of lithium, ensuring controlled SEI formation compared to Li||Cu cells. Addition of VC has been found to improve the capacity retention of the cells, and increasing the concentration of VC in the electrolyte further improves the reversibility of lithium cycling. However, the performance improvements are accompanied by an increased voltage hysteresis. Ex-situ surface analysis of the electrodes suggests that the SEI generated on the plated lithium is primarily composed of LEDC, Li_2CO_3, and LiF when the 1.2 M $LiPF_6$ in EC:EMC (3:7) electrolyte is utilized. Alternatively, the SEI is dominated by poly(VC) when cells are cycled with the 1.2 M $LiPF_6$ in EC:EMC (3:7) with 5% VC electrolyte. The results suggest incorporating polymeric species within the lithium SEI improves plating/stripping performance of lithium metal in carbonate electrolytes. The results are similar to previously reported investigations with Li||Cu cells and demonstrate the feasibility of Cu||$LiFePO_4$ cells for developing electrolytes for lithium metal electrodes.[10,28] With this knowledge, advantageous characteristics of Cu||$LiFePO_4$ cells can be exploited when investigating other electrolyte additives. Specifically, other additives which can generate polymer surface films are under investigation and will be reported in the future.

REFERENCES

1. M. S. Whittingham, *Science*, **192**, 1126 (1976).

2. R. D. Rauh, T. F. Reise, and S. B. Brummer, *J. Electrochem. Soc.*, **125**, 186 (1978).

3. K. Xu, *Chem. Rev.*, **104**, 4303 (2004).

4. F. Ossola, G. Pistoia, R. Seeber, and P. Ugo, *Electrochim. Acta*, **33**, 47 (1988).

5. E. Plichta, S. Slane, M. Uchiyama, M. Salomon, D. Chua, W. B. Ebner, and H. W. Lin, *J. Electrochem. Soc.*, **136**, 1865 (1989).

6. I. Uchida and S. Hajime, *J. Electrochem. Soc.*, **142**, L139 (1995).

7. M. S. Whittingham, *Proc. IEEE*, **100**, 1518 (2012).

8. W. Xu, J. Wang, F. Ding, X. Chen, E. Nasybulin, Y. Zhang, and J.-G. Zhang, *Energy Environ. Sci.*, **7**, 513 (2014).

9. D. Aurbach, O. Youngman, Y. Gofer, A. Meitav, and P. Dan, *Electrochim. Acta*, **35**, 625 (1990).

10. F. Ding, W. Xu, X. Chen, J.-G. Zhang, M. H. Engelhard, Y. Zhang, B. R. Johnson, J. V. Crum, T.A. Blake, X. Liu, and J.-G. Zhang, *J. Electrochem. Soc.*, **160**, A1894 (2013).

11. F. Ding, W. Xu, X. Chen, J. Zhang, Y. Shao, M. H. Engelhard, Y. Zhang, T. A. Blake, G. L. Graff, X. Liu, and J. G. Zhang, *J. Phys. Chem. C*, **118**, 4043 (2014).

12. G. Bieker, M. Winter, and P. Bieker, *Phys. Chem. Chem. Phys.*, **17**, 8670 (2015).

13. J. Qian, W. A. Henderson, W. Xu, P. Bhattacharya, M. Engelhard, O. Borodin, and J.-G. Zhang, *Nat. Commun.*, **6**, 6362 (2015).

14. E. Peled, *J. Electrochem. Soc.*, **126**, 2047 (1979).

15. J. Qian, B. D. Adams, J. Zheng, W. Xu, W. A. Henderson, J. Wang, M. E. Bowden, S. Xu, J. Hu, and J. G. Zhang, *Adv. Funct. Mater.*, **26**, 7094 (2016).

16. B. J. Neudecker, N. J. Dudney, and J. B. Bates, *J. Electrochem. Soc.*, **147**, 517 (2000).

17. C. Jehoulet, P. Biensan, J. M. Bodet, M. Broussely, C. Moteau, and C. Tessier-Lescourret, *Batteries for Portable Applications and Electric Vehicles* A. R. Landgrebe and C. F. Holmes, Editors, p. 974, The Electrochemical Society, (1997).

18. D. Aurbach, K. Gamolsky, B. Markovsky, Y. Gofer, M. Schmidt, and U. Heider, *Electrochim. Acta*, **47**, 1423 (2002).

19. M. Nie, J. Demeaux, B. T. Young, D. R. Heskett, Y. Chen, A. Bose, J. C. Woicik, and B. L. Lucht, *J. Electrochem. Soc.*, **162**, A7008 (2015).

20. B. Zhang, M. Metzger, S. Solchenbach, M. Payne, S. Meini, H. A. Gasteiger, A. Garsuch, and B. L. Lucht, *J. Phys. Chem. C*, **119**, 11337 (2015).

21. H. Ota, Y. Sakata, A. Inoue, and S. Yamaguchi, *J. Electrochem. Soc.*, **151**, A1659 (2004).

22. L. El Ouatani, R. Dedryvère, C. Siret, P. Biensan, and D. Gonbeau, *J. Electrochem. Soc.*, **156**, A468 (2009).

23. J. C. Burns, R. Petibon, K. J. Nelson, N. N. Sinha, A. Kassam, B. M. Way, and J. R. Dahn, *J. Electrochem. Soc.*, **160**, A1668 (2013).

24. R. Petibon, L. Rotermund, K. J. Nelson, A. S. Gozdz, J. Xia, and J. R. Dahn, *J. Electrochem. Soc.*, **161**, A1167 (2014).

25. H. Ota, K. Shima, M. Ue, and J. ichi Yamaki, *Electrochim. Acta*, **49**, 565 (2004).

26. H. Ota, Y. Sakata, Y. Otake, K. Shima, M. Ue, and J. Yamaki, *J. Electrochem.*

Soc., **151**, A1778 (2004).

27. R. Mogi, M. Inaba, S.-K. Jeong, Y. Iriyama, T. Abe, and Z. Ogumi, *J. Electrochem. Soc.*, **149**, A1578 (2002).

28. J. Guo, Z. Wen, M. Wu, J. Jin, and Y. Liu, *Electrochem. Commun.*, **51**, 59 (2015).

29. R. Dedryvère, M. Maccario, L. Croguennec, F. Le Cras, C. Delmas, and D. Gonbeau, *Chem. Mater.*, **20**, 7164 (2008).

30. D. Aurbach and A. Zaban, *J. Electroanal. Chem.*, **365**, 41 (1994).

31. D. M. Seo, C. C. Nguyen, B. T. Young, D. R. Heskett, J. C. Woicik, and B. L. Lucht, *J. Electrochem. Soc.*, **162**, A7091 (2015).

32. K. Xu, G. R. V Zhuang, J. L. Allen, U. Lee, S. S. Zhang, P. N. Ross, and T. R. Jow, *J. Phys. Chem. B*, **110**, 7708 (2006).

33. A. L. Michan, B. S. Parimalam, M. Leskes, R. N. Kerber, T. Yoon, C. P. Grey, and B. L. Lucht, *Chem. Mater.*, **28**, 8149 (2016).

34. J. F. Moulder, W. F. Stickle, P. E. Sobol, and K. D. Bomben, *Handbook of X-ray Photoelectron Spectroscopy* J. Chastan, Editor, p. 11, Perkin-Elmer Corporation, (1992).

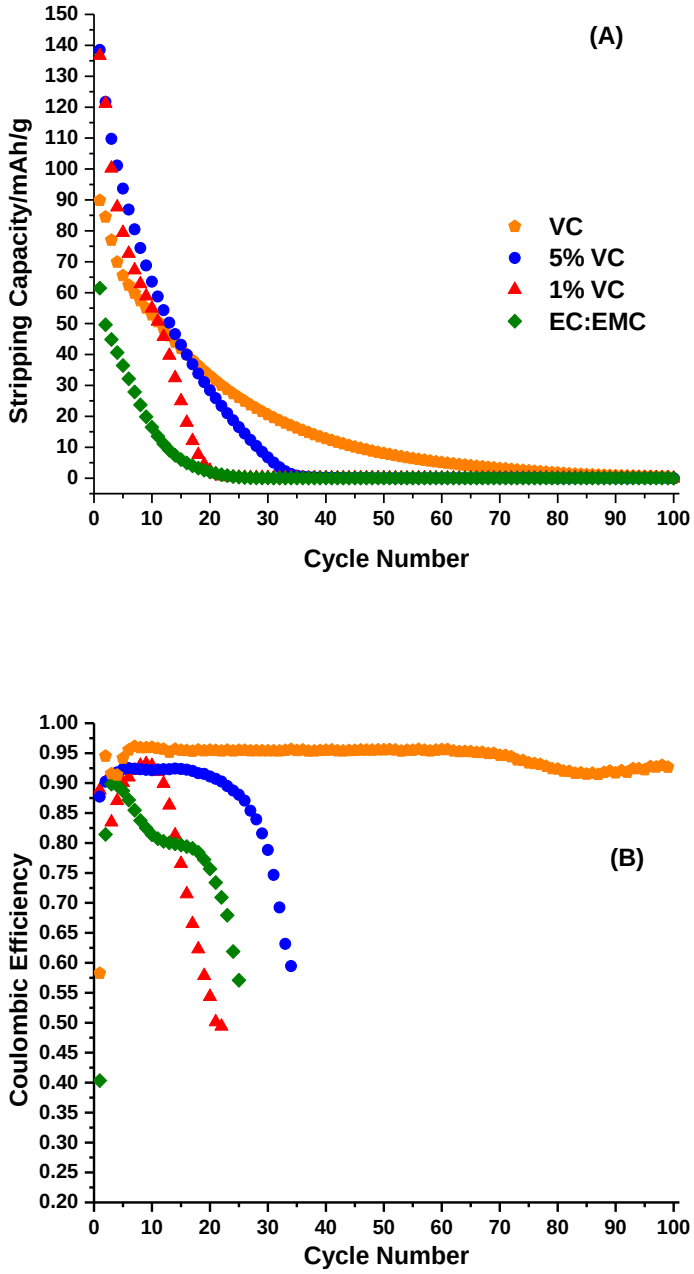

Figure 2-1. Stripping specific capacity vs. cycle number for the EC:EMC, 1% VC, 5% VC, and VC-S electrolytes (A) and corresponding Coulombic efficiency vs. cycle number (B).

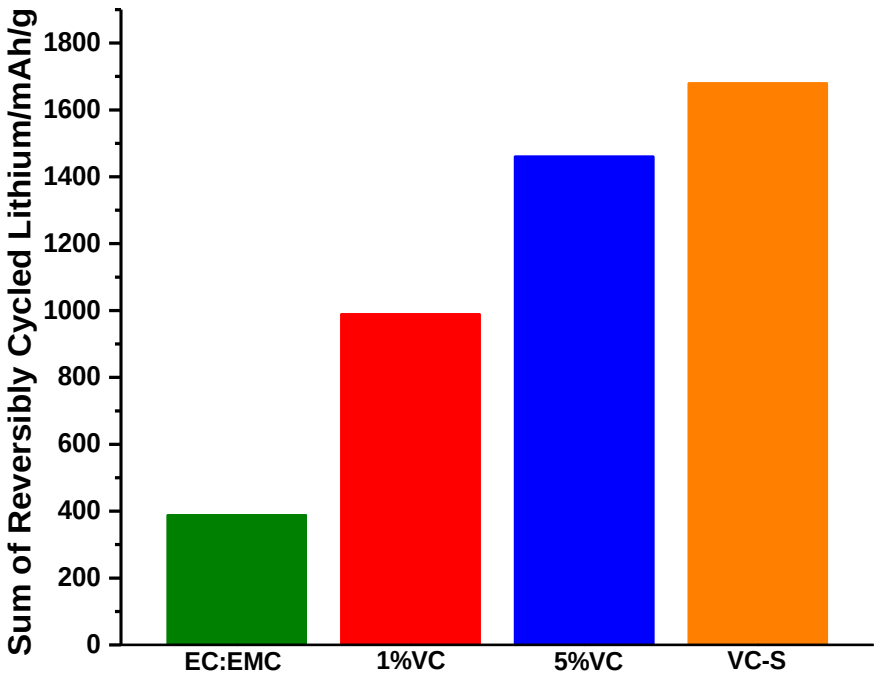

Figure 2-2. Total sum of reversibly cycled lithium after 100 cycles for the EC:EMC, 1% VC, 5% VC, and VC-S electrolytes.

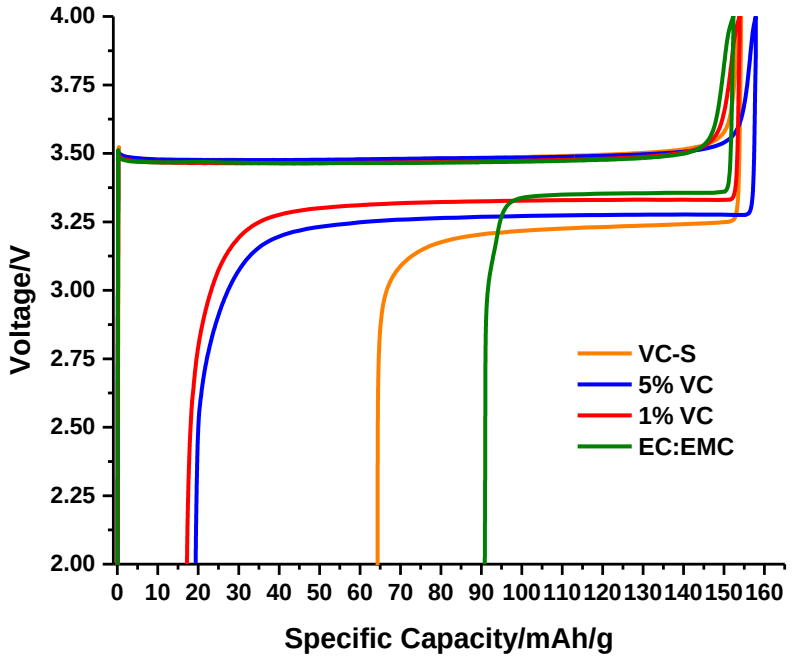

Figure 2-3. Voltage vs. specific capacity plots for the first plating and stripping of lithium with EC:EMC, 1% VC, 5% VC, and VC-S electrolytes.

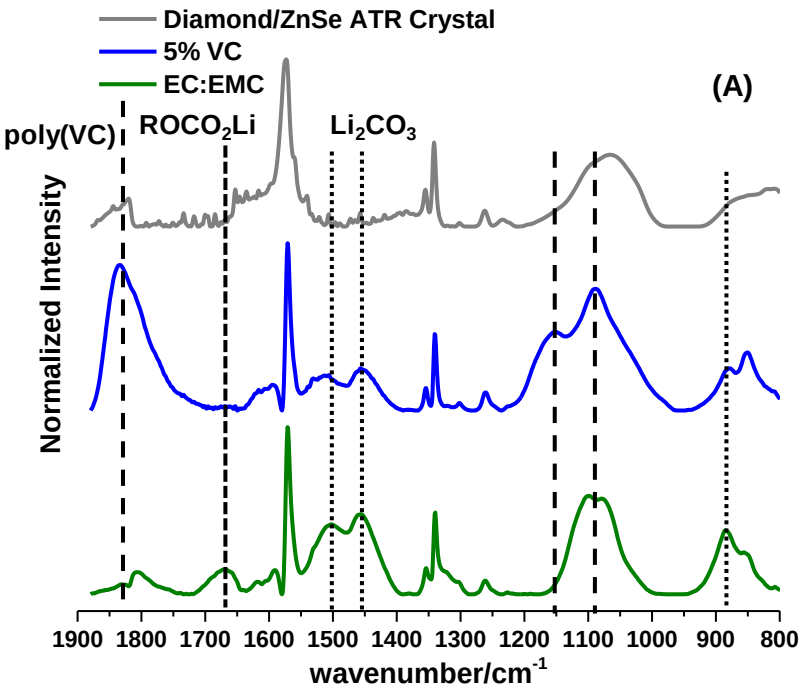

Figure 2-4. Normalized ATR-FTIR spectra of lithium plated with EC:EMC and 5% VC electrolytes for regions 1900 – 800 cm^{-1}. A spectrum of the diamond/ZnSe ATR crystal is shown to emphasize overlapping regions.

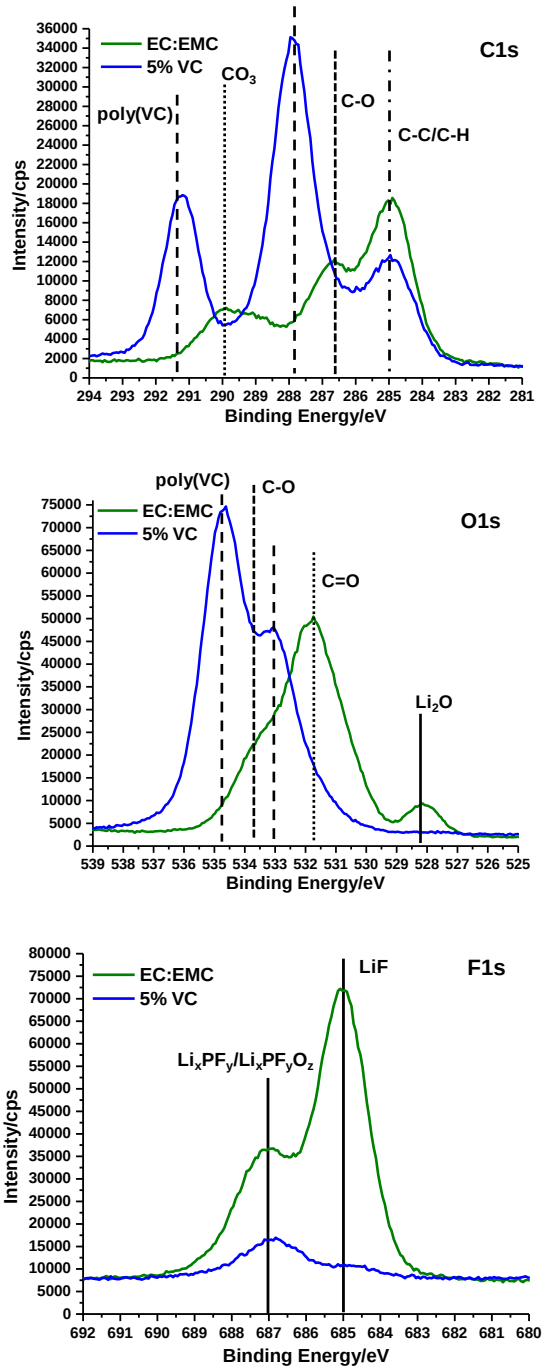

Figure 2-5. C1s, O1s, F1s XPS spectra plotted for lithium plated with EC:EMC and 5% VC electrolytes.

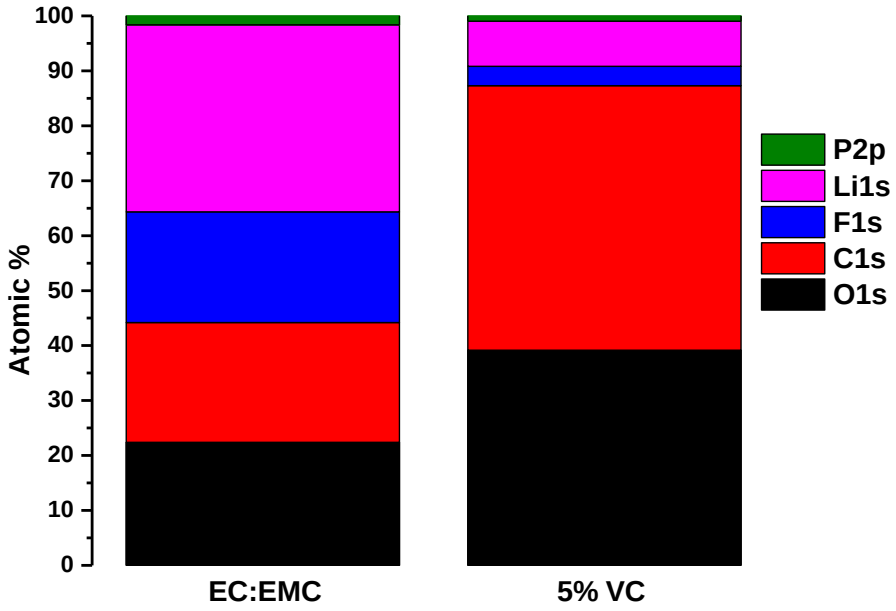

Figure 2-6. Corresponding relative atomic concentrations from XPS spectra for lithium plated with EC:EMC and 5% VC electrolytes.

CHAPTER 3

Effect of Fluoroethylene Carbonate Electrolytes on the Nanostructure of the Solid Electrolyte Interphase and Performance of Lithium Metal Anodes

Zachary L. Brown[1], Sunhyung Jurng[1], Cao Cuong Nguyen[1] and Brett L. Lucht[1]

[1]*Department of Chemistry, University of Rhode Island, Kingston, Rhode Island 02881, USA*

**Corresponding author: blucht@chm.uri.edu*

The following was published in the ACS Applied Energy Materials, and is presented here in manuscript format

ABSTRACT

The mechanism for the performance enhancement of lithium metal electrodes by fluoroethylene carbonate (FEC) is revealed. Electrolytes containing FEC, 1.2 M $LiPF_6$ in ethylene carbonate (EC):ethyl methyl carbonate (EMC) (3:7, vol) with 10% FEC (mass %) and 1.2 M $LiPF_6$ in FEC, improve the electrochemical performance of both Li||Li and Cu||$LiFePO_4$ cells compared to the baseline electrolyte, 1.2 M $LiPF_6$ in EC:EMC (3:7, vol). Ex situ surface analysis of lithium metal electrodes after the initial plating demonstrates that the solid electrolyte interphase (SEI) generated from FEC containing electrolytes is similar to the SEI generated from the baseline electrolyte, yet the corresponding Coulombic efficiencies are markedly different. Electron microscopy investigations reveal the presence of a unique SEI containing nanostructured LiF particles for the lithium electrode plated from the 1.2 M $LiPF_6$ in FEC electrolyte. The presence of the nanostructured LiF particles correlate with the improved cycling performance, suggesting that the morphology of the SEI is as important as the composition of the SEI.

INTRODUCTION

Fluoroethylene carbonate (FEC) has been investigated as an electrolyte additive for lithium-ion batteries which improves the performance of commercial negative electrode materials, such as graphite and silicon.[1–9] Incorporation of FEC has also been reported to significantly improve the cycling performance of lithium metal electrodes,[10,11] which are proposed to be the next generation anodes for lithium batteries.[12] However, the mechanism of performance improvement for lithium metal anodes cycled with electrolytes containing FEC is not well understood.

Previous investigations provide insight into the composition of the solid electrolyte interphase (SEI)[13] generated from FEC containing electrolytes on silicon electrodes.[4,14] The improved electrochemical performance for FEC containing electrolytes has been attributed to the generation of a stable SEI composed of polymeric species.[4,14] The elastomeric properties of the polymeric SEI have been reported to be stable to the volumetric expansion and contraction of silicon electrodes, minimizing SEI fracture leading to further electrolyte decomposition.[4] The composition of the SEI generated from FEC containing electrolytes on lithium metal anodes is likely related to that observed on silicon. FEC containing electrolytes have been reported to improve the performance of lithium metal electrodes via the generation of polymeric species similar to that reported for silicon anodes.[11] It has also been reported that FEC generates LiF deposits which may contribute to the improved cycling performance of lithium metal anodes.[15–17] In other studies, uniform plating and stripping of lithium metal electrodes have been reported to be improved by the

presence of preformed microstructured LiF deposits.[18,19] However, LiF is observed in nearly every SEI generated on the surface of anode materials, including lithium.[11] Therefore, a strong understanding of the source of the improved performance for lithium metal anodes in the presence of LiF and polymeric species is lacking.

The mechanism of performance enhancement for lithium metal electrodes cycled with FEC containing electrolytes has been investigated via a combination of electrochemical analysis of Li||Li and Cu||$LiFePO_4$ cells and ex situ surface analysis of the cycled electrodes. The in situ formation of lithium metal and low reactivity of $LiFePO_4$ in Cu||$LiFePO_4$ cells ensure that the FEC does not react with the electrode surfaces prior to the initial lithium plating cycle, as previously reported.[20,21] The cells were analyzed by electrochemical cycling and electrochemical impedance spectroscopy (EIS) followed by ex situ diffuse reflectance infrared Fourier transform spectroscopy (DRIFTS), X-ray photoelectron spectroscopy (XPS), and transmission electron microscopy (TEM). The analysis reveals that both the composition and the nanostructure of the SEI are important for improving the cycling efficiency of lithium metal electrodes.

EXPERIMENTAL

Electrochemical characterization was performed using 2032 coin cells with Li||Li or Cu||$LiFePO_4$ cells. The Li||Li cells were assembled with either Li foil (16 mm diameter) and a Celgard 3501 separator. The Cu||$LiFePO_4$ cells were assembled with a Cu metal foil negative electrode (15 mm diameter, MTI Corporation), Celgard 3501 separator (19 mm diameter), and a $LiFePO_4$ positive electrode (91% active material,

13.7 mm diameter, MTI corporation), the other 9% of the composite electrode is composed of conductive carbon and PVDF coated on aluminum. The cells were prepared with 75 μL of electrolyte. Electrolytes investigated include 1.2 M $LiPF_6$ in EC:EMC (3:7, vol, EC:EMC electrolyte), EC:EMC electrolyte with 10% FEC (10% FEC electrolyte), and 1.2 M $LiPF_6$ in FEC solvent (FEC electrolyte). The copper metal foil was sonicated with 1 M HCl (2 x 2 minutes) followed by sonication with isopropanol (1 x 2 minutes), punched to the specified diameter, and dried at 110°C, overnight under vacuum (approx. $3x10^{-3}$ atm) prior to cell assembly. The $LiFePO_4$ electrodes were punched to the specified diameter, and dried at 110°C overnight under vacuum (approx. $3x10^{-3}$ atm) prior to cell assembly. The cycling procedure consisted of plating Li metal at 0.1 mA/cm^2 (approx. C/20 rate, where C represents the theoretical capacity of $LiFePO_4$) with subsequent stripping and plating at 0.5 mA/cm^2 (approx. C/4 rate), within a voltage window of 2.0 – 4.0 V, using an Arbin BT2000 battery cycler at 25°C. There was a rest period of one hour between cell construction and the beginning of the electrochemical protocol. After the first plating of lithium metal (100% state-of-charge, SOC), electrochemical impedance spectroscopy (EIS) was recorded using a potentiostat with an amplitude of 10 mV and frequency range of 500 kHz–10 mHz, in 10 hour periods for 50 hours, at a cell voltage of 3.45 V.

IR spectra were acquired with a Bruker Tensor 27 spectrometer equipped with an UpIR Diffuse Reflectance accessory (Pike Technologies) and LaDTG detector. Lithium metal was deposited onto Cu foil according to the first charge procedure outlined in the electrochemistry section (charge to 4.0 V at C/20 rate) and held at rest for approximately 48 hours to ensure cell equilibration before disassembly. Lithium

metal was also deposited at a C/20 rate, followed by 10 plating/stripping cycles at a C/4 rate, and held at rest for approximately 48 hours before disassembly. Electrodes were washed with 4x500 μL battery grade EMC and dried under vacuum (approx. 3x10-3 atm) for 10 minutes, then overnight in the argon glovebox. The electrodes were transferred from an argon glove box to another argon-filled glove box in a sealed Nalgene vial and measured with DRIFTS. The spectra were acquired in the argon glove box with a resolution of 4 cm^{-1} and 256 scans. Spectra were normalized according to the most intense peak.

XPS measurements were acquired with a K-alpha Thermo system using Al Kα radiation (hν = 1486.6 eV) under ultra-high vacuum (<$1x10^{-12}$ atm) and a measured spot size of 400 μm in diameter. Lithium metal was deposited onto Cu foil according to the first charge procedure outline in the electrochemistry section (charge to 4.0 V at C/20 rate), and held at rest for approx. 48 hours to ensure cell equilibration before disassembly. Lithium metal was also deposited at C/20 rate, followed by 10 plating/stripping cycles at C/4 rate, and held at rest for approximately 48 hours before disassembly. Electrodes were washed with 4x500 μL battery grade EMC and dried under vacuum (approx. $3x10^{-3}$ atm) for 10 minutes, then overnight in the argon glovebox. The samples were transferred from the argon glove box in an air-free transfer case. The binding energy was corrected based on the F1s spectrum, assigning LiF to 685 eV. Relative atomic concentrations were calculated by integrating respective peaks with a Shirley background, using Thermo Avantage v5.932 software, accounting for respective atomic sensitivity factors. Spectra were normalized

according to the most intense peak. Minor amounts of contaminating CFx species are present in XPS spectra.

TEM measurements were acquired with a JEM-2100 Transmission Electron Microscope equipped with a LaB_6 electron emission source, operating at 200 kV. PELCO Cu TEM grids, 500 mesh, were placed on a Cu foil electrode during coin cell assembly. Approximately 15 mol% of Li from the $LiFePO_4$ electrodes were deposited and held for approx. 48 hours to ensure cell equilibration before disassembly. TEM grids were removed and washed with 4x500 μL battery grade EMC and dried under vacuum (approx. $3x10^{-3}$ atm) for 10 minutes, then overnight in the argon glovebox. After drying, the TEM grid was placed in a Cryo-Transfer Holder, shutter closed, assembly placed in a sealable Aldrich AtmosBab, allowing for transfer into the TEM without air exposure. Energy dispersive X-ray analysis (EDX) was used to analyze the elemental composition of the surface films on the plated lithium.

RESULTS AND DISCUSSION

The stripping capacity vs. cycle number, Coulombic efficiency vs. cycle number, and sum of reversibly cycled lithium for Cu||$LiFePO_4$ cells after 100 cycles are provided in Figure 3-1. The 10% FEC electrolyte has an initial Coulombic efficiency above 90%, compared to ~31% for cells cycled with the EC:EMC electrolyte. The stripping capacity of the cells containing the 10% FEC electrolyte is also improved. Upon increasing the FEC content, the Coulombic efficiency is improved to 98% while retention of the stripping capacity is further improved. The improvement in electrochemical performance is further illustrated wherein the sum of

the stripping capacities (reversibly cycled lithium), over 100 cycles,[21] increases with increasing FEC content in the electrolyte (Figure 3-1C). As previously reported,[21] similar increases in the content of vinylene carbonate (VC) also improve the quantity of reversibly cycled lithium. Employing FEC as a solvent provides a large improvement in the sum of reversibly cycled lithium compared to the 10% FEC electrolyte. The corresponding voltage vs. capacity plots and voltage hysteresis upon cycling are also provided in Figure 3-2. The difference between average plating and average stripping voltages is reduced with FEC present in the electrolyte (Figure 3-2A). The beneficial reduction in voltage hysteresis is sustained upon additional cycling for cells containing FEC (Figure 3-2B). It should be noted that employing FEC as a solvent increases the electrolyte viscosity and likely increases the potential for gas generation.[22]

While the performance of the $LiFePO_4$ cathode has been reported to be better with added FEC,[23] the minor improvement of the $LiFePO_4$ cathode does not account for the large observed enhancement in capacity retention and efficiency. Further, Li||Li cells (Figure 3-3) containing 10% FEC and FEC electrolytes continue to cycle significantly longer than cells with EC:EMC electrolytes. The observation is consistent with other electrochemical investigations of lithium metal electrodes with electrolytes containing FEC.[10,11,17] Further, visual images of stripped electrodes (Figure 3-4) demonstrate that FEC electrolytes clearly strip more lithium.

Electrochemical impedance spectra have been acquired for cells after the first plating of lithium metal at 100% SOC[24] and are provided in Figure 3-5. The initial impedance of each cell was measured, followed by periodic 10-hour measurements at

constant voltage. Overall, the impedance of the cell is reduced with increasing FEC content in the electrolyte, suggesting the generation of a low resistance SEI for FEC containing electrolytes. Further, the impedance appears to grow over time for the EC:EMC electrolyte, whereas the FEC containing electrolytes have a relatively minimal impedance change over time. This observation suggests the SEI generated from the FEC-containing electrolytes is more stable than the SEI generated from the EC:EMC electrolyte, consistent with the improved electrochemical performance. Therefore, the large enhancement observed in electrochemical performance for the plating/stripping of lithium in Cu||$LiFePO_4$ cells results from the addition of FEC.

The DRIFTS spectra of the lithium electrode after the first plating cycle and the lithium electrode plated after 10 plating and stripping cycles from the EC:EMC, 10% FEC, and FEC electrolytes are provided in Figure 3-6. The peaks at 1573 and 1342 cm^{-1} are artifact peaks of the DRIFTS accessory. The DRIFTS spectrum of the lithium electrode after the first plating cycle contains major peaks assigned to lithium carbonate (Li_2CO_3; 1510, 1450, and 878 cm^{-1}) and lithium alkyl carbonates ($ROCO_2Li$; 1660 and 1319 cm^{-1}).[5,25,26] The peaks associated with $ROCO_2Li$ and Li_2CO_3 have comparable intensity, suggesting comparable concentrations of these two SEI components.[21] Upon increasing the concentration of FEC in the electrolyte, a change in the ratio of the intensities of the peaks is observed. The $ROCO_2Li$ has a weaker relative intensity than the peaks associated with Li_2CO_3. The cells containing FEC have dramatically improved initial Coulombic efficiency and higher relative concentrations of Li_2CO_3, suggesting that Li_2CO_3 may be an important SEI component for lithium metal anodes. After 10 cycles, the DRIFTS spectra of the lithium electrode

plated from the EC:EMC electrolyte is similar to the DRIFTS spectrum after the first plating cycle. Given the poor electrochemical performance, it is likely that the EC:EMC electrolyte continuously decomposes to generate a thicker SEI with the same composition. Conversely, significant changes are observed for lithium plated with the FEC containing electrolytes. Specifically, peaks assigned to $ROCO_2Li$, polycarbonates (ROCOOR; 1806 and 1756 cm−1),[5,11] and possibly lithium carboxylates (RCOOLi; 1625 cm^{-1})[27] are observed, consistent with a change in the composition of the SEI upon additional cycling. Interestingly, the presence of polycarbonate correlates with the improved cycling efficiency for lithium metal anodes similar to that previously reported for silicon electrodes.[4,14]

The C1s, O1s, and F1s XPS spectra of the lithium electrode plated from the EC:EMC, 10% FEC, or FEC electrolytes after the first plating cycle and after 10 plating and stripping cycles are provided in Figure 3-7. After the first plating cycle, the C1s, O1s, and F1s spectra are very similar for the lithium metal electrode plated from the EC:EMC and 10% FEC electrolytes. The C1s spectra contain peaks associated with CO_3 at 290.0 eV, C-O at 286.9 eV and C-C/C-H at 284.9 eV consistent with the generation of a combination of $ROCO_2Li$ and Li_2CO_3, as observed by IR spectroscopy.[21] The O1s spectrum contains a broad beak centered at ~532.5 eV, consistent with a mixture of C-O and C=O containing species. The F1s spectrum contains a strong peak at 685 eV characteristic of LiF and a small peak at 687 eV characteristic of $Li_xPF_yO_z$. Small differences are observed for the lithium electrode plated from the FEC electrolyte. The relative intensity of the CO_3 peak in the C1s (~290 eV)[28,29] and O1s (~532 eV)[21] is reduced compared to the XPS spectra of the

lithium electrode plated with the other electrolytes, consistent with the decrease in the intensity of the lithium alkyl carbonates observed by IR spectroscopy. However, the F1s spectra are very similar containing peaks at 685 and 687 consistent with LiF and $Li_xPF_yO_z$, respectively.[21]

The elemental concentrations of the surface films on the lithium metal electrodes are also very similar after the first plating cycle, as depicted in Figure 3-8. After 10 cycles, the XPS spectra for lithium metal electrodes plated from EC:EMC, 10% FEC, and FEC electrolytes have similar element spectra to the spectra after the first plating (Figure 3-7). However, as the concentration of FEC in the electrolyte is increased the concentration of F, which is predominantly LiF, decreases and the concentrations of C and O increase (Figure 3-8). The relative increase in C1s and O1s and decrease in F1s intensity suggests a change in the composition of the SEI upon additional cycling for FEC containing electrolytes, which is in agreement with the IR data, and is consistent with the generation of a poly(carbonate) containing SEI on lithium metal, similar to that previously reported for VC containing electrolytes[21]

Representative TEM images of lithium plated from the EC:EMC, 10% FEC, and FEC electrolytes are provided in Figure 3-9. There is no consistent morphology observed for lithium plated from the EC:EMC electrolyte, and the lithium is plated nonuniformly (Figure 3-9A,B). Small lithium particles nucleate on the copper TEM grid for lithium plated from the 10% FEC electrolyte, and the lithium is plated uniformly (Figure 3-9C,D). Lithium is plated more uniformly from the FEC electrolyte, and a consistent morphology is observed containing nanostructured particles on both the copper grid and the larger areas of plated lithium (Figure 3-9E,F).

Higher magnification reveals the presence of a uniform nanostructured LiF surface film on the lithium metal electrode plated from the FEC electrolyte (Figure 3-9G,H). The presence of the nanostructured LiF particles is likely important for the high efficiency for plating and stripping of the lithium metal electrode. The IR, XPS, and TEM data suggest that the initial SEI generated on the lithium metal anode during the first plating cycle is primarily composed of nanostructured LiF with a smooth coating of Li_2CO_3. Similar nanostructured LiF containing surface films have been recently reported for lithium metal anodes.[30,31] Upon further cycling, polymeric species generated via FEC reduction are observed which likely further contribute to the good long-term cycling performance of the lithium metal electrodes in the presence of the FEC electrolyte.

EDX analysis was performed on the surface films on the plated lithium for each electrolyte, as depicted in Figure 3-10. From examination of the O Kα (0.525 keV) and F Kα (0.677 keV) peaks,[32] the surface film on the lithium plated from the EC:EMC electrolyte is oxygen rich. In contrast, the small particles on the surface of the lithium plated from FEC containing electrolytes are fluorine rich. The fluorine rich particles are predominantly LiF as determined by XPS.

The dramatic improvement of the electrochemical cycling performance of lithium metal anodes in the presence of electrolytes containing FEC is proposed to result from the generation of nanostructured LiF particles via a Li_2CO_3 capping mechanism, as previously reported.[30] As lithium is plated from the FEC electrolyte, both LiF and Li_2CO_3 are formed during the reductive decomposition of FEC.[22] As LiF particle formation is initiated, a high local concentration Li_2CO_3 is also present

resulting in LiF particle capping by a layer of Li_2CO_3, thereby controlling the size of LiF nanoparticles.[33–35] Upon precipitation, the size of the LiF nanoparticles in the surface film on the lithium metal electrode is smaller than the critical dimension required for ultramicroelectrode behavior affording a uniform lithium-ion diffusion field for the lithium electrode.[36–38] This uniform diffusion field allows for plating and stripping of lithium with high efficiency and minimal dendrite growth, similar to that reported for lithium difluoro(oxalate) borate electrolytes.[30] The systematic development of electrolyte formulations which favorably control the nucleation and growth of LiF nanoparticles leads to improved cycling performance and dendrite inhibition for lithium metal electrodes.

CONCLUSION

The effect of FEC containing electrolytes on the plating and stripping efficiency of lithium metal electrodes has been investigated. Increasing the content of FEC in the electrolyte improves the electrochemical performance of both Li||Li and Cu||$LiFePO_4$ cells. Ex situ surface analysis via a combination of IR, XPS, and TEM with EDX suggests that FEC containing electrolytes generate an initial SEI on the lithium metal electrode which is primarily composed of nanostructured LiF particles coated with Li_2CO_3. The presence of the nanostructured LiF particles leads to a uniform diffusion field resulting in more uniform plating and stripping of lithium. Upon additional cycling, polymeric species are also observed on the outer surface of SEI on lithium metal for the FEC containing electrolytes, further contributing to good cycling performance. While there have been many investigations of the composition of the SEI on anodes in lithium batteries, the results of this investigation suggest that the morphology and nanostructure of the SEI components is critical for lithium metal anodes. The SEI morphology is also likely responsible for the requirement for slow formation cycling of commercial graphite anodes in lithium-ion batteries.[39,40] Developing a better understanding of the role of the nanostructure of the SEI components is required to develop the next generation of lithium batteries.

REFERENCES

(1) Mcmillan, R.; Slegr, H.; Shu, Z. X.; Wang, W. Fluoroethylene Carbonate Electrolyte and Its Use in Lithium Ion Batteries with Graphite Anodes. *J. Power Sources* **1999**, *81–82*, 20–26.

(2) Choi, N.; Yew, K. H.; Lee, K. Y.; Sung, M.; Kim, H.; Kim, S. Effect of Fluoroethylene Carbonate Additive on Interfacial Properties of Silicon Thin-Film Electrode. *J. Power Sources* **2006**, *161*, 1254–1259.

(3) Etacheri, V.; Haik, O.; Goffer, Y.; Roberts, G. A.; Stefan, I. C.; Fasching, R.; Aurbach, D. Effect of Fluoroethylene Carbonate (FEC) on the Performance and Surface Chemistry of Si-Nanowire Li-Ion Battery Anodes. *Langmuir* **2012**, *28* (1), 965–976.

(4) Shkrob, I. A.; Wishart, J. F.; Abraham, D. P. What Makes Fluoroethylene Carbonate Different? *J. Phys. Chem. C* **2015**, *119* (27), 14954–14964.

(5) Nguyen, C. C.; Lucht, B. L. Comparative Study of Fluoroethylene Carbonate and Vinylene Carbonate for Silicon Anodes in Lithium Ion Batteries. *J. Electrochem. Soc.* **2014**, *161* (12), A1933–A1938.

(6) Nie, M.; Demeaux, J.; Young, B. T.; Heskett, D. R.; Chen, Y.; Bose, A.; Woicik, J. C.; Lucht, B. L. Effect of Vinylene Carbonate and Fluoroethylene Carbonate on SEI Formation on Graphitic Anodes in Li-Ion Batteries. *J. Electrochem. Soc.* **2015**, *162* (13), A7008–A7014.

(7) Jung, R.; Metzger, M.; Haering, D.; Solchenbach, S.; Marino, C.; Tsiouvaras, N.; Stinner, C.; Gasteiger, H. A. Consumption of Fluoroethylene Carbonate

(FEC) on Si-C Composite Electrodes for Li-Ion Batteries. *J. Electrochem. Soc.* **2016**, *163* (8), A1705–A1716.

(8) Mcarthur, M. A.; Trussler, S.; Dahn, J. R. In Situ Investigations of SEI Layer Growth on Electrode Materials for Lithium-Ion Batteries Using Spectroscopic Ellipsometry. *J. Electrochem. S* **2012**, *159* (3), A198–A207.

(9) Xu, K. Electrolytes and Interphases in Li-Ion Batteries and Beyond. *Chem. Rev.* **2014**, *114* (23), 11503–11618.

(10) Ding, F.; Xu, W.; Chen, X.; Zhang, J.; Engelhard, M. H.; Zhang, Y.; Johnson, B. R.; Crum, J. V.; Blake, T. A.; Liu, X.; Zhang, J.-G. Effects of Carbonate Solvents and Lithium Salts on Morphology and Coulombic Efficiency of Lithium Electrode. *J. Electrochem. Soc.* **2013**, *160* (10), A1894–A1901.

(11) Markevich, E.; Salitra, G.; Chesneau, F.; Schmidt, M.; Aurbach, D. Very Stable Lithium Metal Stripping − Plating at a High Rate and High Areal Capacity in Fluoroethylene Carbonate-Based Organic Electrolyte Solution. *ACS Energy Lett.* **2017**, *2*, 1321–1326.

(12) Cheng, X.; Zhang, R.; Zhao, C.-Z.; Zhang, Q. Toward Safe Lithium Metal Anode in Rechargeable Batteries : A Review. *Chem. Rev.* **2017**, *117* (15), 10403–10473.

(13) Peled, E. The Electrochemical Behavior of Alkali and Alkaline Earth Metals in Nonaqueous Battery Systems—The Solid Electrolyte Interphase Model. *J. Electrochem. Soc.* **1979**, *126* (12), 2047–2051.

(14) Jin, Y.; Kneusels, N.-J. H.; Magusin, P. C. M. M.; Kim, G.; Castillo-Martinez, E.; Marbella, L. E.; Kerber, R. N.; Howe, D. J.; Paul, S.; Liu, T.; Grey, C. P.

Identifying the Structural Basis for the Increased Stability of the Solid Electrolyte Interphase Formed on Silicon with the Additive Fluoroethylene Carbonate. *J. Am. Chem. Soc.* **2017**, *139* (42), 14992–15004.

(15) Alvarado, J.; Schroeder, M. A.; Zhang, M.; Borodin, O.; Gobrogge, E.; Olguin, M.; Ding, M. S.; Gobet, M.; Greenbaum, S.; Meng, Y. S.; Xu, K. A Carbonate-Free, Sulfone-Based Electrolyte for High-Voltage Li-Ion Batteries. *Mater. Today* **2018**, *21* (4), 341–353.

(16) Fan, X.; Chen, L.; Ji, X.; Deng, T.; Hou, S.; Chen, J.; Zheng, J.; Wang, F.; Jiang, J.; Xu, K.; Wang, C. Highly Fluorinated Interphases Enable High-Voltage Li-Metal Batteries. *Chem* **2018**, *4*, 174–185.

(17) Zhang, X.-Q.; Cheng, X.-B.; Chen, X.; Yan, C.; Zhang, Q. Fluoroethylene Carbonate Additives to Render Uniform Li Deposits in Lithium Metal Batteries. *Adv. Funct. Mater.* **2017**, *27*, 1605989.

(18) Lu, Y.; Tu, Z.; Archer, L. A. Stable Lithium Electrodeposition in Liquid and Nanoporous Solid Electrolytes. *Nat. Mater.* **2014**, *13*, 961–969.

(19) Fan, L.; Zhuang, H.; Gao, L.; Lu, Y.; Archer, L. Regulating Li Deposition at Artificial Solid Electrolyte Interphases. *J. Mater. Chem. A* **2017**, *5*, 3483–3492.

(20) Qian, J.; Adams, B. D.; Zheng, J.; Xu, W.; Henderson, W. A.; Wang, J.; Bowden, M. E.; Xu, S.; Hu, J.; Zhang, J. G. Anode-Free Rechargeable Lithium Metal Batteries. *Adv. Funct. Mater.* **2016**, *26* (39), 7094–7102.

(21) Brown, Z. L.; Jurng, S.; Lucht, B. L. Investigation of the Lithium Solid Electrolyte Interphase in Vinylene Carbonate Electrolytes Using Cu||$LiFePO_4$ Cells. *J. Electrochem. Soc.* **2017**, *164* (9), A2186–A2189.

(22) Michan, A. L.; Parimalam, B. S.; Leskes, M.; Kerber, R. N.; Yoon, T.; Grey, C. P.; Lucht, B. L. Fluoroethylene Carbonate and Vinylene Carbonate Reduction: Understanding Lithium-Ion Battery Electrolyte Additives and Solid Electrolyte Interphase Formation. *Chem. Mater.* **2016**, *28* (22), 8149–8159.

(23) Wu, B.; Ren, Y.; Mu, D.; Liu, X.; Zhao, J.; Wu, F. Enhanced Electrochemical Performance of $LiFePO_4$ Cathode with the Addition of Fluoroethylene Carbonate in Electrolyte. *J. Solid State Electrochem.* **2013**, *17* (3), 811–816.

(24) Schmidt, J. P.; Chrobak, T.; Ender, M.; Illig, J.; Klotz, D.; Ivers-Tiffée, E. Studies on $LiFePO_4$ as Cathode Material Using Impedance Spectroscopy. *J. Power Sources* **2011**, *196*, 5342–5348.

(25) Seo, D. M.; Nguyen, C. C.; Young, B. T.; Heskett, D. R.; Woicik, J. C.; Lucht, B. L. Characterizing Solid Electrolyte Interphase on Sn Anode in Lithium Ion Battery. *J. Electrochem. Soc.* **2015**, *162* (13), A7091–A7095.

(26) Zhuang, G. V.; Yang, H.; Ross, P. N.; Xu, K.; Jow, T. R. Lithium Methyl Carbonate as a Reaction Product of Metallic Lithium and Dimethyl Carbonate. *Electrochem. Solid-State Lett.* **2006**, *9* (2), A64–A68.

(27) Nguyen, C. C.; Seo, D. M.; Chandrasiri, K. W. D. K.; Lucht, B. L. Improved Cycling Performance of a Si Nanoparticle Anode Utilizing Citric Acid as a Surface-Modifying Agent. *Langmuir* **2017**, *33* (37), 9254–9261.

(28) Zhuang, G. V.; Yang, H.; Ross, P. N.; Xu, K.; Jow, T. R. Lithium Methyl Carbonate as a Reaction Product of Metallic Lithium and Dimethyl Carbonate. *Electrochem. Solid-State Lett.* **2006**, *9*, A64–A68.

(29) Seo, D. M.; Nguyen, C. C.; Young, B. T.; Heskett, D. R.; Woicik, J. C.; Lucht,

B. L. Characterizing Solid Electrolyte Interphase on Sn Anode in Lithium Ion Battery. *J. Electrochem. Soc.* **2015**, *162*, A7091–A7095.

(30) Jurng, S.; Brown, Z. L.; Kim, J.; Lucht, B. L. Effect of Electrolyte on the Nanostructure of the Solid Electrolyte Interphase (SEI) and Performance of Lithium Metal Anodes. *Energy Environ. Sci.*, **2018,** Advance Article.

(31) Wang, X.; Zhang, M.; Akvarado, J.; Wang, S.; Sina, M.; Lu, B.; Bouwer, J.; Xu, W.; Xiao, J.; Zhang, J.; Liu, J.; Meng, Y. S. New Insights on the Structure of Electrochemically Deposited Lithium Metal and Its Solid Electrolyte Interphases via Cryogenic TEM. *Nano Lett.* **2017**, *17* (12), 7606–7612.

(32) Bruker. Periodic Table of Elements and X-ray Energies https://www.bruker.com/fileadmin/user_upload/8-PDF-Docs/X-rayDiffraction_ElementalAnalysis/HH-XRF/Misc/Periodic_Table_and_X-ray_Energies (accessed 12/19/2017).

(33) Xia, Y.; Xiong, Y.; Lim, B.; Skrabalak, S. E. Shape-Controlled Synthesis of Metal Nanocrystals : Simple Chemistry Meets Complex Physics? *Angew. Chem. Int. Ed. Engl.* **2009**, *48*, 60–103.

(34) Phan, C. M.; Nguyen, H. M. Role of Capping Agent in Wet Synthesis of Nanoparticles. *J. Phys. Chem. A* **2017**, *121* (17), 3213–3219.

(35) Campisi, S.; Schiavoni, M.; Chan-Thaw, C. E.; Villa, A. Untangling the Role of the Capping Agent in Nanocatalysis : Recent Advances and Perspectives. *Catalysts* **2016**, *6* (12), 185.

(36) Bard, A. J.; Faulkner, L. R. *Electrochemical Methods: Fundamentals and Applications*, 2nd ed.; John Wiley & Sons, 2000.

(37) Zoski, C. G. *Electroanalysis* **2002**, *14*, 1041–1051.

(38) Aoki, K. *Electroanalysis* **1993**, *5*, 627–639.

(39) Buqa, H.; Golob, P.; Winter, M.; Besenhard, J. O. Modified Carbons for Improved Anodes in Lithium Ion Cells. *J. Power Sources* **2001**, *97–98*, 122–125.

(40) Andersson, A. M.; Edström, K. Chemical Composition and Morphology of the Elevated Temperature SEI on Graphite. *J. Electrochem. Soc.* **2001**, *148* (10), A1100–A1109.

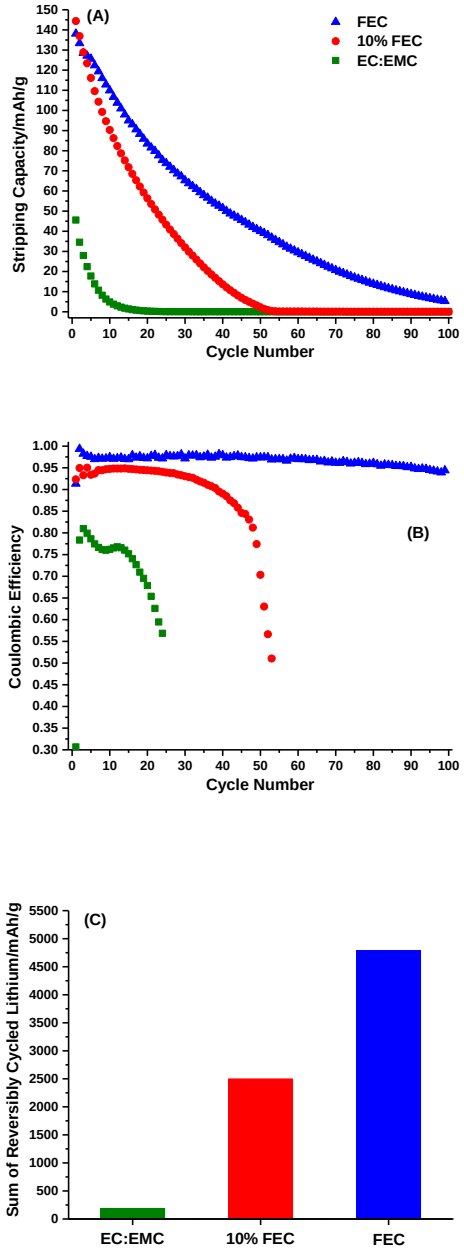

Figure 3-1. Stripping specific capacity vs. cycle number (A), Coulombic efficiency vs. cycle number (B) and corresponding total sum of reversibly cycled lithium after 100 cycles for the EC:EMC, 10% FEC, and FEC electrolytes (C).

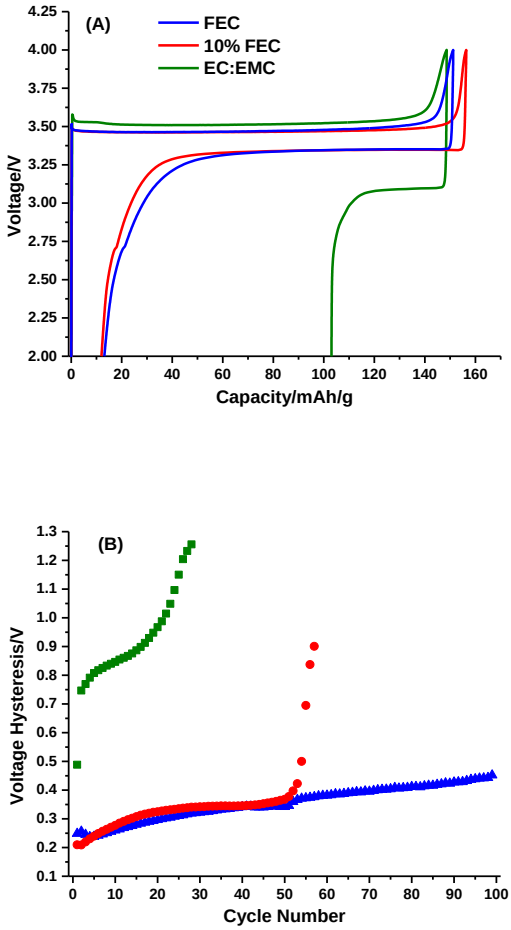

Figure 3-2. Corresponding voltage vs. specific capacity plots for the first plating and stripping of lithium with EC:EMC, 10% FEC, FEC electrolytes (A) and corresponding voltage hysteresis upon prolonged cycling (B).

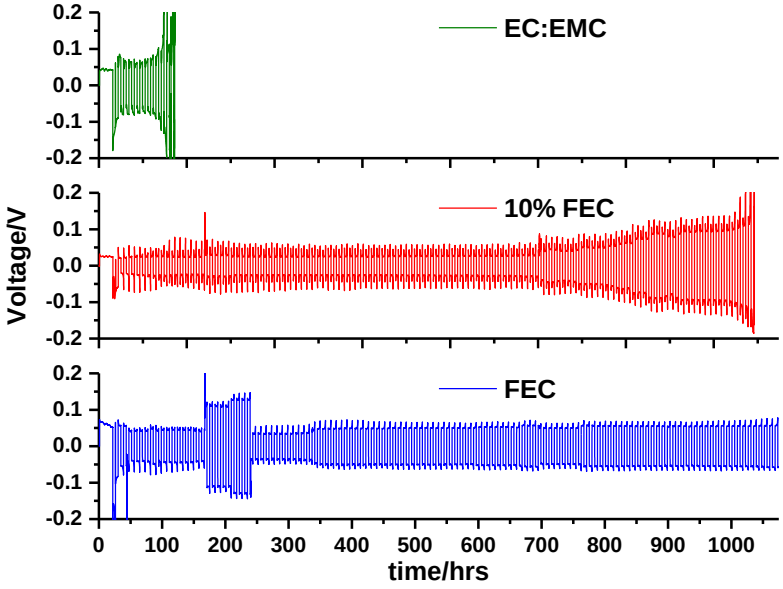

Figure 3-3. Li||Li cells cycled with EC:EMC, 10% FEC, and FEC electrolytes.

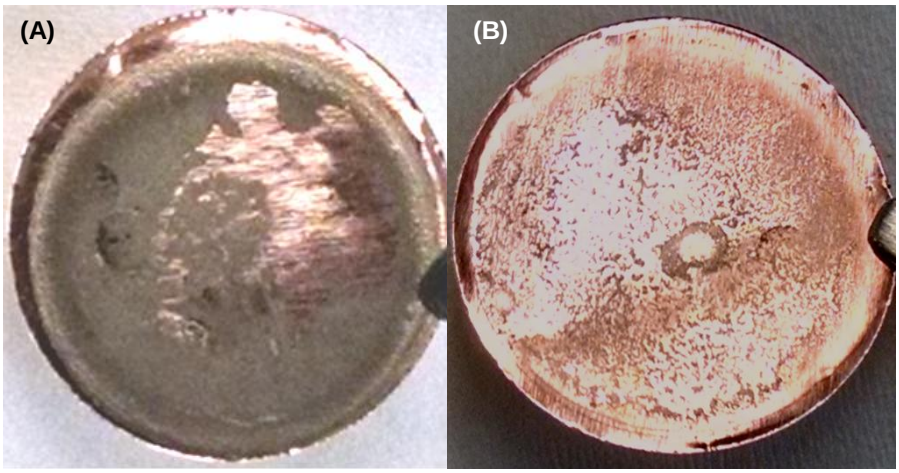

Figure 3-4. Images of the stripped lithium electrode for EC:EMC (A) and 10% FEC (B) electrolytes.

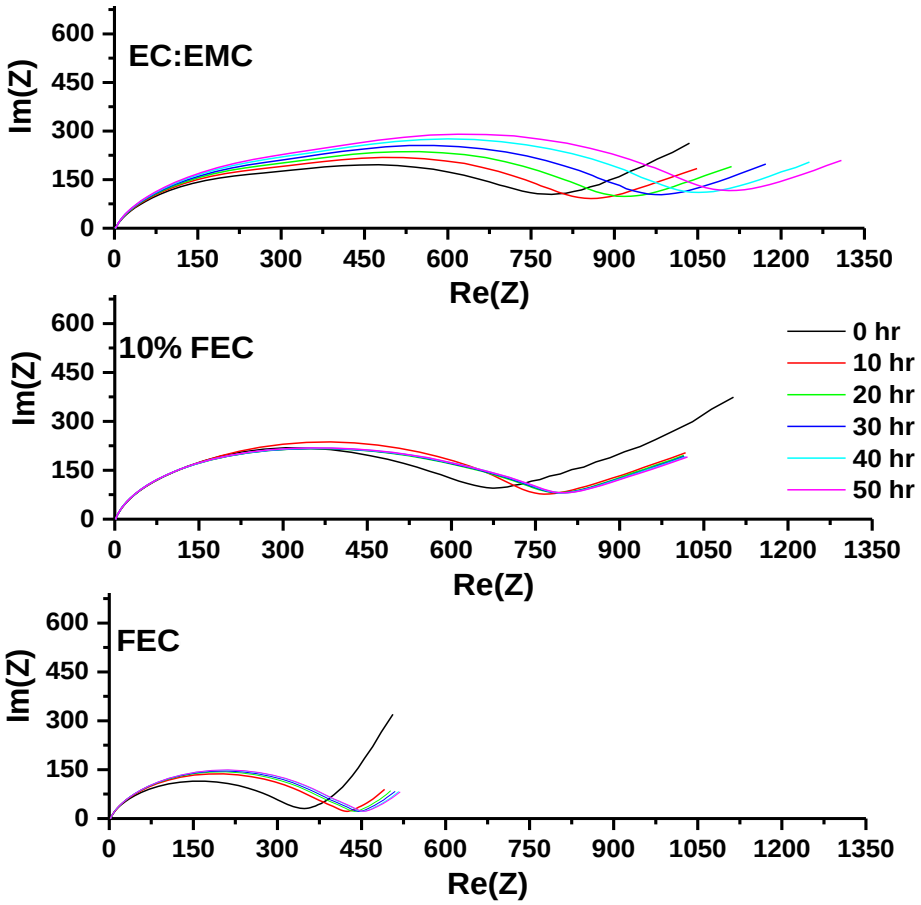

Figure 3-5. Electrochemical Impedance Spectroscopy measurements of EC:EMC (top), 10% FEC (middle), and FEC (bottom) electrolytes after the first plating of lithium metal.

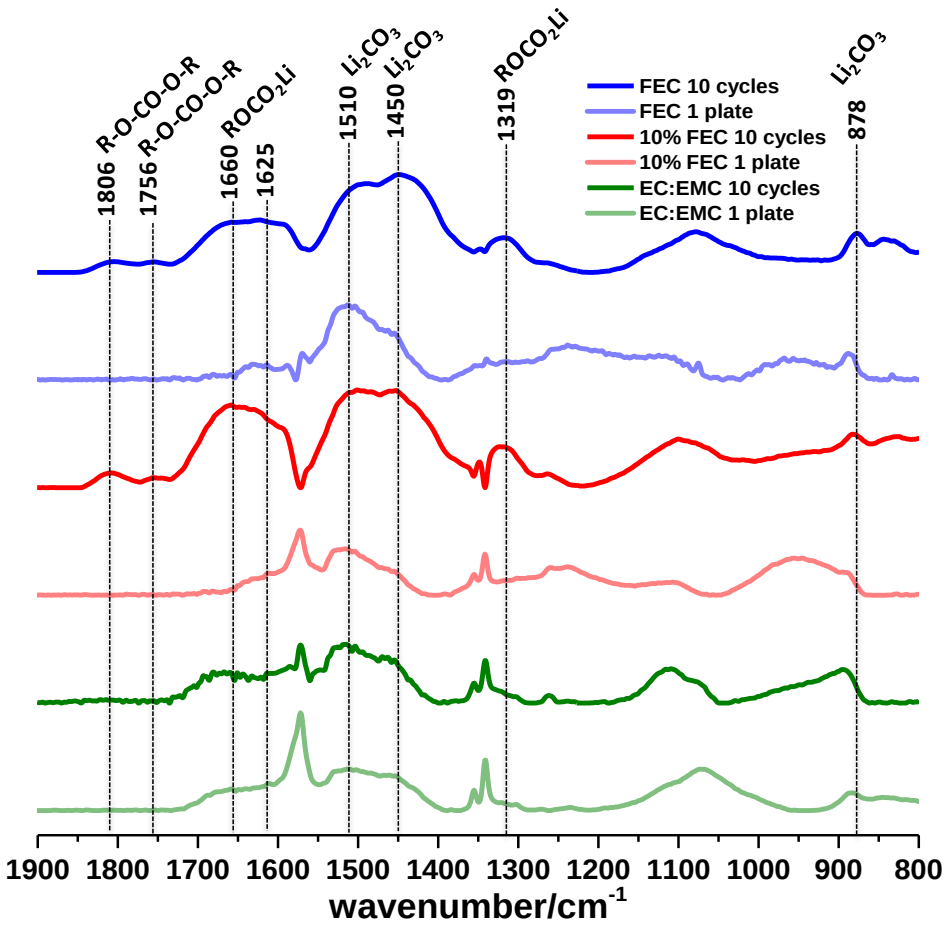

Figure 3-6. Normalized DRIFTS spectra of of lithium plated with EC:EMC, 10% FEC, and FEC electrolytes for the 1st plate and after 10 cycles within regions 1900 – 800 cm^{-1}.

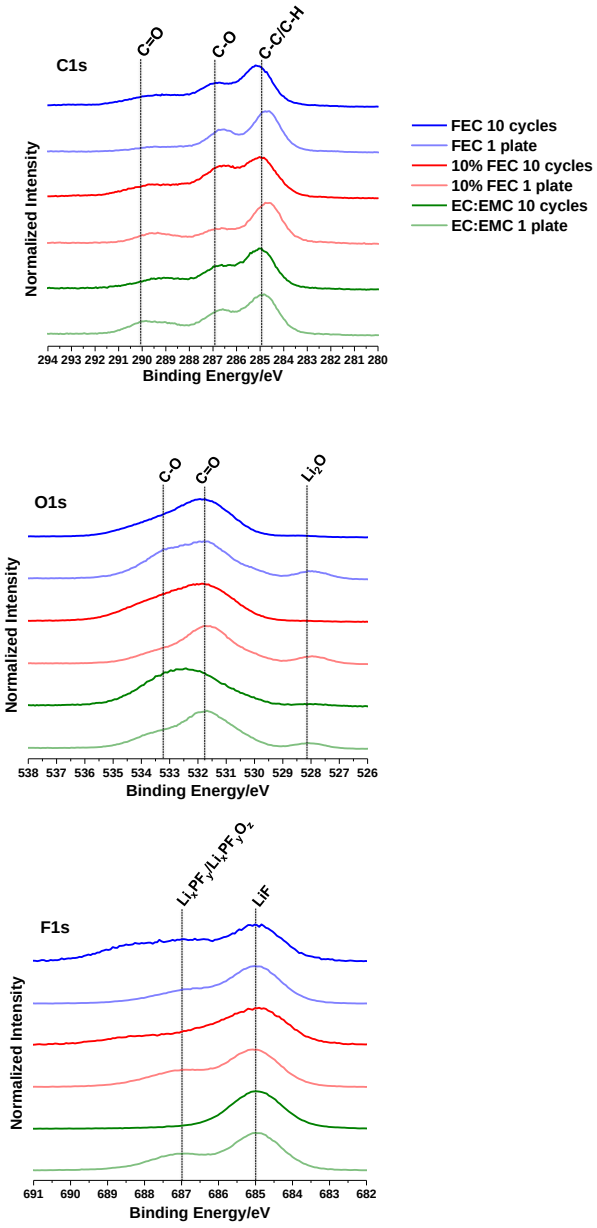

Figure 3-7. Normalized C1s, O1s, and F1s XPS spectra for lithium plated with EC:EMC, 10% FEC, and FEC electrolytes after the first plating of lithium metal and after 10 plating/stripping cycles.

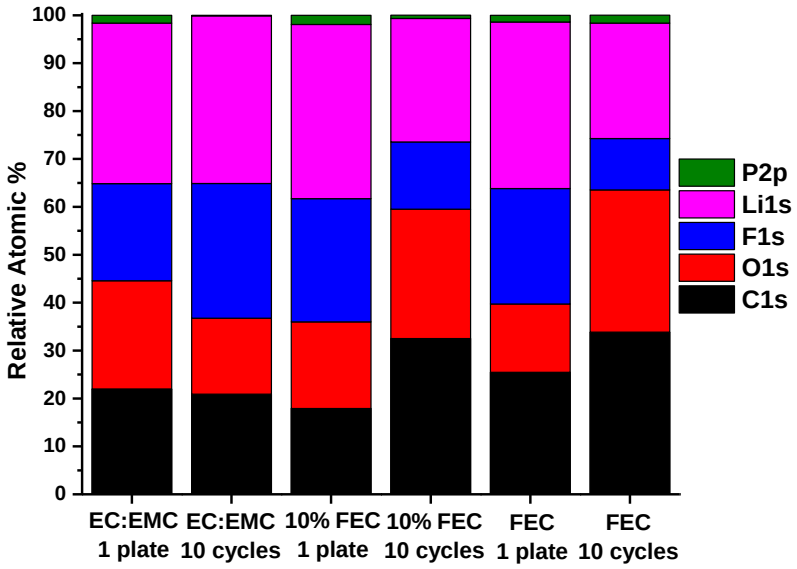

Figure 3-8. Corresponding relative atomic concentrations for lithium plated with EC:EMC, 10% FEC, and FEC electrolytes after the first plating of lithium metal and after 10 plating/stripping cycles.

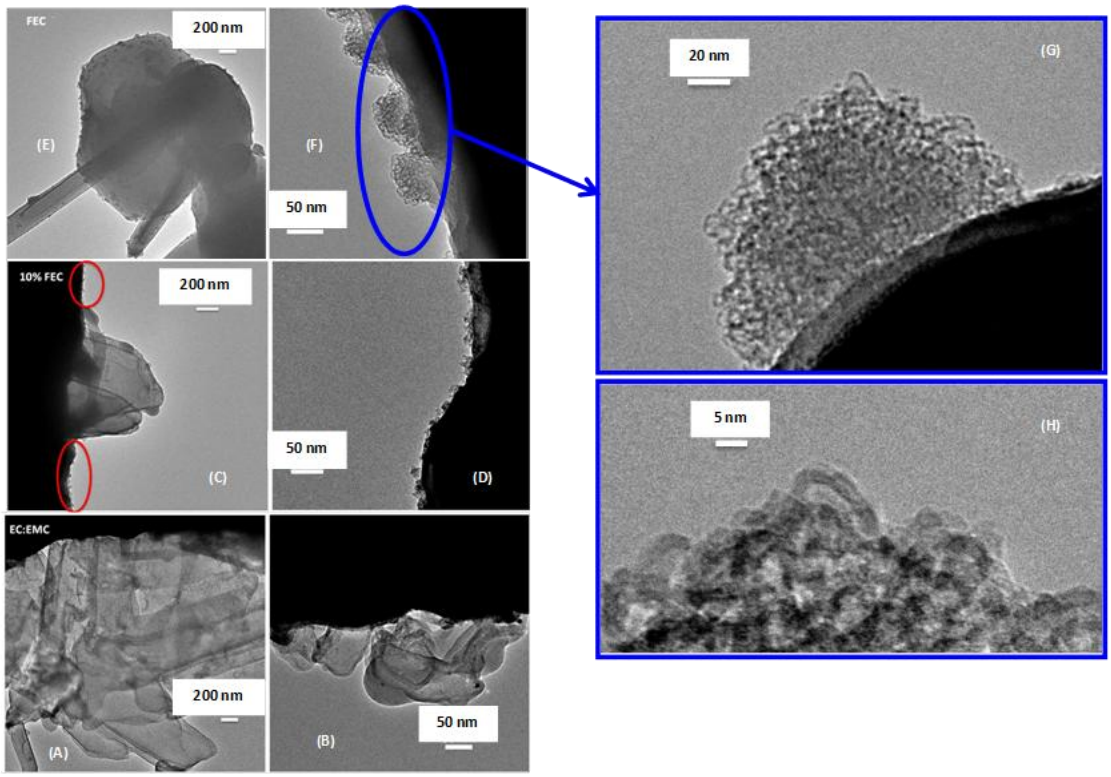

Figure 3-9. TEM images of lithium plated with the EC:EMC electrolyte (A, B), lithium plated with 10% FEC electrolyte (C, D), and lithium plated with the FEC electrolyte (E, F). Corresponding higher magnification TEM images of the unique lithium structure plated with FEC electrolyte are also shown (G, H).

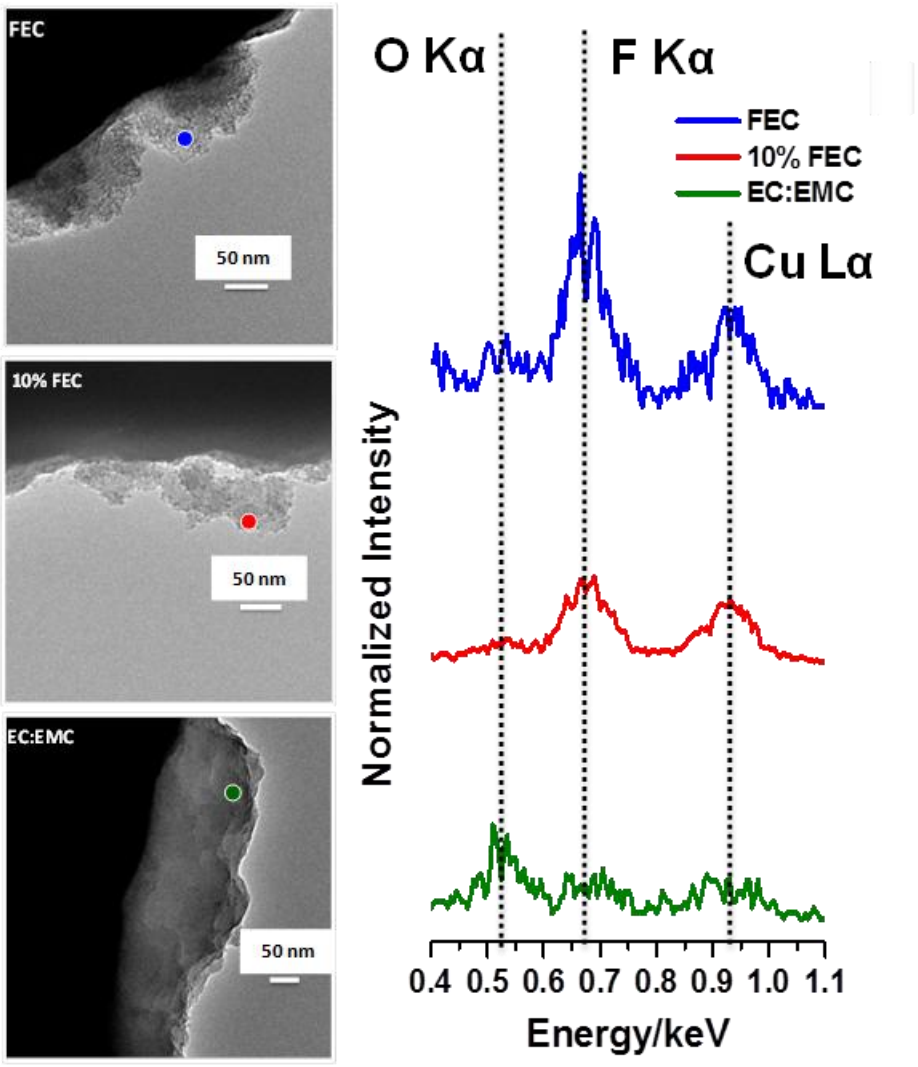

Figure 3-10. EDX analysis of lithium plated with EC:EMC, 10% FEC, and FEC electrolytes

CHAPTER 4

Effect of electrolyte on the nanostructure of the solid electrolyte interphase (SEI) and performance of lithium metal anodes

Sunhyung Jurng[1], Zachary L. Brown[1], Jiyeon Kim[1] and Brett L. Lucht[1]

[1]*Department of Chemistry, University of Rhode Island, Kingston, Rhode Island 02881, USA*

**Corresponding author: blucht@chm.uri.edu*

The following was published in RSC Energy & Environmental Science and is presented here in manuscript format

ABSTRACT

Developing electrolytes that enable commercially viable lithium metal anodes for rechargeable lithium batteries remains challenging, despite recent exhaustive efforts. Electrolytes of similar composition, yet different structure, have been investigated to understand key mechanisms for improving the cycling performance of lithium metal anodes. Specifically, the electrolytes investigated include $LiPF_6$, $LiBF_4$, lithium bis(oxalato)borate (LiBOB), and lithium difluoro(oxalato)borate (LiDFOB) dissolved in a mixture of ethylene carbonate (EC) and ethyl methyl carbonate (EMC). There is a remarkable difference in the cycling performance of 1.2 M LiDFOB in EC:EMC (3:7) compared to 0.6 M $LiBF_4$ + 0.6 M LiBOB in EC:EMC (3:7), despite the effectively equivalent chemical composition. The LiDFOB electrolyte has significantly better cycling performance. Furthermore, the chemical compositions of the SEI generated on the lithium metal electrode from the two electrolytes are very similar, especially after the 1st plating, suggesting that the chemical composition of the SEI may not be the primary source for the difference in cycling performance. Ex situ transmission electron microscopy (TEM) reveals that the difference in cycling performance can be traced to the presence of nanostructured LiF particles in the SEI from the LiDFOB electrolyte. It is proposed that the capping ability of the oxalate moiety from LiDFOB, in combination with simultaneous generation of LiF, leads to generation of uniform and evenly distributed nanostructured LiF particles. The presence of nanostructured LiF in the SEI results in uniform diffusion field gradients on the lithium electrode which leads to improved cycling performance. The proposed mechanism not only provides insight for improving lithium metal anodes for batteries,

but also expands upon the understanding of the role of LiF in the SEI on graphite electrodes in commercial lithium ion batteries. A superior understanding of the structure and function of the SEI will facilitate the development of next-generation energy storage systems.

INTRODUCTION

Lithium metal is a promising negative electrode material for future high-energy batteries for consumer electronics and electric vehicles. Lithium metal anodes have a very high theoretical specific capacity of 3860 mAh g^{-1}, extremely low negative potential (-3.04 V vs. standard hydrogen electrode) and low gravimetric density of 0.534 g cm^{-3}. Thus, application of lithium metal to secondary lithium batteries has been investigated intensively.[1,2] However several barriers exist in commercializing lithium metal anodes, including the formation of lithium dendrites, safety risks caused by dendritic lithium, and low Coulombic efficiency.

Since lithium metal reacts with most common electrolytes, a solid electrolyte interphase (SEI)[3] is generated from the decomposition of the electrolyte on the lithium metal anode during the plating process. The SEI stabilizes lithium metal and prevents further reaction with the electrolyte. While the SEI on lithiated graphite electrodes used in commercial lithium ion batteries has reasonable stability to afford long term cycling performance, a stable SEI on lithium metal anodes has not been observed. The instability of the SEI on lithium metal leads to poor efficiency and irreversible consumption of lithium. Thus, the generation of a thin and stable SEI for lithium metal anodes is critical. Variation of the electrolyte used with lithium metal anodes has been reported to result in significant changes to cycling efficiency and lithium dendrite growth. These variations in electrolyte include, but not are limited to, solid-state or polymer electrolytes,[4–6] concentrated electrolytes,[7] ionic liquids,[8] and electrolyte additives.[9–11] At this time, an effective electrolyte for lithium metal anodes still

remains elusive. However, establishing a better understanding of how electrolyte modification results in improved performance of lithium metal anodes is critical for the systematic design of the next generation of electrolytes.

Development of carbonate electrolytes for lithium metal anodes is desired, given their versatile properties,[12] such as a high dielectric constant, chemical stability, and wide electrochemical window.[10,13–15] Recent work has demonstrated that LiF is a key SEI component for enabling rechargeable lithium metal batteries in carbonate electrolytes.[13,16–19] However, LiF is a common component of nearly every SEI generated on the surface of the lithium metal anode, regardless of electrochemical performance.[20] Therefore, the mechanism of LiF generation from the electrolyte and the structure of the LiF particles must strongly influence the electrochemical performance of lithium metal. In addition, the importance of the morphology or nanostructure of SEI components, including LiF, has been proposed for decades,[21,22] however, direct evidence has not been reported. Herein, a unique mechanism for the generation of nanostructured LiF is proposed along with a mechanistic rationale for the improved electrochemical performance of an SEI on lithium metal containing nanostructured LiF. The results suggest the significance of the SEI nanostructure to electrochemical performance of battery electrodes, as previously proposed with limited experimental justification.[23–25] This finding furthers the understanding of the nature of lithium metal anode and provides insight regarding the rational design of the SEI for electrode materials in lithium-ion batteries. In particular, this insight can facilitate the development of commercial graphite or silicon anodes, where the nature of the SEI plays a crucial role in determining electrochemical performance.

The effect of lithium salt on the performance of lithium metal anodes has been investigated. Lithium tetrafluoroborate ($LiBF_4$), lithium bis(oxalato)borate (LiBOB) and lithium difluoro(oxalato)borate (LiDFOB) have been compared to lithium hexafluorophosphate ($LiPF_6$) in a common blend of carbonate solvents, ethylene carbonate (EC) and ethyl methyl carbonate (EMC) which is widely used commercially.[26] In order to minimize reactivity of cell components with the electrolyte, $LiFePO_4$/Cu cells[27] were used to investigate the SEI generated by each electrolyte on lithium metal anodes.[28] The 1.2 M LiDFOB in EC :EMC (3:7) electrolyte was observed to dramatically improve the plating and stripping performance of lithium metal anodes, while the effectively identical chemical composition, 0.6 M $LiBF_4$ + 0.6 M LiBOB in EC:EMC (3:7) had poor plating and stripping performance. It is proposed that the capping ability of the oxalate moiety from LiDFOB, in combination with simultaneous generation of LiF, leads to optimal growth of the nanostructured LiF particles. The presence of nanostructured LiF in the SEI results in uniform diffusion field gradients on the lithium anode which leads to improved cycling performance.

EXPERIMENTAL

2032-type coin cells containing $LiFePO_4$ and copper foil electrodes were used for electrochemical testing. $LiFePO_4$/Cu cells were assembled for each electrolyte (135 mL), consisting of a $LiFePO_4$ positive electrode (13.7 mm diameter, MTI Corporation), a PP/PE/PP separator (19 mm diameter, Celgard 2325) and a

copper foil negative electrode (19mm diameter, MTI Corporation). The $LiFePO_4$ cathodes are composed of 91% active material and 9% of PVDF binder and conductive carbon. The average active mass loading and areal capacity of $LiFePO_4$ cathodes is 10.5 mg cm^{-2} and 1.75 mAh cm^{-2}, respectively. The copper foil was cleaned with 1 M HCl solution followed by sonication with distilled water and hexane. Both $LiFePO_4$ and copper foil electrodes were punched to a specific diameter, and dried at 110°C under vacuum overnight before cell assembly. $LiFePO_4$/Cu cells were assembled in an argon glove box (M-Braun) with oxygen and water contents <1 ppm. The electrolytes investigated are: 1.2 M $LiPF_6$ in EC:EMC ($LiPF_6$ electrolyte), 1.2 M $LiBF_4$ in EC:EMC ($LiBF_4$ electrolyte), 1.2 M LiDFOB in EC:EMC (LiDFOB electrolyte), the mixture of 0.6 M $LiBF_4$ and 0.6 M LiBOB in EC:EMC ($LiBF_4$ + LiBOB electrolyte), and 0.6 M LiBOB in EC:EMC (LiBOB electrolyte). The mixture of ethylene carbonate and ethyl methyl carbonate (EC:EMC = 3:7, volume:volume) is the solvent for all electrolytes. All electrolyte components (salts and solvents) were supplied from a commercial supplier as battery grade with less than 50 ppm water, and used as received.

Galvanostatic cycling (lithium plating/stripping) of $LiFePO_4$/Cu cells was conducted using an Arbin BT2000 battery cycler at room temperature (25°C) in a constant temperature oven. The cycling procedure of $LiFePO_4$/Cu cells consists of plating lithium at a rate of 0.1 mA cm^{-2} with subsequent cycling at a rate of 0.5 mA cm^{-2}, within a voltage cut-off of 2.0–4.0 V vs. Li/Li+. A 3 h rest period was inserted at the beginning of each cycling protocol to ensure uniform wetting of all cell components. 2032-type coin cells containing two identical lithium electrodes and two

separators (PP/PE/PP and glass fiber) were assembled to perform electrochemical testing. Li/Li cells were cycled with current density of 0.5 mA/cm^2 and limited charge/discharge capacity of 2 mAh/cm^2.

Electrochemical impedance spectroscopy (EIS) was conducted on Li/Li symmetric cells at 25°C. Li/Li cells for EIS were prepared from two identical $LiFePO_4$/Cu cells cycled with the procedure mentioned above until the 10^{th} lithium plating. The cells were then disassembled in an argon glove box and Li/Li cells were assembled with a PP/PE/PP separator using the same electrolyte and allowed to equilibrate for 2 hours. The cells were tested using a Biologic VSP in a frequency range from 100 kHz to 100 mHz with a 5 mV amplitude excitation.

XPS measurements were conducted with a K-alpha spectrometer (Thermo Scientific) using Al Ka radiation ($h\nu$ = 1486.6 eV) under ultra-high vacuum ($<1x10^{-12}$ atm). The spot size and pass energy were 400 mm in diameter and 60 eV respectively. After cycling, the $LiFePO_4$/Cu cells were allowed to equilibrate for 48 hours and disassembled in an argon glove box. Lithium electrodes were washed with an EC:EMC (3:7) solution followed by only EMC to remove the salt residue and EC, dried overnight under vacuum (approx. $3x10^{-3}$ atm), and then transferred in an air-free container from the glove box to the XPS chamber. The binding energy scale was corrected using the LiF peak (685 eV) in the F 1s spectra. Relative atomic concentrations were determined from integration of the XPS peaks, accounting for respective atomic sensitivity factors.

TEM measurements were conducted with a JEOL JEM-2100F at 200 kV, equipped with a LaB_6 electron emission source. Pelco copper TEM grids, 500 mesh,

were placed on a copper foil electrode and assembled with $LiFePO_4$, as described above. Approximately 15% of the lithium from the $LiFePO_4$ electrode was plated at constant current with voltage of approximately 3.45 V, characteristic of the $LiFePO_4$ electrode vs. Li/Li+, and allowed to equilibrate for 48 hours. After cell equilibration, the TEM grid was collected and washed with EMC and dried under vacuum (approx. $3x10^{-3}$ atm). After drying, the grid was transferred to the TEM chamber without air exposure using a Cryo-Transfer holder and a sealable Aldrich AtmosBag. Energy-dispersive X-ray spectroscopy (EDX, INCAx-act, Oxford Instrument) was also conducted to analyze the element composition using beam diameters between 10–25 nm.

RESULTS AND DISCUSSION

The cycling performance of these cells is depicted with Coulombic efficiency versus cycle number (Figure 4-1a) and the total amount of lithium stripped each cycle (Figure 4-1b). The stripping capacity versus cycle number is also presented in Figure 4-2. The cycling performance is clearly dependent upon the salt used in the electrolyte, suggesting that the salt is involved in either SEI formation or mossy lithium generation. The performance differences are easily discernible with the $LiFePO_4$/Cu cells since there is no excess lithium as there is for the Li/Li or Li/Cu cells. Thus, lithium loss during plating and stripping is more dramatic for the $LiFePO_4$/Cu cells than in Li/Li symmetric cells. The cells cycled with the $LiBF_4$, LiBOB, and $LiBF_4$ + LiBOB electrolytes have better initial capacity retention (Figure 4-2b) and cycling efficiency than cells cycled with the $LiPF_6$ electrolyte, but retained capacity is

insignificant after only 10 cycles. However, the cell cycled with the LiDFOB electrolyte has dramatically better efficiency and capacity retention over the first 50 cycles, maintaining >95% efficiency through the 50th cycle. It is noteworthy that the performance of the cell cycled with $LiBF_4$ + LiBOB electrolyte is much worse than the cell cycled with LiDFOB electrolyte, despite the effectively equivalent chemical composition of the electrolytes (see the chemical structures depicted in Fig. 4-1), suggesting that the DFOB anion has a unique interaction with the lithium metal surface. In addition, variation of the LiDFOB salt concentration from 1.2 to 1.8 M resulted in only small changes in performance (Figure 4-3).

The 1st plating and stripping cycle of lithium with the different electrolytes in $LiFePO_4$/Cu cells is provided in Figure 4-2a. Significant changes in the stripping capacities are observed when comparing the electrochemical performance of all electrolytes. This suggests that either the quantity of electrolyte decomposition to generate a solid electrolyte interphase (SEI) is much greater for cells with poor first cycle efficiency or significant mossy lithium is generated resulting in poor stripping. All of the cells containing the alternative salts have better first cycle efficiency than cells containing $LiPF_6$ (25.1%).

Nyquist plots of Li/Li symmetric cells, in which lithium electrodes were generated from $LiFePO_4$/Cu cells cycled with the different electrolytes, are provided in Figure 4-4. Upon the 10th plating, the overall impedance of cells is inversely related to the capacity retention ($LiPF_6$ > $LiBF_4$ > LiBOB ≈ $LiBF_4$ + LiBOB > LiDFOB). The strong correlation suggests that cell performance is dominated by the plating and stripping of lithium on copper and not the $LiFePO_4$ electrode. Differences in the

structure and stability of the SEI on the lithium metal are likely responsible for the differences in impedance and cycling performance.

Galvanostatic cycling results observed for Li/Li symmetric cells cycled with the different electrolytes are shown in Figure 4-5. Except for the cell containing the LiDFOB electrolyte (Figure 4-5c) a rapidly increasing voltage is observed during both charge/discharge steps where the voltage limit (3.5 V) is reached in less than 50 cycles. This voltage increase is characteristic of a significant increase in the impedance of lithium electrodes in the cells during cycling.[7,29] Upon reaching this voltage limit, lithium is no longer being cycled and the cells have reached ‘‘high impedance failure’’.[7,29] Conversely, the cell containing the LiDFOB electrolyte demonstrates stable charge/discharge behavior for more than 2000 hours (250 cycles) and do not undergo impedance failure. This improvement in cycling confirms that observations with $LiFePO_4$/Cu are representative of behavior with Li/Li cells, i.e. the LiDFOB electrolyte improves the electrochemical performance of the lithium metal anode.[30–32]

The surface of lithium metal was investigated with XPS. Spectra of the electrodes were acquired after the 1st and the 10^{th} plating (Figure 4-6). The spectra of the electrodes acquired after 15% of the available lithium was removed from $LiFePO_4$ (i. e. 15% state-of-charge) during the 1st plating are depicted in Figure 4-7. The corresponding relative atomic concentrations from XPS spectra are provided in Figure 4-8. The C 1s spectrum of the lithium electrode plated with the $LiPF_6$ electrolyte contains peaks characteristic of Li_2CO_3 or lithium alkyl carbonates (290.3 eV) along with a C–O peak (286.8 eV).[20,33–35] There are corresponding peaks at 531.8 and 533.5

eV in the O 1s spectra, which are characteristic of C=O and C–O, respectively,[20,33–35] supporting the presence of lithium alkyl carbonates and Li_2CO_3. The F 1s spectrum has an intense peak at 685 eV, characteristic of LiF.[20,33–35] The XPS spectra do not change significantly upon prolonged cycling. The relative atomic concentrations calculated from corresponding XPS spectra (Figure 4-8) illustrate that the surface of the lithium electrode plated with the $LiPF_6$ electrolyte has high concentrations of inorganic species, especially LiF, as can be observed in the F 1s spectra.

The surface of the lithium electrode plated with the $LiBF_4$ electrolyte has much less Li_2CO_3 or lithium alkyl carbonates (C 1s) compared to the lithium electrode plated with the $LiPF_6$ electrolyte, however, an intense C–O peak is observed. This C–O peak grows notably after prolonged cycling. In the F 1s spectrum, the LiF peak (685 eV) is present during the very early stage of plating (15% of lithium from the $LiFePO_4$ electrode, Figure 4-7), however, the additional peaks are observed at higher binding energies (687–690 eV) and these additional peaks have significantly increased intensity upon prolonged cycling (Figure 4-6). The peaks observed at higher binding energies are characteristic of B–F compounds from the decomposition of $LiBF_4$ salt.[36,37] The changes in peak intensity indicate that the film generated from $LiBF_4$ is not stable during cycling. A corresponding change in atomic concentration is also observed upon cycling where the concentration of B increases and F decreases (Figure 4-8). A broad B–F peak is observed in the B 1s spectrum from 191–195 eV characteristic of a combination of B–F and B–O species.[36–41] The data suggest the film generated from $LiBF_4$ reacts with carbonate solvents to generate B–O–C and B–F containing species after prolonged cycling. The surface of the lithium electrode plated

with the LiBOB electrolyte has a characteristic peak assigned to lithium carboxylate or lithium oxalate at 289 eV, as well as C–O at 286.8 eV in the C 1s spectrum (Figure 4-6). The corresponding peaks characteristic of C=O and C–O are observed at 531.8 and 533.5 eV, respectively, in the O 1s spectra. The B 1s spectrum contains a peak at 193.5 eV assigned to B–O species.[39–41] The elemental concentration of the surface film on the lithium electrodes plated with the LiBOB electrolyte is dominated by C and O containing species,[42] as depicted in Figure 4-8.

The XPS spectra of the lithium electrode plated with the LiDFOB and $LiBF_4$ + LiBOB electrolytes are very similar for the 1st plating, as both surface films contain lithium carboxylate or lithium oxalate (289 eV, C 1s) along with a C–O peak (286.8 eV, C 1s). Upon additional cycling, the surface film on the lithium electrode cycled with the LiDFOB electrolyte does not change significantly. However, upon additional cycling the surface film on lithium electrode plated with the $LiBF_4$ + LiBOB electrolyte changes significantly. After 10 cycles the element spectra and elemental concentrations are very similar to the surface film on lithium electrode cycled with the LiBOB electrolyte (Figures 4-6 and 4-8) For example, the concentration of F and the intensity of the LiF peak (685 eV, F 1s) decreases considerably after prolonged cycling with the $LiBF_4$ + LiBOB electrolyte. Further, the peak assigned to B–O (193.5 eV, B 1s) increases in intensity upon cycling, as observed for the lithium electrode cycled with the LiBOB electrolyte. The results suggest that the LiDFOB and $LiBF_4$ + LiBOB electrolytes generate an initial surface film with very similar composition. However, upon cycling, the surface film of the lithium metal electrode cycled with the LiDFOB electrolyte is stable, affording good capacity retention and high efficiency,

while the surface film of the lithium electrode cycled with the $LiBF_4$ + LiBOB electrolyte is unstable, evolving into a surface film which causes poor efficiency for the lithium metal electrode.

Depth profiling with argon ion-beam sputtering has been performed on cycled lithium electrodes (i.e. at the 10th plating) with the LiDFOB and $LiBF_4$ + LiBOB electrolytes (Figure 4-9). The electrode cycled with the $LiBF_4$ + LiBOB electrolyte contains more C and O and less F than the electrode cycled with the LiDFOB electrolyte. As the sputtering time is increased, the composition of the surface of electrode cycled with the $LiBF_4$ + LiBOB electrolyte changes more than the surface of electrode cycled with the LiDFOB electrolyte. This change in atomic concentration upon sputtering suggests that the SEI composition changes as a function of depth, consistent with an SEI composed of primarily of LiBOB decomposition products on the exterior and $LiBF_4$ decomposition products on the interior, as discussed above. The elemental composition of the surface of electrode cycled with the LiDFOB electrolyte, has much smaller changes upon sputtering suggesting that a stable and homogeneous surface film is generated. The results suggest that the presence of the LiDFOB salt generates favorable and stable SEI on lithium surface which minimizes surface film changes during prolonged cycling.

To understand the morphology of plated lithium and SEI nanostructure, TEM analysis has been conducted on lithium electrodes with representative images and EDX spectra shown in Figure 4-10. Since the chemical composition of the surface films are very similar for the LiDFOB and $LiBF_4$ + LiBOB electrolytes, the morphology of the surface films has been analyzed to develop a better understanding

for the source of the significant performance differences. The morphology was also investigated for the $LiPF_6$ electrolyte for further comparison.

The morphology of plated lithium is dependent on the electrolyte used. Specifically, the appearance of lithium plated from the $LiPF_6$ electrolyte is non-uniform (Figure 4-10a). There is no unique morphology observed and many different shapes of lithium (light and dark gray, Figure 4-10b) are present on the copper TEM grid (black, Figure 4-10b) consistent with the formation of dendritic and mossy lithium. Due to this non-uniformity, the features of the SEI are inconsistent and difficult to resolve.

By comparison, lithium plated from the LiDFOB electrolyte is uniform, smooth, and contains very small particles (5–10 nm) evenly distributed on the surface (Figure 4-10c). While most of the small particles are evenly distributed, some of the small particles cluster together to form larger secondary particles. High resolution imaging of the secondary particles reveals that the particles covered by a smooth layer (Figure 4-10d). The primary particles have a darker contrast than the outer layer, suggesting that they have a higher atomic number. Analysis of surface of the lithium plated from the LiDFOB electrolyte by EDX (Figure 4-10g,h) indicates that the clusters of the primary particles (point 1, secondary particle) are largely composed of F while the surrounding coating (point 2) is largely composed of O. Therefore, the TEM data coupled with the XPS suggest that electrodes cycled with LiDFOB electrolyte have an SEI composed of nanostructured LiF particles covered with a smooth layer of lithium alkyl carbonates, Li_2CO_3 and lithium oxalate. This also correlates with the argon sputtering investigations with XPS (Figure 4-9) which

demonstrate that the inner region contains more F than the outer surface. These observations are also consistent with recent exploration of similar SEI structures on lithium metal using the cryogenic TEM technique.[43]

Similar LiF-containing particles are also observed on lithium plated from the $LiBF_4$ + LiBOB electrolyte, however, the secondary particles are much larger (200–400 nm) than the particles plated from the LiDFOB electrolyte (Figure 4-10e), and are not covered by a smooth layer (Figure 4-10f). From EDX characterization (Figure 4-11), these larger particles have a relatively high concentration of F, while the surrounding area is composed of O. It is suggested that the $LiBF_4$ + LiBOB electrolyte is able to generate similar particles, compared to particles generated by the LiDFOB electrolyte. However, the growth of these secondary particles is not controlled upon generation from the $LiBF_4$ + LiBOB electrolyte. Given the similar chemical composition of the SEI generated from the LiDFOB and $LiBF_4$ + LiBOB electrolytes (15% of 1st plating, Figure 4-7) the distribution and size of these nanostructured LiF particles must significantly influence the cycling performance of lithium metal anodes.

It is proposed that during the reductive decomposition of LiDFOB, the decomposition products, likely oxalate or CO_2 act as a capping agent[44–46] for LiF nanoparticle generation (Figures 4-12a,b). Similar capping agents have been widely used for the synthesis of nanoparticles. A capping agent enables control over the size or shape of particles without agglomeration by modifying the surface of particles. Oxalates are one of the typical capping agents used to prepare metal oxide nanomaterials.[47,48] Therefore, the oxalate moiety of LiDFOB and LiBOB may be functioning as a capping agent to generate nanostructured LiF. LiDFOB contains both

fluorine and oxalate moieties (Figure 4-12a), enhancing the capping process for LiDFOB compared to LiBOB, since both the LiF and lithium oxalate are derived from reduction of the same molecular structure. This enhanced capping results in the generation of smaller particles (Figure 4-12b) from the LiDFOB electrolyte compared to the $LiBF_4$ + LiBOB electrolyte. The morphology of the SEI appears to strongly influence the plating and stripping performance of lithium electrodes,[7,49] since the molecular composition of the SEI after the first plating is very similar for the LiDFOB and $LiBF_4$ + LiBOB electrolytes (Figure 4-6). The presence of an SEI comprised of nanostructured LiF on lithium electrode plated from the LiDFOB electrolyte has dramatically better capacity retention, efficiency and exhibits the smallest impedance.

Based on all the observed data, a model for surface film formation for lithium metal plated with the LiDFOB and $LiBF_4$ + LiBOB electrolytes has been proposed as illustrated in Figure 4-12c,d. Decomposition of the electrolyte is initiated immediately as the lithium metal is plated. The LiDFOB salt participates in film formation during lithium plating from the LiDFOB electrolyte. Both $LiBF_4$ and LiBOB also participate in film formation for lithium plated with the $LiBF_4$ + LiBOB electrolyte. During film formation, LiF particles are generated on the surface of lithium or copper. Effective capping by LiDFOB results in the generation of very small (<5 nm) LiF particles covered by a layer of lithium oxalate or Li_2CO_3 (Fig. 4c). Interestingly, the LiF/Li_2CO_3 interface at the nanostructured level has been computationally predicted to have high lithium ion conductivity which could also contribute to the good performance of the LiDFOB electrolyte.[50] However, when lithium is plated with the $LiBF_4$ + LiBOB electrolyte, the size and distribution of the LiF particles is not

controlled well due to the poor capping ability of LiBOB compared to LiDFOB. The LiF particles grow much larger and do not evenly coat the surface. In addition, continuous LiBOB reduction during prolonged cycling generates a more resistive surface film on the lithium electrode which quickly leads to cell failure (Figure 4-12d).

The differences in cycling performance can be related to differences in diffusion field gradients at the nanometer scale. Schematic diagrams of the diffusion field on lithium plated with the LiDFOB and $LiBF_4$ + LiBOB electrolytes are depicted in Figure 4-12e and f. Since LiF has an electronically insulating nature[51] and its cation diffusivity is lower than other SEI components,[52] the surface covered with LiF can be considered as an inactive area for lithium plating/stripping. Thus, the surface film on the lithium metal electrode has both active and inactive areas, affecting both electrochemical performance and lithium deposition. Active areas of the electrode generate a lithium diffusion field, and these individual diffusion fields extend over the projected boundaries of the inactive areas. If the size of each inactive area (e.g. LiF) is smaller than a critical dimension, the separated diffusion fields merge into a linear single field[53] (Figure 4-12e). Under these conditions, lithium ion diffusion is not hindered by the presence of the inactive areas, having an area equal to the geometric area of the entire surface, even including inactive areas. This phenomenon is commonly observed in ultramicroelectrodes (UMEs),[53–55] which are used in various electrochemical measurements or electrochemical sensors. On the contrary, if the size of each inactive area is larger than a critical dimension (Figure 4-12f), the separated diffusion fields do not merge, and the overall diffusion field is hindered by the presence of inactive areas. The disturbance in the diffusion field results in poor

efficiency and irregular dendrite growth, due to a non-uniform lithium ion distribution.[56,57] The differences in diffusion fields provide an explanation for an SEI containing nanostructured LiF particles improving the performance of lithium metal anodes plated from the LiDFOB electrolyte.

CONCLUSIONS

The common $LiBF_4$, LiBOB, and LiDFOB salts were utilized to understand key mechanisms for improving the cycling performance of lithium metal anodes, providing insight for future electrolyte development. The LiDFOB electrolyte provides a dramatic improvement in electrochemical performance compared to the other salts. However, lithium cycled with the $LiBF_4$ + LiBOB electrolyte has rapid performance decay even though it has an equivalent chemical composition to the LiDFOB electrolyte. Ex situ surface analysis (XPS) suggests that the surface film generated on lithium is primarily composed of lithium alkyl carbonate, Li_2CO_3, lithium oxalate, and LiF. The initial composition of the surface film generated on lithium with the $LiBF_4$ + LiBOB electrolyte is very similar to the composition of the surface film generated on lithium with the LiDFOB electrolyte. However, after 10 cycles with the $LiBF_4$ + LiBOB electrolyte the capacity fades and the surface film evolves into a surface film with a similar composition to that observed with the LiBOB electrolyte. This suggests LiBOB is continuously decomposed covering the initially formed unstable SEI on lithium metal electrode. TEM analysis reveals

the LiDFOB electrolyte generates a uniform film composed of nanostructured LiF particles covered by a smooth layer of Li_2CO_3 and lithium oxalate on the lithium surface, while the $LiBF_4$ + LiBOB electrolyte generates an inhomogeneous film containing much larger LiF particles which are not homogenously covered by a film of Li_2CO_3 and lithium oxalate. Based on this analysis, the generation of nanostructured LiF particles has been proposed to result from the presence of oxalate based capping agents within the same molecular component as the source of the LiF (LiDFOB). The presence of the nanostructured LiF particles results in the generation of uniform diffusion field gradients which afford uniform lithium plating. Thus, the controlled generation of nanostructured LiF plays a critical role in the improved plating/stripping performance of lithium metal anodes, in addition to the composition of stable SEI generated from the LiDFOB electrolyte. Based on this model, researchers are motivated to pursue new synthetic routes for energy storage materials, applicable not only to liquid organic electrolytes for lithium metal batteries, but for next-generation energy storage systems as well.

REFERENCES

1. J. S. Dunning, W. H. Tiedemann, L. Hsueh and D. N. Bennion, *J. Electrochem. Soc.*, 1971, **118**, 1886-1890.
2. V. R. Koch, *J. Power Sources*, 1981, **6**, 357-370.
3. E. Peled, *J. Electrochem. Soc.*, 1979, **126**, 2047-2051.
4. Z. Tu, P. Nath, Y. Lu, M. D. Tikekar and L. A. Archer, *Acc. Chem. Res.*, 2015, **48**, 2947-2956.
5. S. Choudhury, A. Agrawal, S. Wei, E. Jeng and L. A. Archer, *Chem. Mater.*, 2016, **28**, 2147-2157.
6. N.-W. Li, Y.-X. Yin, C.-P. Yang and Y.-G. Guo, *Adv. Mater.*, 2016, **28**, 1853-1858.
7. J. Qian, W. A. Henderson, W. Xu, P. Bhattacharya, M. Engelhard, O. Borodin and J. G. Zhang, *Nat Commun*, 2015, **6**, 6362.
8. S. Fang, L. Qu, D. Luo, S. Shen, L. Yang and S.-i. Hirano, *RSC Adv.*, 2015, **5**, 33897-33904.
9. J. Qian, W. Xu, P. Bhattacharya, M. Engelhard, W. A. Henderson, Y. Zhang and J.-G. Zhang, *Nano Energy*, 2015, **15**, 135-144.
10. S. M. Wood, C. H. Pham, R. Rodriguez, S. S. Nathan, A. D. Dolocan, H. Celio, J. P. de Souza, K. C. Klavetter, A. Heller and C. B. Mullins, *ACS Energy Letters*, 2016, **1**, 414-419.
11. J. Zheng, M. H. Engelhard, D. Mei, S. Jiao, B. J. Polzin, J.-G. Zhang and W. Xu, *Nature Energy*, 2017, **2**, 17012.

12. K. Xu, *Chem. Rev.*, 2004, **104**, 4303-4418.

13. E. Markevich, G. Salitra, F. Chesneau, M. Schmidt and D. Aurbach, *ACS Energy Letters*, 2017, **2**, 1321-1326.

14. H. Xiang, P. Shi, P. Bhattacharya, X. Chen, D. Mei, M. E. Bowden, J. Zheng, J.-G. Zhang and W. Xu, *J. Power Sources*, 2016, **318**, 170-177.

15. S. Choudhury and L. A. Archer, *Advanced Electronic Materials*, 2016, **2**, 1500246.

16. X.-Q. Zhang, X.-B. Cheng, X. Chen, C. Yan and Q. Zhang, *Adv. Funct. Mater.*, 2017, **27**, 1605989.

17. Y. Lu, Z. Tu and L. A. Archer, *Nat Mater*, 2014, **13**, 961.

18. L. Fan, H. L. Zhuang, L. Gao, Y. Lu and L. A. Archer, *J Mater Chem A*, 2017, **5**, 3483-3492.

19. M. Nie, D. P. Abraham, Y. Chen, A. Bose and B. L. Lucht, *The Journal of Physical Chemistry C*, 2013, **117**, 13403-13412.

20. P. Verma, P. Maire and P. Novak, *Electrochim. Acta*, 2010, **55**, 6332-6341.

21. H. Buqa, P. Golob, M. Winter and J. O. Besenhard, *J. Power Sources*, 2001, **97-98**, 122-125.

22. A. M. Andersson and K. Edström, *J. Electrochem. Soc.*, 2001, **148**, A1100-A1109.

23. H.-G. Steinrück, C. Cao, Y. Tsao, C. J. Takacs, O. Konovalov, J. Vatamanu, O. Borodin and M. F. Toney, *Energy Environ. Sci.*, 2018, **11**, 594-602.

24. N. Takenaka, Y. Suzuki, H. Sakai and M. Nagaoka, *The Journal of Physical Chemistry C*, 2014, **118**, 10874-10882.

25. A. Tokranov, B. W. Sheldon, P. Lu, X. Xiao and A. Mukhopadhyay, *J. Electrochem. Soc.*, 2014, **161**, A58-A65.

26. M. Nie and B. L. Lucht, *J. Electrochem. Soc.*, 2014, **161**, A1001-A1006.

27. J. Qian, B. D. Adams, J. Zheng, W. Xu, W. A. Henderson, J. Wang, M. E. Bowden, S. Xu, J. Hu and J.-G. Zhang, *Adv. Funct. Mater.*, 2016, **26**, 7094-7102.

28. Z. L. Brown, S. Jurng and B. L. Lucht, *J. Electrochem. Soc.*, 2017, **164**, A2186-A2189.

29. E. Kazyak, K. N. Wood and N. P. Dasgupta, *Chem. Mater.*, 2015, **27**, 6457-6462.

30. F. Wu, J. Qian, R. Chen, J. Lu, L. Li, H. Wu, J. Chen, T. Zhao, Y. Ye and K. Amine, *ACS Applied Materials & Interfaces*, 2014, **6**, 15542-15549.

31. Q. Xu, Y. Yang and H. Shao, *Electrochim. Acta*, 2018, **259**, 534-541.

32. B. Qin, S. Zhang, Z. Hu, Z. Liu, J. Zhang, J. Zhao, J. Xiong and G. Cui, *Ionics*, 2017, **23**, 1399-1406.

33. R. Dedryvère, S. Laruelle, S. Grugeon, L. Gireaud, J.-M. Tarascon and D. Gonbeau, *J. Electrochem. Soc.*, 2005, **152**, A689-A696.

34. A. M. Andersson and K. Edstrom, *J. Electrochem. Soc.*, 2001, **148**, A1100-A1109.

35. R. Dedryvere, H. Martinez, S. Leroy, D. Lemordant, F. Bonhomme, P. Biensan and D. Gonbeau, *J. Power Sources*, 2007, **174**, 462-468.

36. E. A. Il'inchik, V. V. Volkov and L. N. Mazalov, *J. Struct. Chem.*, 2005, **46**, 523-534.

37. A. M. Andersson, M. Herstedt, A. G. Bishop and K. Edström, *Electrochim. Acta*, 2002, **47**, 1885-1898.

38. T. Schedlbauer, U. C. Rodehorst, C. Schreiner, H. J. Gores and M. Winter, *Electrochim. Acta*, 2013, **107**, 26-32.

39. G. V. Zhuang, K. Xu, T. R. Jow and P. N. Ross, *Electrochem. Solid-State Lett.*, 2004, **7**, A224-A227.

40. E. M. Wigayati, T. Lestariningsih, A. Subhan, C. R. Ratri and I. Purawiardi, *Ionics*, 2016, **22**, 43-50.

41. T. Lestariningsih, E. Wigayati, C. Ratri and Q. Sabrina, *Journal of Physics: Conference Series*, 2017, **817**, 012030.

42. K. Xu, U. Lee, S. Zhang, M. Wood and T. R. Jow, *Electrochem. Solid-State Lett.*, 2003, **6**, A144.

43. X. Wang, M. Zhang, J. Alvarado, S. Wang, M. Sina, B. Lu, J. Bouwer, W. Xu, J. Xiao, J. G. Zhang, J. Liu and Y. S. Meng, *Nano Lett.*, 2017, **17**, 7606-7612.

44. Y. Xia, Y. Xiong, B. Lim and S. E. Skrabalak, *Angewandte Chemie (International ed. in English)*, 2009, **48**, 60-103.

45. S. Campisi, M. Schiavoni, C. Chan-Thaw and A. Villa, *Catalysts*, 2016, **6**, 185.

46. C. M. Phan and H. M. Nguyen, *The Journal of Physical Chemistry A*, 2017, **121**, 3213-3219.

47. S. Vaidya, T. Ahmad, S. Agarwal and A. K. Ganguli, *J. Am. Ceram. Soc.*, 2007, **90**, 863-869.

48. R. Pegu, K. J. Majumdar, D. J. Talukdar and S. Pratihar, *RSC Adv.*, 2014, **4**, 33446-33456.

49. K. Yan, H.-W. Lee, T. Gao, G. Zheng, H. Yao, H. Wang, Z. Lu, Y. Zhou, Z. Liang, Z. Liu, S. Chu and Y. Cui, *Nano Lett.*, 2014, **14**, 6016-6022.

50. Q. Zhang, J. Pan, P. Lu, Z. Liu, M. W. Verbrugge, B. W. Sheldon, Y.-T. Cheng, Y. Qi and X. Xiao, *Nano Lett.*, 2016, **16**, 2011-2016.

51. M. Gauthier, T. J. Carney, A. Grimaud, L. Giordano, N. Pour, H.-H. Chang, D. P. Fenning, S. F. Lux, O. Paschos, C. Bauer, F. Maglia, S. Lupart, P. Lamp and Y. Shao-Horn, *The Journal of Physical Chemistry Letters*, 2015, **6**, 4653-4672.

52. L. Benitez and J. M. Seminario, *J. Electrochem. Soc.*, 2017, **164**, E3159-E3170.

53. A. J. Bard and L. R. Faulkner, *Electrochemical Methods: Fundamentals and Applications, 2nd Edition*, John Wiley & Sons, 2000.

54. C. G. Zoski, *Electroanalysis*, 2002, **14**, 1041-1051.

55. K. Aoki, *Electroanalysis*, 1993, **5**, 627-639.

56. X.-B. Cheng, M.-Q. Zhao, C. Chen, A. Pentecost, K. Maleski, T. Mathis, X.-Q. Zhang, Q. Zhang, J. Jiang and Y. Gogotsi, *Nature Communications*, 2017, **8**, 336.

57. F. Sagane, K.-I. Ikeda, K. Okita, H. Sano, H. Sakaebe and Y. Iriyama, *J. Power Sources*, 2013, **233**, 34-42.

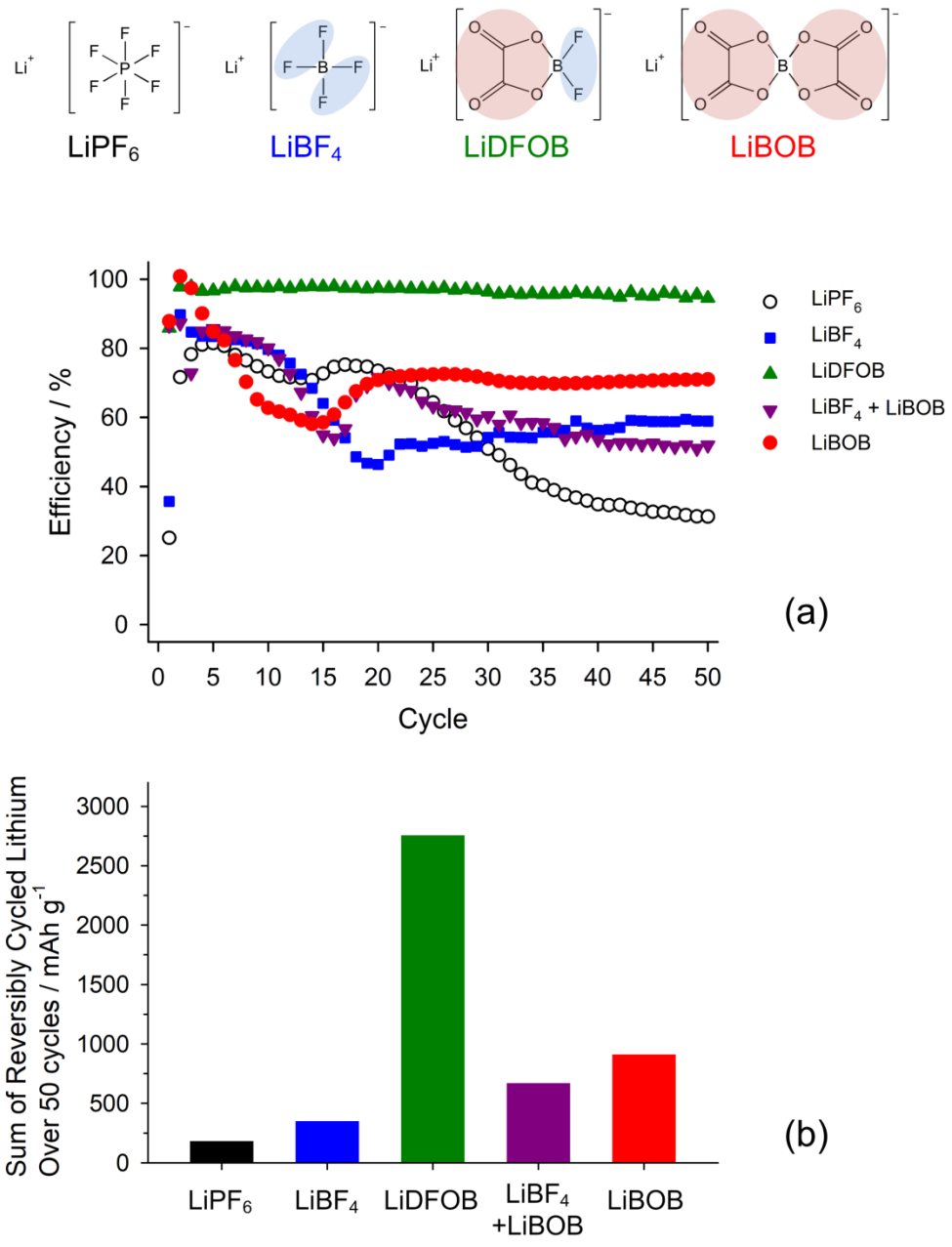

Figure 4-1. Comparison of (a) Coulombic efficiency vs. cycle number and (b) total sum of reversibly cycled lithium over 50 cycles obtained from $LiFePO_4$/Cu cells.

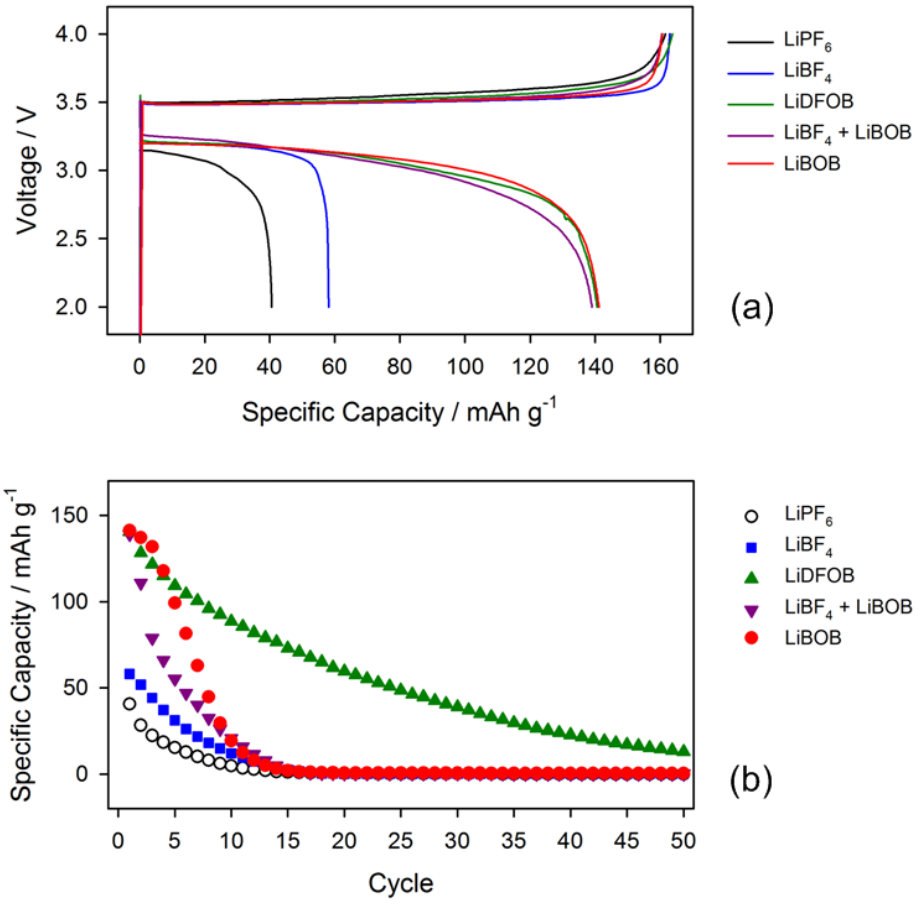

Figure 4-2. Comparison of the (a) 1st lithium plating/stripping profile and (b) stripping capacity vs. cycle number obtained from $LiFePO_4$/Cu cells using the investigated electrolytes.

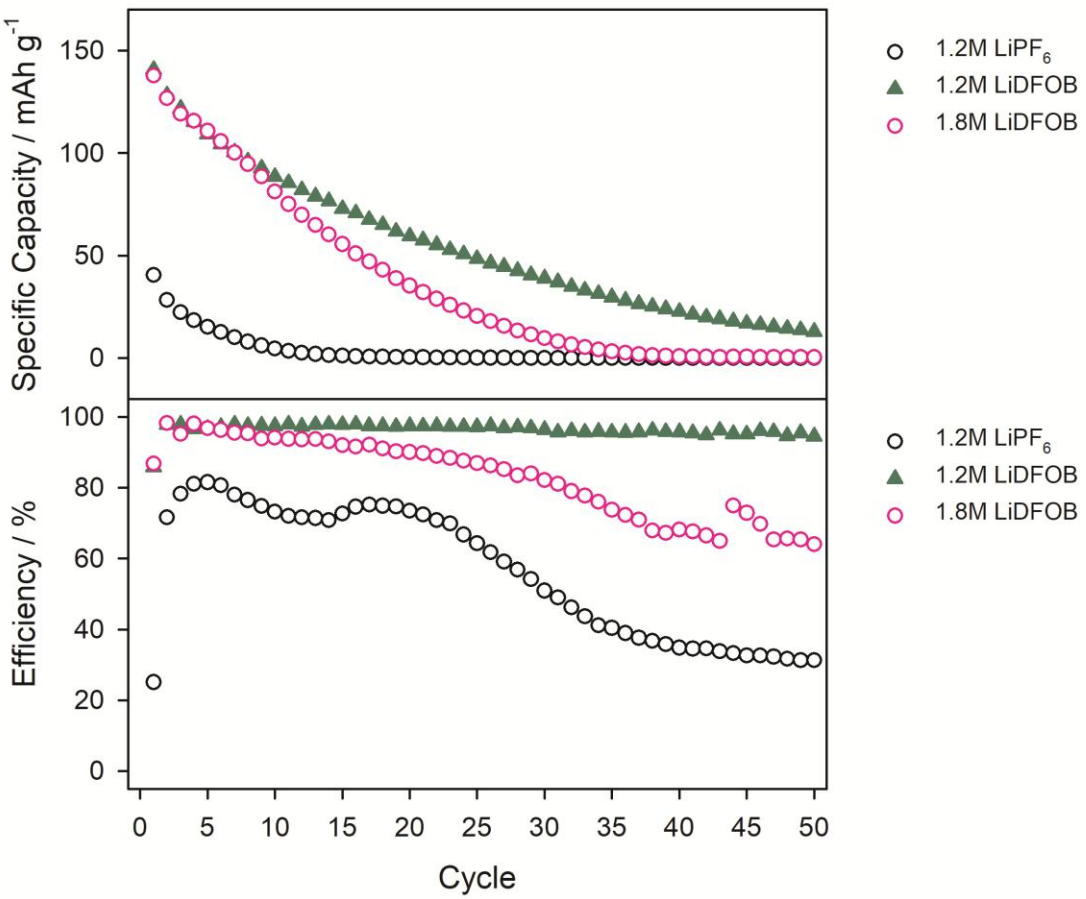

Figure 4-3. Comparison of the (a) stripping capacity and (b) efficiency vs. cycle number obtained from $LiFePO_4$/Cu cells using the investigated electrolytes.

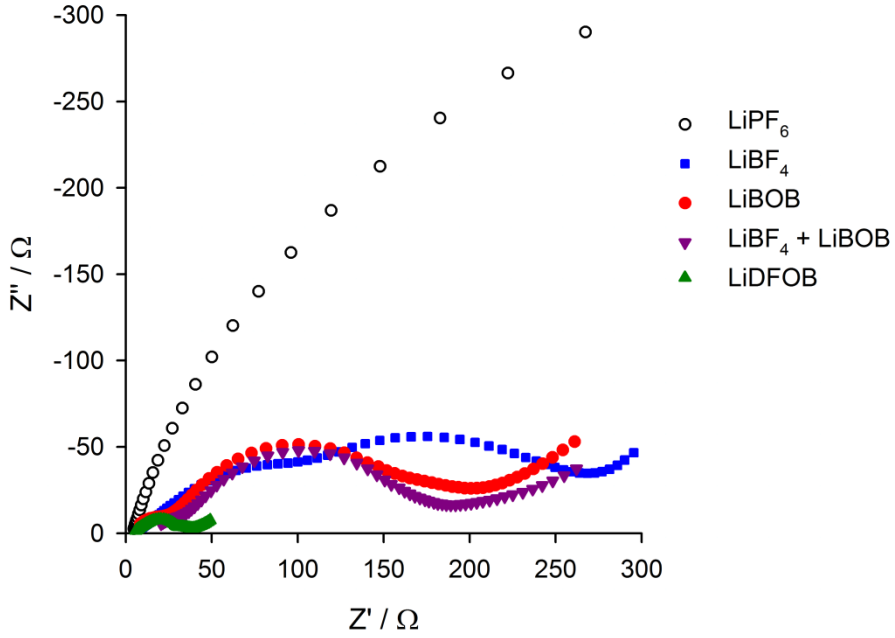

Figure 4-4. The Nyquist plots obtained from the Li/Li symmetric cells, in which lithium electrodes were generated from $LiFePO_4$/Cu cells containing the investigated electrolytes.

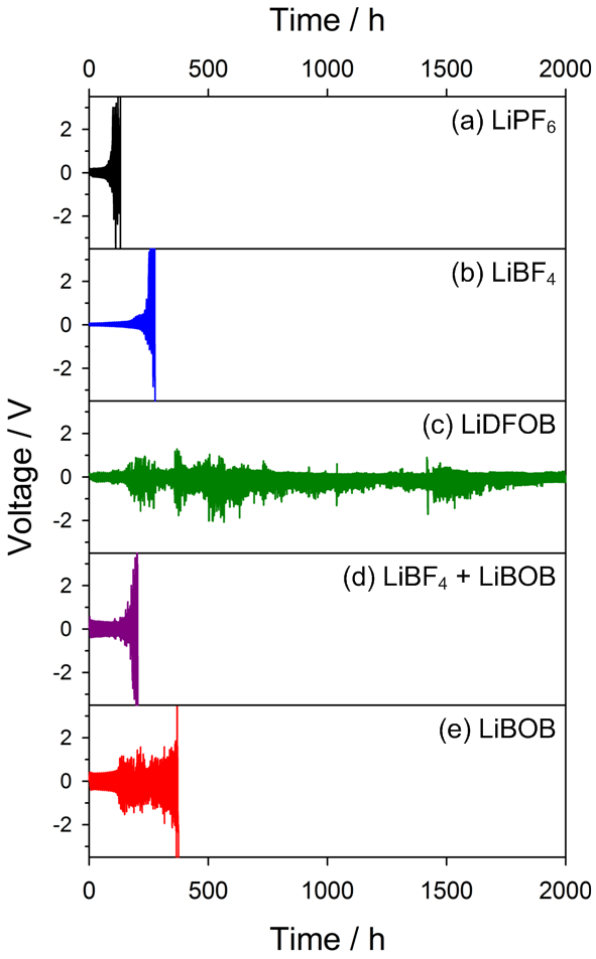

Figure 4-5. Galvanostatic cycling results of Li/Li symmetric cells with current density of 0.5 mA cm^{-2} and limited charge/discharge capacity of 2 mAh cm^{-2}.

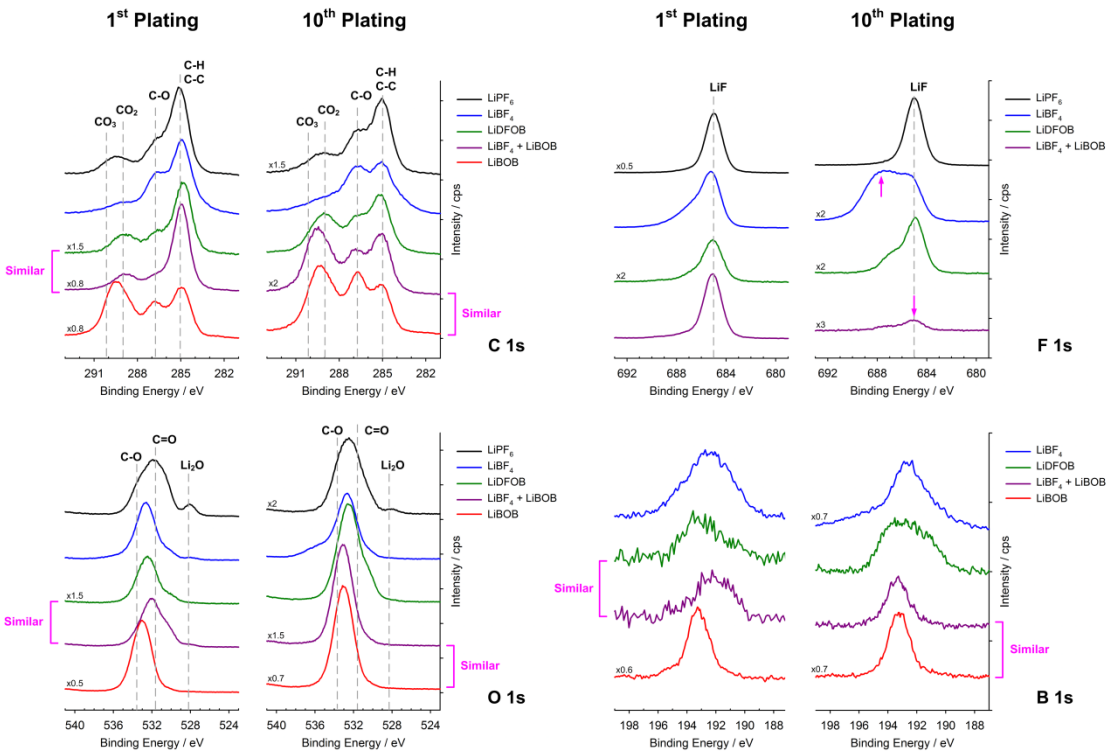

Figure 4-6. XPS spectra obtained from lithium plated using the investigated electrolytes after the 1st and the 10th plating (100% state-of-charge).

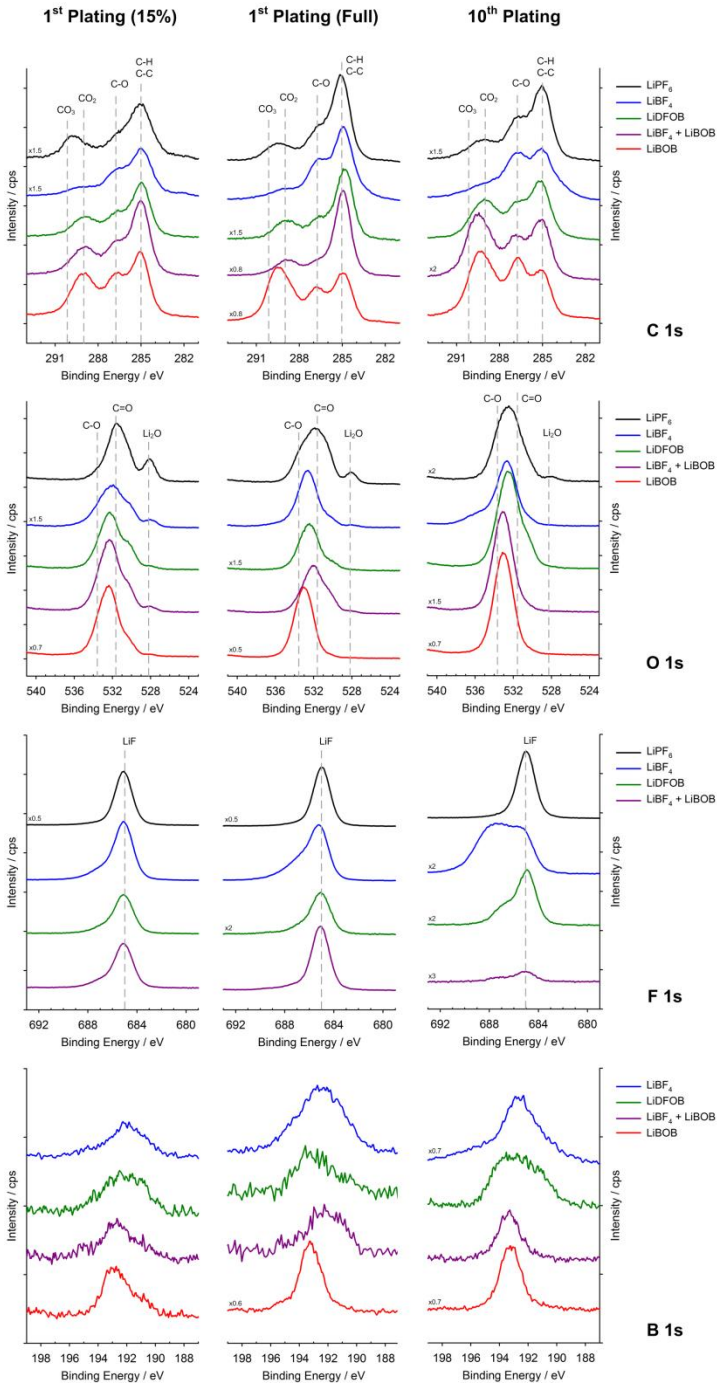

Figure 4-7. XPS spectra obtained from lithium plated using the investigated electrolytes

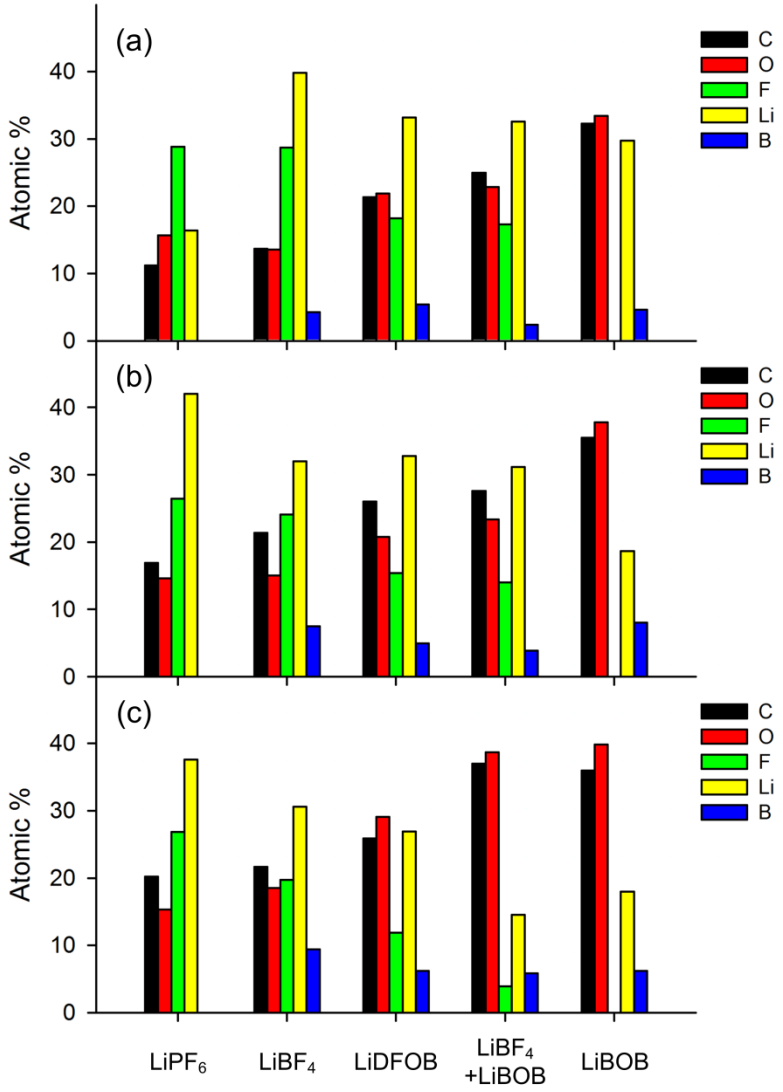

Figure 4-8. Corresponding relative atomic concentrations from XPS spectra for lithium at the (a) 15% of 1st plating, (b) full 1st plating, and (c) 10th plating.

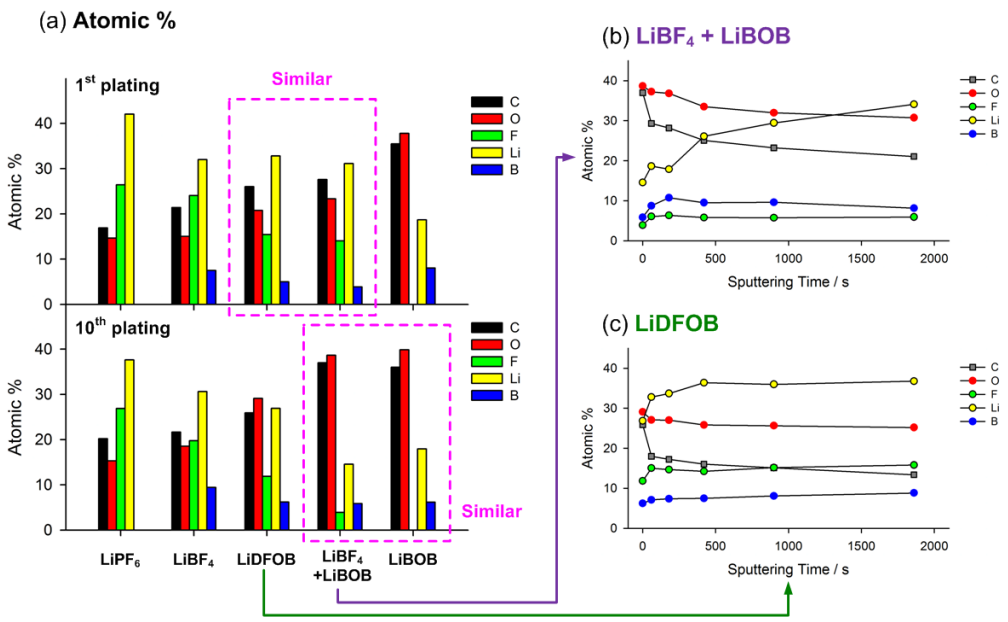

Figure 4-9. (a) Corresponding relative atomic concentrations from XPS spectra and the relative XPS atomic concentration profile upon argon sputtering of lithium plated from (b) 0.6 M $LiBF_4$ + 0.6 M LiBOB in EC:EMC and (c) 1.2 M LiDFOB in EC:EMC.

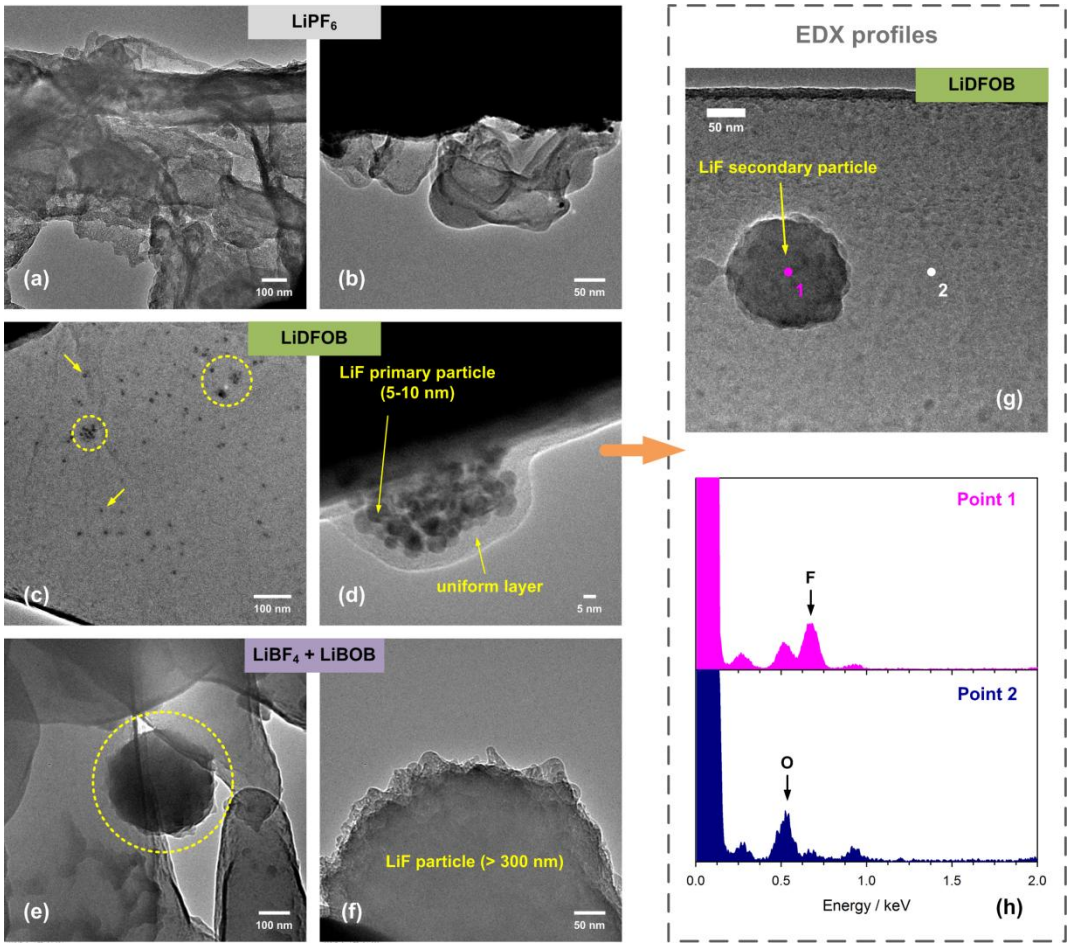

Figure 4-10. TEM images of lithium plated from (a, b) 1.2 M $LiPF_6$ in EC:EMC; (c, d) 1.2 M LiDFOB in EC:EMC; (e, f) 0.6 M $LiBF_4$ + 0.6 M LiBOB in EC:EMC and (g, h) EDX spectra of lithium plated from 1.2 M LiDFOB in EC:EMC.

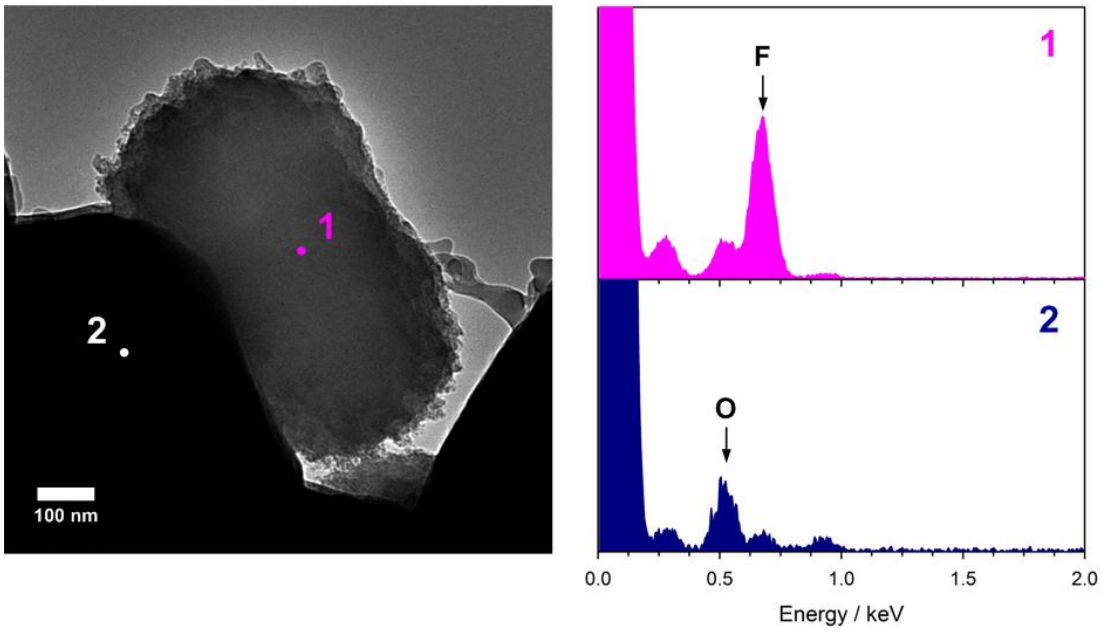

Figure 4-11. EDX spectra of lithium plated from 0.6 M $LiBF_4$ + 0.6 M LiBOB in EC:EMC.

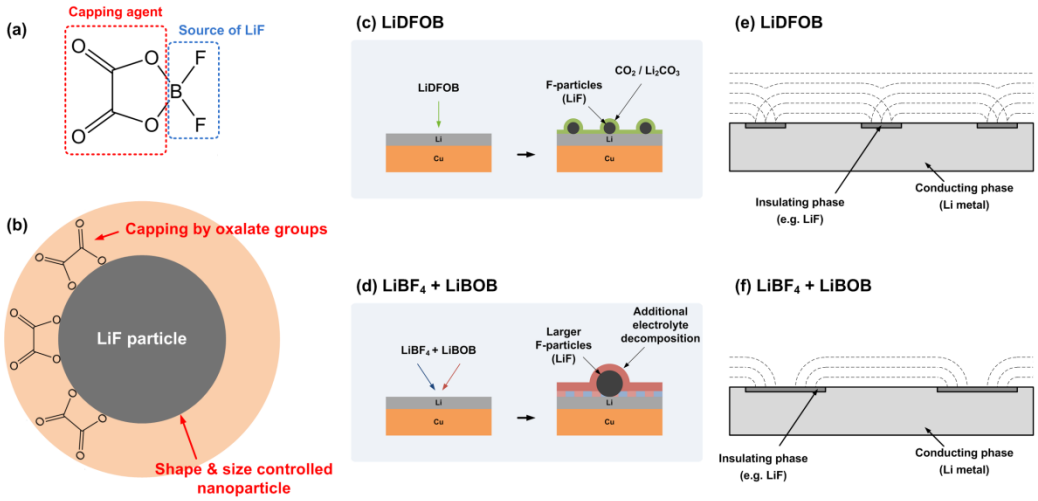

Figure 4-12. (a, b) Proposed mechanisms of LiDFOB acting as a capping agent for LiF nanoparticle generation; (c, d) models of SEI from the (c) LiDFOB and (d) $LiBF_4$+LiBOB electrolyte; and (e, f) schematic of diffusion fields at lithium plated from each electrolyte. Each lithium electrode has active and inactive areas on its surface.

CHAPTER 5

Synergistic Performance of Lithium Difluoro(oxalate)borate and Fluoroethylene Carbonate in Carbonate Electrolytes for the Lithium Metal Anode

Zachary L. Brown[1] and Brett L. Lucht[1]

[1]*Department of Chemistry, University of Rhode Island, Kingston, Rhode Island 02881, USA*

**Corresponding author: blucht@chm.uri.edu*

The following has been submitted for publication in the Journal of the Electrochemical Society and is presented here in manuscript format

ABSTRACT

There is significant interest in the development of rechargeable high-energy density batteries which utilize the lithium metal anode. Recently, fluoroethylene carbonate (FEC) and lithium difluoro(oxalate)borate (LiDFOB) have been reported to significantly improve the electrochemical performance of the lithium metal anodes. This investigation focuses exploring the synergy between LiDFOB and FEC in carbonate electrolytes for lithium metal anodes. In ethylene carbonate (EC) electrolytes, LiDFOB is optimal when used in high salt concentrations, such as 1.0 M, to improve the electrochemistry of the lithium metal anode in Cu||$LiFePO_4$ cells. However, in FEC electrolytes, LiDFOB is optimal when used in smaller concentrations, such as 0.05 – 0.10 M. From surface analysis, LiDFOB is observed to favorably react on the surface of lithium metal to improve the performance of the lithium metal anode, in both EC and FEC-based electrolytes. This research demonstrates progress towards developing feasible high-energy density lithium-based batteries.

INTRODUCTION

The development of energy storage technology is an important topic for facilitating the employment of renewable energy in society. Therefore, current energy storage research is heavily focused on enabling rechargeable high-energy density lithium-based batteries.[1–3] In particular, permitting reversible electrochemical plating and stripping of the lithium metal anode in carbonate electrolytes can achieve this goal.[4] Unfortunately, the performance of the lithium metal anode in carbonate electrolytes is plagued by unsafe dendrite formation and poor Coulombic efficiency upon cycling. However, recent developments in electrolyte chemistry have improved upon these limitations significantly.[2,3]

Fluoroethylene carbonate (FEC) containing electrolytes have been reported to improve the performance of lithium metal electrodes via the generation of polymeric species within the Solid Electrolyte Intephase (SEI)[5] of lithium metal, similar to that reported for silicon anodes.[6,7] It has also been reported that FEC generates LiF deposits which may contribute to the improved cycling performance of lithium metal anodes.[8,9] Recent work suggests that FEC can generate nano-structured LiF, creating a uniform diffusion field on the lithium metal electrode, leading to uniform plating and stripping.[9] Furthermore, it has been demonstrated that employing FEC in co-solvent amounts is optimal for achieving high performance lithium metal anodes.[6]

Lithium difluoro(oxalate)borate (LiDFOB) has also been reported to generate nano-structured LiF for lithium metal electrodes, thereby improving the electrochemical performance of the lithium metal anode.[10] However, the optimal

amount of LiDFOB to use in carbonate electrolytes for the lithium metal anode has not been explored. Further, the synergy between FEC and LiDFOB has not been investigated in carbonate electrolytes for the lithium metal anode. Given the reported improvement in plating/stripping of the lithium metal anode with FEC and LiDFOB containing electrolytes, exploring their synergy can assist researchers in developing high performance electrolytes for the lithium metal anode.

Several carbonate electrolyte compositions containing FEC and LiDFOB have been investigated via a combination of electrochemical analysis with Cu||$LiFePO_4$ cells and ex-situ surface analysis of the cycled electrodes. The in-situ formation of lithium metal and low reactivity of $LiFePO_4$ in Cu||$LiFePO_4$ cells ensure that the FEC does not react with the electrode surfaces prior to the initial lithium plating cycle, as previously reported.[9,11] In particular, ex-situ diffuse reflectance infrared fourier transform spectroscopy (DRIFTS), and X-ray photoelectron spectroscopy (XPS) were used to confirm the role of LiDFOB in the optimized electrolytes. The analysis reveals that LiDFOB can be used in additive concentrations to synergistically work with FEC co-solvent electrolytes.

EXPERIMENTAL

Electrochemistry – Electrochemical characterization was performed using 2032 coin cells with Cu||$LiFePO_4$ cells. The Cu||$LiFePO_4$ cells were assembled with a Cu metal foil negative electrode (15 mm diameter, MTI Corporation), two Celgard 2400 separators (19 mm diameter), and a $LiFePO_4$ positive electrode (91% active material, 13.7 mm diameter, MTI corporation), the other 9% of the composite

electrode is composed of conductive carbon and PVDF coated on aluminum. The cells were prepared with 60 µL of electrolyte. Electrolytes investigated include (1-x) M $LiPF_6$ + x M LiDFOB in ethylene carbonate: dimethyl carbonate (1g:4g, EC:DMC) solvent and (1-x) M $LiPF_6$ + x M LiDFOB in fluoroethylene carbonate: dimethyl carbonate (1g:4g, FEC:DMC) solvent. The compositions studied consisted of 1.0 M $LiPF_6$, (1.0 M $LiPF_6$ EC electrolyte), 0.95 M $LiPF_6$ + 0.05 M LiDFOB (0.05 M LiDFOB EC electrolyte), 0.90 M $LiPF_6$ + 0.10 M LiDFOB (0.10 M LiDFOB EC electrolyte), 0.50 M $LiPF_6$ + 0.50 M LiDFOB (0.50 M LiDFOB EC electrolyte), and 1.0 M LiDFOB (1.0 M LiDFOB EC electrolyte). The identical compositions studied in FEC:DMC electrolytes are abbreviated as 1.0 M $LiPF_6$ FEC electrolyte, 0.05 M LiDFOB FEC electrolyte, 0.1 M LiDFOB FEC electrolyte, 0.5 M LiDFOB FEC electrolyte, and 1.0 M LiDFOB FEC electrolyte. The copper metal foil was sonicated with isopropanol (2 x 2 minutes), punched to the specified diameter, and dried at 110°C, overnight under vacuum prior to cell assembly. The $LiFePO_4$ electrodes were punched to the specified diameter, and dried at 110°C overnight under vacuum prior to cell assembly. The cycling procedure consisted of plating Li metal at 0.1 mA/cm^2 (approx. C/20 rate, where C represents the theoretical capacity of $LiFePO_4$) with subsequent stripping and plating at 0.4 mA/cm^2 (approx. C/4 rate), within a voltage window of 2.0 – 4.0 V, using an Arbin BT2000 battery cycler at 25°C. There was a rest period of one hour between cell construction and the beginning of the electrochemical protocol.

DRIFTS – IR spectra of lithium metal electrodes were acquired with a Bruker Tensor 27 spectrometer equipped with an UpIR Diffuse Reflectance accessory (Pike

Technologies) and LaDTG detector. Lithium metal was deposited onto Cu foil according to the first charge procedure outlined in the electrochemistry section (charge to 4.0 V at C/20 rate) and held at rest for approximately 4 hours to ensure cell equilibration before disassembly. Electrodes were washed with 4x500 µL battery grade DMC and dried under vacuum for 20 minutes, then overnight in an argon-filled glovebox. The electrodes were transferred from an argon glove box to a nitrogen-filled glove box in a sealed Nalgene vial and measured immediately with DRIFTS. There is no evidence for reaction of the lithium metal anodes with N_2 during the timeframe of the analysis. The spectra were acquired in the nitrogen glove box with a resolution of 4 cm^{-1} and 32 scans.

XPS – XPS measurements were acquired with a K-alpha Thermo system using Al Kα radiation (hν = 1486.6 eV) under ultra-high vacuum ($<1x10^{-12}$ atm) and a measured spot size of 400 µm in diameter. Lithium metal was deposited onto Cu foil according to the first charge procedure outlined in the electrochemistry section (charge to 4.0 V at C/20 rate), and held at rest for approx. 4 hours to ensure cell equilibration before disassembly. Electrodes were washed with 4x500 µL battery grade DMC and dried under vacuum for 10 minutes, then overnight in the argon glovebox. The samples were transferred from the argon glove box in an air-free transfer case, while sealed under vacuum. The binding energy was corrected based on the F1s spectrum, assigning LiF to 685 eV.

RESULTS AND DISCUSSION

The concentration of Li^+ is maintained at 1.0 M for all electrolytes investigated, emphasizing the influence of the PF_6^- and $DFOB^-$ anions on electrochemical performance. The stripping capacity vs. cycle number, Coulombic efficiency vs. cycle number and sum of reversibly cycled lithium for Cu||$LiFePO_4$ cells after 50 cycles for the EC:DMC electrolytes investigated are provided in Figure 5-1A, 5-1B, and 5-1C, respectively. The stripping capacity of the cells containing the 1.0 M $LiPF_6$ EC electrolyte (see electrolyte abbreviations in experimental section) is extremely poor, with no significant reversible capacity upon cycling (Fig. 5-1A), as evidenced by the low initial Coulombic efficiency of 15%. In general, the cycling performance is improved as the concentration of LiDFOB is increased in the electrolyte, with the 1.0 M LiDFOB EC electrolyte having the best performance, achieving 30 cycles before the cell drops below 20 % of the initial capacity (Fig. 5-1A). This trend is evident in Fig. 5-1B, with initial efficiencies of 52%, 69%, 87%, and 89% for the 0.05 M LiDFOB EC, 0.10 M LiDFOB EC, 0.50 M LiDFOB EC, and 1.0 M LiDFOB electrolytes, respectively. The improvement in electrochemical performance is further illustrated by the sum of the stripping capacities (reversibly cycled lithium) over 100 cycles,[11] which increases with increasing LiDFOB content in the electrolyte (Fig. 5-1C). With EC-containing electrolytes, it is optimal to use LiDFOB as the pure salt instead of as an additive, supporting previous investigations of LiDFOB electrolytes.[9]

The stripping capacity vs. cycle number, Coulombic efficiency vs. cycle number and sum of reversibly cycled lithium for Cu||$LiFePO_4$ cells after 100 cycles

for the FEC:DMC electrolytes investigated are provided in Figure 5-2A, 5-2B, and 5-2C, respectively. The 1.0 M $LiPF_6$ FEC electrolyte, out performs all EC electrolytes described above, achieving 40 cycles before the cells drops below 20 % of the initial capacity and higher efficiencies stabilizing around 98% (Figs. 5-2A, 5-2B), consistent with previous work.[6,9] This is also evident in Figure 5-2C, since the quantity of reversibly cycled lithium exceeds the best EC electrolyte by more than 1000 mAh/g. Upon addition of LiDFOB to the electrolyte, there are minor improvements in Coulombic efficiency, extending the lifetime of the cell for more cycles (Figs. 5-2A, 5-2B). This observation suggests that, upon incorporation of LiDFOB into the electrolyte, parasitic reactions of the lithium metal electrode with the electrolyte are mitigated. The optimal concentration of LiDFOB required is much lower for the FEC electrolytes, with the 0.05 M LiDFOB FEC and 0.10 M LiDFOB FEC electrolytes having the slightly better electrochemical performance. This trend is also clear for the sum of reversibly cycled lithium (Fig. 5-2C). Therefore, incorporation of LiDFOB in additive concentrations to FEC based electrolytes improves performance synergistically with FEC to improve the cycling performance of the lithium metal anode.

The DRIFTS spectra of the lithium electrode after the first plating cycle of lithium from 1.0 M $LiPF_6$ EC, 1.0 M LiDFOB EC, 1.0 M $LiPF_6$ FEC, and 0.10 M LiDFOB FEC electrolytes, are provided in Figure 5-3. The peak at 1573 cm^{-1} is an artifact peak of the DRIFTS accessory.[9] The DRIFTS spectrum of the lithium electrode plated with 1.0 M $LiPF_6$ EC, and 1.0 M $LiPF_6$ FEC after the first plating

cycle contains major peaks assigned to lithium carbonate (Li_2CO_3; 1510, 1460 cm^{-1}) and lithium alkyl carbonates ($ROCO_2Li$; 1690 cm^{-1}), as previously reported.[9,12–15] The peaks associated with $ROCO_2Li$ and Li_2CO_3 have comparable intensity, suggesting comparable concentrations of these two SEI components for lithium metal plated with both 1.0 M $LiPF_6$ EC and FEC electrolytes, consistent with previous work.[9] The similar IR spectra for lithium plated with the 1.0 M $LiPF_6$ EC and FEC but significant difference in cycling performance have been discussed previously, suggesting that the nanostructure of the SEI products is a major factor in electrochemical performance.[9,10]

For lithium metal plated with 1.0 M LiDFOB EC and 0.10 M LiDFOB FEC electrolytes, Li_2CO_3 is observed, along with similar concentration of $Li_2C_2O_4$ species (1625 cm^{-1}).[16,17] This observation supports the favorable decomposition of LiDFOB on the electrode surface. There also appears to be a minor amount of polycarbonates observed at 1780 and 1815 cm^{-1}, as well, suggesting LiDFOB facilitates the decomposition of EC, consistent with previous work.[17] There is a relatively higher concentration of $Li_2C_2O_4$ for lithium metal plated with the LiDFOB EC electrolyte compared to the 0.10 M LiDFOB FEC electrolyte, consistent with the significant difference in concentration of LiDFOB in the respective electrolytes. Given that $ROCO_2Li$ is not observed for lithium plated with the superior LiDFOB electrolytes, the generation of $Li_2C_2O_4/Li_2CO_3$ in the SEI products may be preferential to the generation of $ROCO_2Li/Li_2CO_3$ in the SEI. This could be due to the poor stability of $ROCO_2Li$ or the ability of $Li_2C_2O_4$ and Li_2CO_3 to control the growth of LiF nano-particles, as previously reported.[9,10]

The C1s, O1s, and F1s XPS spectra of the lithium electrode after the first plating cycle of lithium from the 1.0 M $LiPF_6$ EC, 1.0 M LiDFOB EC, 1.0 M $LiPF_6$ FEC, and 0.10 M LiDFOB electrolytes, are provided in Figure 5-4. After the first plating cycle, the C1s, O1s, and F1s spectra are very similar for the lithium metal electrode plated from the 1.0 M $LiPF_6$ EC and FEC electrolytes, consistent with previous work.[9] The C1s spectra contain peaks associated with CO_3 at 289.9 eV, C-O at 286.7 eV and C-C/C-H at 285.0 eV consistent with the generation of a combination of $ROCO_2Li$ and Li_2CO_3, as observed by IR spectroscopy.[11,13,18] The O1s spectrum contains a broad beak centered at ~531.8 eV, consistent with a mixture of C-O and C=O containing species.[11,13,18] A peak for Li_2O is also observed at 528 eV in the O1s spectrum.[11,13,18] Further, The F1s spectra are very similar, containing peaks at 685 eV and 687 eV consistent with LiF and $Li_xPF_yO_z$, respectively.[18,19] All of these observations are consistent with previous work.[9]

The XPS spectra of the lithium metal plated from the 1.0 M LiDFOB EC electrolyte, contains C1s and O1s peaks at 289.3 eV and 533.0 eV, respectively, consistent with the presence of oxalate functional groups, as observed in the DRIFTS spectrum.[10] Further, Li_2O is not observed in the O1s spectrum. The F1s spectrum contains a peak consistent with LiF although the concentration of F is relatively low, 8%, suggesting the oxalate products are dominant on the surface. A high concentration of LiDFOB (1 M) was used in the electrolyte, thus the concentration of oxalate species on the surface of lithium metal is expected to be relatively high, consistent with the DRIFTS analysis.

For lithium plated from the 0.10 M LiDFOB FEC electrolyte, the spectra have similarities to both the lithium plated from the 1.0 M $LiPF_6$ FEC electrolyte and from the 1.0 M LiDFOB EC electrolyte, as expected, since the electrolytes contain both LiDFOB and FEC. A C1s peak is observed at 289.0 eV, consistent with the presence of $Li_2C_2O_4$ as observed in the DRIFTS spectra.[10] The O1s spectrum contains a broad peak centered at 532 eV consistent with a combination of C-O and C=O containing species.[11,13,18] The observations are slightly different to that of lithium plated from the 1.0 M LiDFOB EC electrolyte, consistent with a lower concentration of LiDFOB decomposition products on the surface of lithium, which is expected for lithium metal plated with the 0.10 M LiDFOB FEC electrolyte since there is a lower concentration of LiDFOB.

Finally, the B1s and P2p spectra are provided in Figure 5-5 supporting the presence of LiDFOB decomposition products on the surface of lithium metal plated from the LiDFOB containing electrolytes. Peaks are observed at 193.4 eV and ~191.5 eV in the B1s spectra for lithium plated from 1.0 M LiDFOB EC and 0.10 M LiDFOB FEC electrolytes, respectively. It should be noted that intensity from the P2s peak overlaps with B1s peak. However, the intensity of the P2p peak at ~135.2 eV, characteristic of Li_xPF_y and $Li_xPF_yO_z$,[18,19] is similar for both the 1.0 M $LiPF_6$ FEC and 0.10 M LiDFOB FEC electrolytes, yet the intensity and peak position of the peaks the B1s spectra are different supporting the presence of boron decomposition products on the surface of lithium metal plated from the 0.10 M LiDFOB FEC electrolyte. The shift in binding energy suggests that the boron containing species in the SEI differ in

structure, but it is unclear at this time how the structures may differ. In addition, as expected the concentration of B is lower for the lithium plated with a lower concentration of LiDFOB. Overall, LiDFOB improves the electrochemical performance of the cells via modification of the SEI, confirming the synergistic behavior of LiDFOB and FEC for lithium metal electrodes.

CONCLUSION

The concentration of LiDFOB was varied in carbonate electrolytes to optimize the performance of the lithium metal anode in Cu||$LiFePO_4$ cells. In EC electrolytes, LiDFOB is optimal in higher concentrations (1.0 M), as the bulk salt. However, in FEC electrolytes, LiDFOB is optimal when used in lower concentrations, 0.05 – 0.10 M. Ex-situ surface analysis suggests that LiDFOB reacts on the surface of lithium metal to generate a more stable SEI improving the performance of lithium metal anodes in both EC and FEC-based electrolytes. Therefore, LiDFOB and FEC can be used in the electrolyte synergistically to optimize the performance of the lithium metal anode. This research demonstrates progress towards feasible high-energy density lithium-based batteries.

REFERENCES

1. P. Albertus, S. Babinec, S. Litzelman, and A. Newman, *Nat. Energy*, **3**, 16–21 (2018).

2. X. Cheng, R. Zhang, C.-Z. Zhao, and Q. Zhang, *Chem. Rev.*, **117**, 10403–10473 (2017).

3. B. Liu, J. G. Zhang, and W. Xu, *Joule*, **2**, 833–845 (2018).

4. K. Xu, *Chem. Rev.*, **104**, 4303–4417 (2004).

5. E. Peled, *J. Electrochem. Soc.*, **126**, 2047–2051 (1979).

6. E. Markevich, G. Salitra, F. Chesneau, M. Schmidt, and D. Aurbach, *ACS Energy Lett.*, **2**, 1321–1326 (2017).

7. I. A. Shkrob, J. F. Wishart, and D. P. Abraham, *J. Phys. Chem. C*, **119**, 14954–14964 (2015).

8. X. Fan, L. Chen, X. Ji, T. Deng, S. Hou, J. Chen, J. Zheng, F. Wang, J. Jiang, K. Xu, and C. Wang, *Chem*, **4**, 174–185 (2018).

9. Z. L. Brown, S. Jurng, C. C. Nguyen, and B. L. Lucht, *ACS Appl. Energy Mater.*, **1**, 3057–3062 (2018).

10. S. Jurng, Z. L. Brown, J. Kim, and B. L. Lucht, *Energy Environ. Sci.*, **11**, 2600–2608 (2018).

11. Z. L. Brown, S. Jurng, and B. L. Lucht, *J. Electrochem. Soc.*, **164**, A2186–A2189 (2017).

12. C. C. Nguyen and B. L. Lucht, *J. Electrochem. Soc.*, **161**, A1933–A1938 (2014).

13. D. M. Seo, C. C. Nguyen, B. T. Young, D. R. Heskett, J. C. Woicik, and B. L.

Lucht, *J. Electrochem. Soc.*, **162**, A7091–A7095 (2015).

14. G. V. Zhuang, K. Xu, H. Yang, T. R. Jow, and P. N. Ross Jr., *J. Phys. Chem. B*, **109**, 17567–17573 (2005).

15. G. V. Zhuang, H. Yang, P. N. Ross Jr., K. Xu, and T. R. Jow, *Electrochem. Solid-State Lett.*, **9**, A64–A68 (2006).

16. G. V Zhuang, K. Xu, T. R. Jow, and P. N. Ross Jr., *Electrochem. Solid State Lett.*, **7**, A224–A227 (2004).

17. M. Nie and B. L. Lucht, *J. Electrochem. Soc.*, **161**, A1001–A1006 (2014).

18. P. Verma, P. Maire, and P. Novák, *Electrochim. Acta*, **55**, 6332–6341 (2010).

19. A. M. Andersson, D. P. Abraham, R. Haasch, S. MacLaren, J. Liu, and K. Amine, *J. Electrochem. Soc.*, **149**, A1358–A1369 (2002).

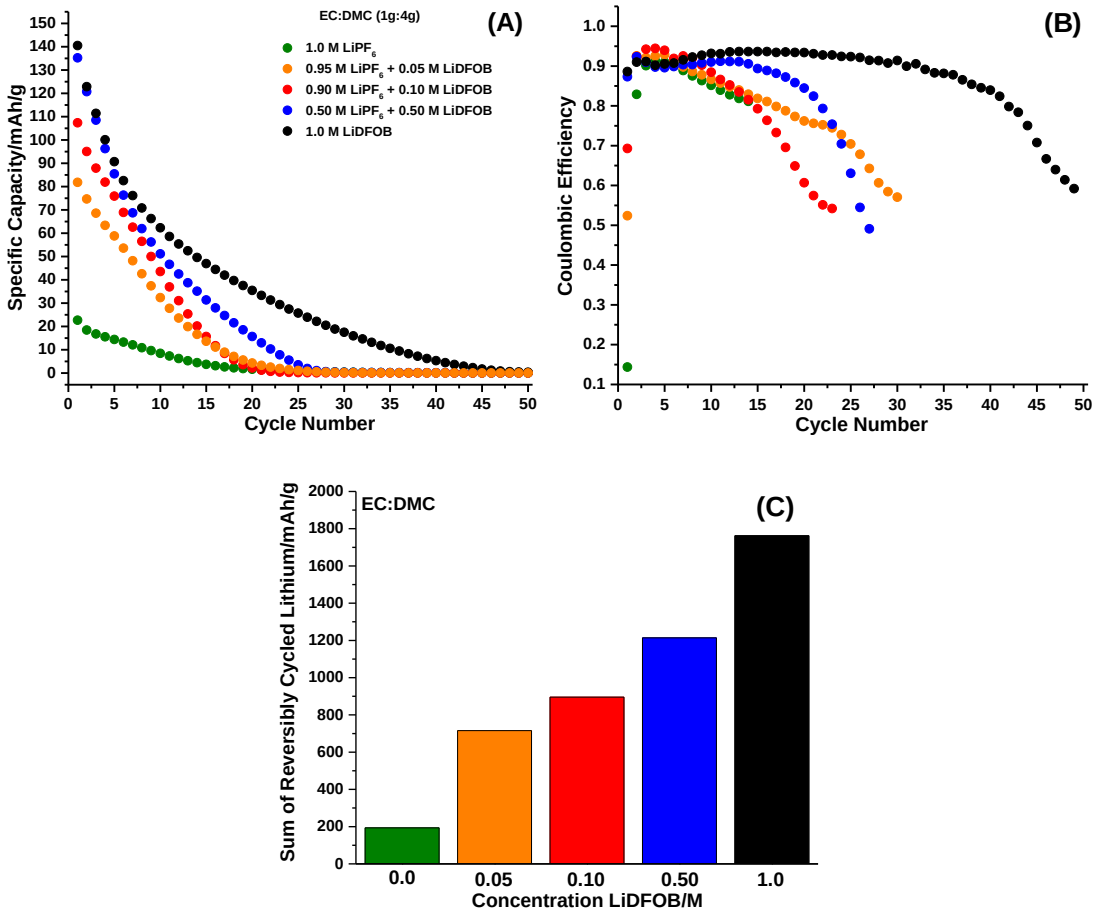

Figure 5-1. The stripping capacity vs. cycle number (A), Coulombic efficiency vs. cycle number (B), and sum of reversibly cycled lithium (C), for EC:DMC electrolytes in Cu||$LiFePO_4$ cells after 50 cycles.

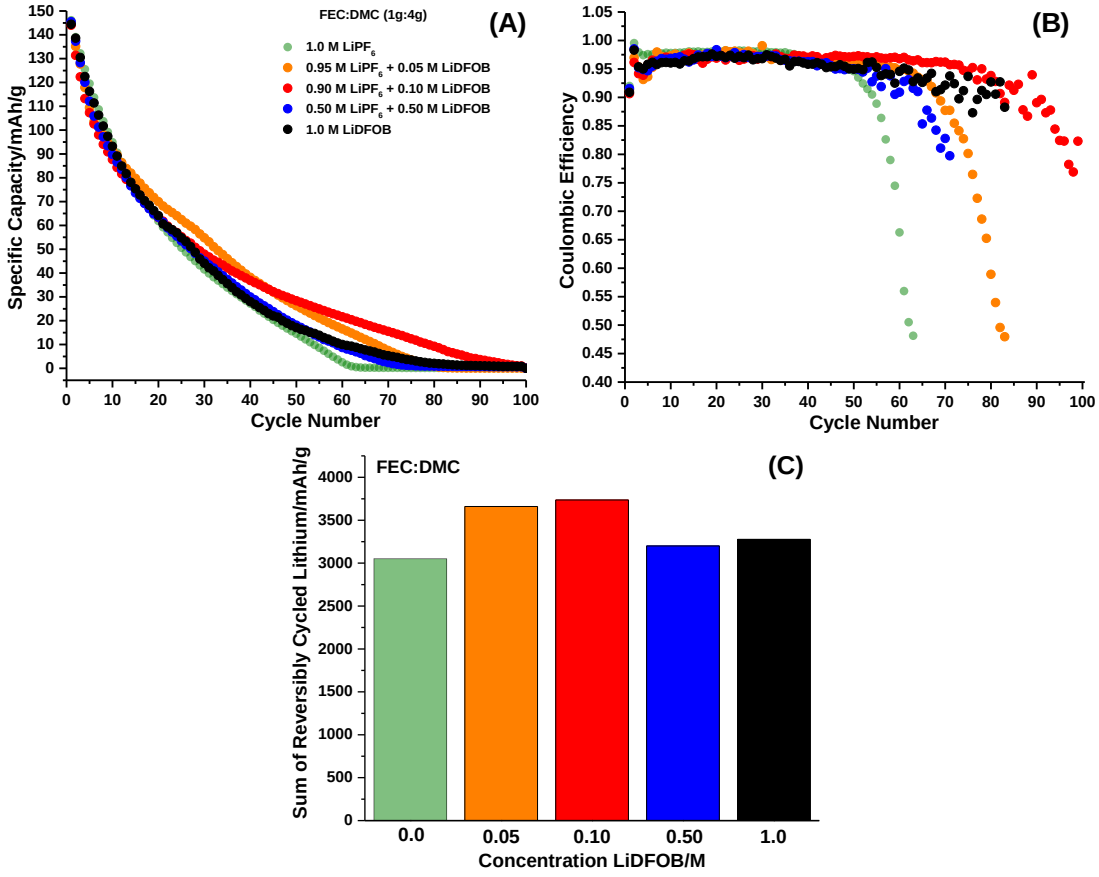

Figure 5-2. The stripping capacity vs. cycle number (A), Coulombic efficiency vs. cycle number (B), and sum of reversibly cycled lithium (C), for FEC:DMC electrolytes in Cu||$LiFePO_4$ cells after 100 cycles.

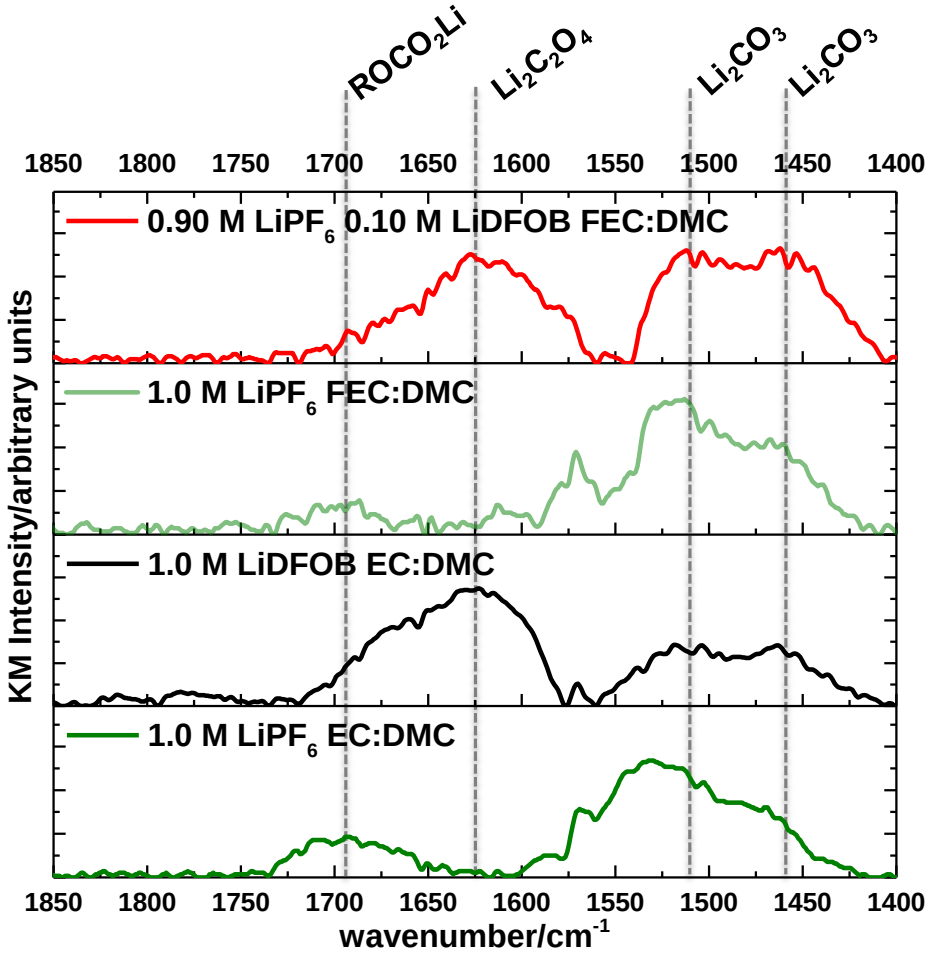

Figure 5-3. DRIFTS of lithium metal plated with the investigated electrolytes.

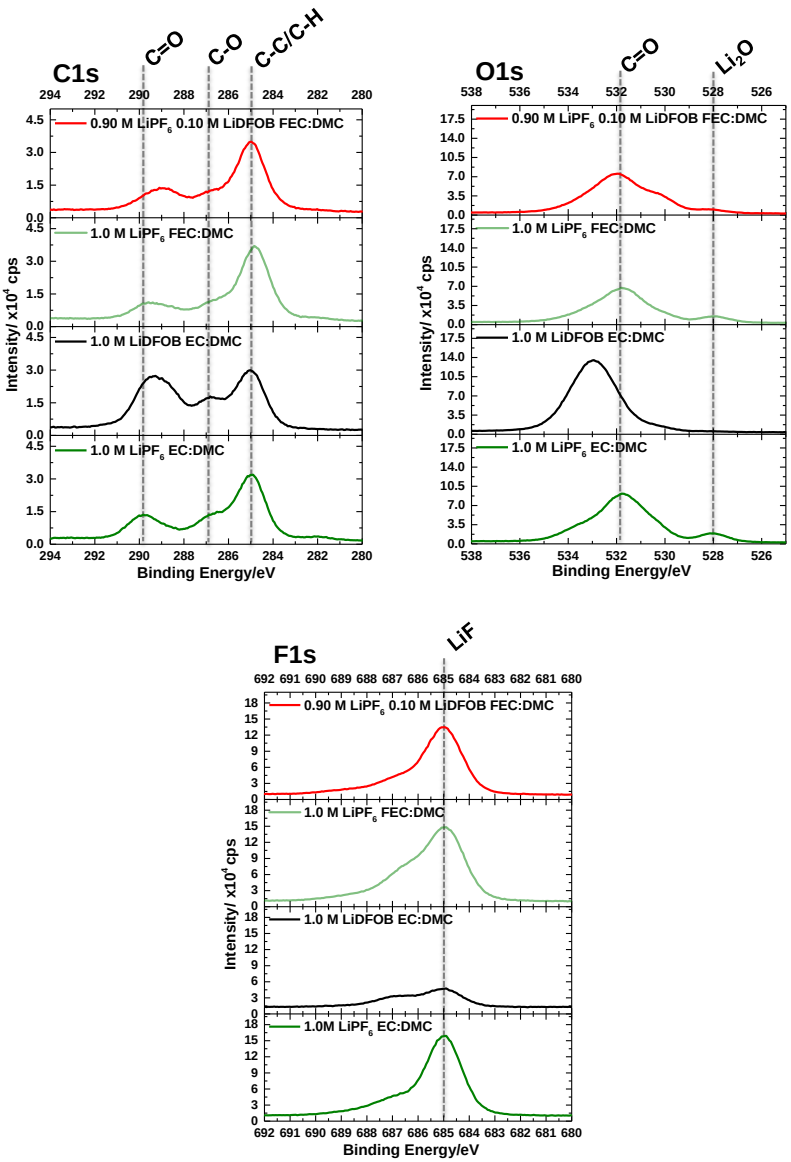

Figure 5-4. C1s, O1s, and F1s spectra of lithium metal plated with the investigated electrolytes.

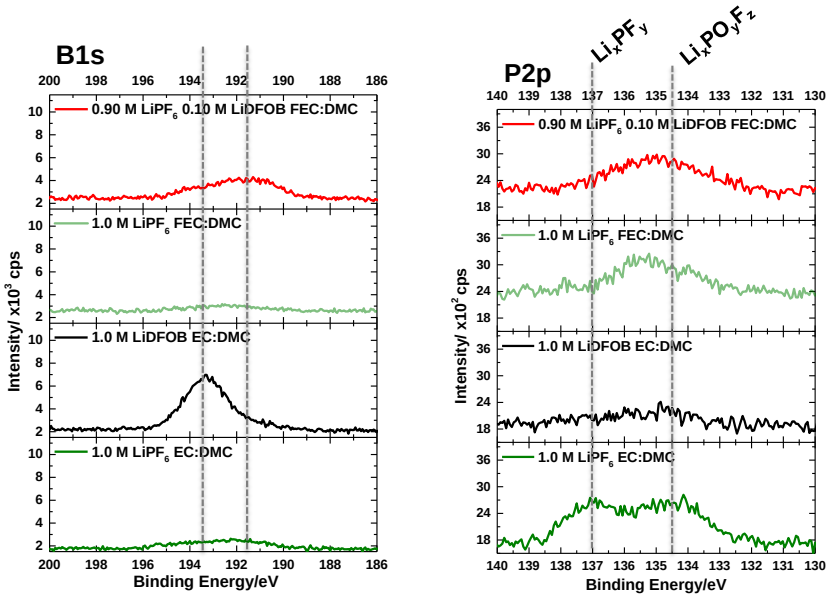

Figure 5-5. B1s and P2p spectra of lithium metal plated with the investigated electrolytes.